Electrically controlled spin dynamics in disordered semiconductors

Inauguraldissertation

zur

Erlangung der Würde eines Doktors der Philosophie

vorgelegt der

Philosophisch-Naturwissenschaftlichen Fakultät

der Universität Basel

von

Mathias Duckheim

aus Reinheim, Deutschland

Basel, 2008

Genehmigt von der Philosophisch-Naturwissenschaftlichen Fakultät auf Antrag von

Prof. Dr. Daniel Loss

Prof. Dr. Dmitrii Maslov

Basel, den 26. November 2008 Prof. Dr. Eberhard Parlow

Dekan

Meinen Eltern gewidmet

Summary

The spin of electrons in a semiconductor environment couples not only to magnetic fields, but also to the orbital motion of the electron. As a consequence, transport in semiconductors includes a class of phenomena in which electrically induced charge motion influences the electron spin. The intricate interplay of spin and charge makes this type of effects a diverse research field of fundamental interest, but is also of practical relevance: Spin-orbit interaction (SOI) provides a mechanism to control the spin with electric fields. Being available in tailored materials, that are routinely used in microelectronics, SOI has therefore attracted intense interest for its potential in applications to use the electron spin alternatively to the charge in new types of electronic devices.

In this thesis we investigate the interplay of spin and charge transport in disordered electron systems, where random impurities not only determine the electrical resistance but also the spin dynamics through spin-orbit interaction. A focus of this work is electric-dipole-induced spin resonance (EDSR), a versatile scheme of spin control using electric fields. Similar to standard paramagnetic resonance where a combination of static and ac magnetic fields drive spin rotations, in EDSR ac electric fields couple resonantly to the spin. Appropriately chosen pulses of these electric fields, which can be generated easier on-chip than ac magnetic fields, allow to achieve arbitrary spin rotations. In a diagrammatic analysis we find that the presence of disorder broadens the line-shape of EDSR and determines the maximal achievable polarization. We identify random internal magnetic fields as the origin of this line-broadening, which limits the efficiency of EDSR, and show that these limitations can be overcome in an optimal geometry where the internal fields are suppressed by the interference of different spin-orbit mechanisms. This leads to a substantial enhancement of the spin polarization at resonance. We moreover link these findings to spin currents giving rise to the spin-Hall effect. We interpret these spin currents in terms of spin polarization components.

The behavior of the spin depends sensitively on whether the orbital motion is diffusive or phase coherent. Indeed, qualitatively different – mesoscopic – effects occur in the spin when electrons flow through phase-coherent systems. Whereas in charge transport such mesoscopic effects are well known, for the spin they have attracted interest only more recently in the context of spintronics. We find that the spin polarization, that arises due to dc transport and SOI, shows large mesoscopic fluctuations that exceed the polarization in incoherent samples with self-averaging. Since this average polarization has been successfully measured we expect this mesoscopic fluctuations to be within experimental reach as well.

Contents

1 Introduction

1.1 Introduction

A conceptually simple picture for charge transport in disordered semiconductors is the Drude model [Drude00]. Electrons scattering randomly from static impurities in the semiconductor can be described simply by classical diffusive drift; a large-scale analogy is the motion of beads falling through a nail bed (also known as Galton box). The electron spin, on the other hand, typically evolves coherently for a duration of many scattering times during this motion. The different behaviour and the robustness of magnetic degrees of freedom has inspired a new paradigm in information technology and solid state physics, termed spintronics [Awschalom02, Awschalom07], which aims at utilizing the electron spin instead of the charge to encode and process information.

A landmark effect attributed to spintronics is the giant magnetoresistance effect (GMR) [Grünberg86, Baibich88, Binasch89] which was awarded the Nobel prize in 2007. Few years after its discovery, GMR turned into a mass production technology applied in reading data from hard drives and also in non-volatile magnetic RAM. Theoretical models and applications of the GMR are based on a two-channel picture of spin transport (with carrier types spin-up and spin-down), but do not focus on superpositions of the two, i. e. on spin coherence.

In addition to such incoherent spintronics devices, intense interest was triggered in spintronics in semiconductors by the long spin coherence times in these materials [Kikkawa97]. Semiconductors provide a unique environment for spintronics with tailored material properties such as the confinement energy, scattering time (mobility), electron g-factor, and effective mass. The availability of optical measurements [Meier84, Baumberg94, Kikkawa98, Kato04a], moreover, allows for time- and spatially resolved measurements of the spin polarization in these systems which has enabled the observation of coherent spin phenomena, e.g. the precession in crystal magnetic fields [Kato04a] and the spin-Hall effect [D'yakonov71, Sinova04, Hirsch99, Kato04c, Wunderlich05, Sih05].

With magnetic elements being absent in semiconductors[1] the control and the generation of non-equilibrium spin polarization without magnetic fields becomes a central issue of semiconductor spintronics. This task is enabled by the strong spin-orbit interaction (SOI) [cf. Sec. 1.2] in these materials giving rise to zero-field, momentum-dependent spin splittings. These splittings lead to effects involving the interaction between the orbital transport processes and the spin dynamics which will be a central topic of this thesis and have received a strong interest for their applicability in schemes to control and generate spin with electric fields. An illustrative example for such spin-orbit related effects is the magnetoelectric effect (MEE) [Levitov85, Edelstein90, Kato05, Meier07]. Analogous to Pauli paramagnetism where a magnetic field causes an energy difference between aligned and anti-aligned spin leading to an imbalance between spin populations in thermal equilibrium, in the MEE internal fields generated by SOI and transport give rise to a spin-polarized steady-state. Of fundamental interest is, moreover, the spin-Hall effect(SHE) [D'yakonov71, Sinova04, Hirsch99, Kato04c, Wunderlich05, Sih05] which is similar to the classical Hall effect, where charges of different sign are deflected in opposite directions as they flow through a conductor immersed in a magnetic field. In the spin Hall effect spin-up and spin-down electrons transported through a semiconductor separate due to spin-orbit coupling and accumulate non-equilibrium spin polarization at the edges of the sample. For the SHE one generally distinguishes two types, the intrinsic and extrinsic SHE. The origin of the extrinsic SHE [D'yakonov71,Engel05,Engel06] is attributed to spin currents arising from spin-selective scattering from impurities. These spin currents are not directly observable, but manifest as spin polarization at the sample edges transverse to an electric current (and without magnetic fields). Edge spin accumulation due to the extrinsic SHE has first been observed in bulk semiconductors [Kato04c, Wunderlich05, Sih06], later in metals [Valenzuela06] and at room-temperature [Stern06]. The intrinsic SHE shows similar boundary spin accumulation [Sih05], but a more intricate polarization profile with additional spatial oscillations resulting from the intrinsic SOI. [2]

While the MEE and the SHE might be applied in schemes to generate spin polarization without magnetic fields, interest also focusses on the manipulation of an existing, non-equilibrium polarization. A set of devices proposed for this purpose rely on alternative gating mechanisms. For instance, the Datta-

[1] Intense efforts focus on the fabrication and characterization of magnetic semiconductors such as GaMnAs. See for a review [Ohno98, Dietl02].

[2] Theoretical descriptions of the intrinsic SHE are based on spin diffusion equations for which appropriate boundary conditions have to be posed. The solution to such equations depends sensitively on these boundary conditions making their correct derivation an important theoretical problem [Maslov93, Mal'shukov05, Bleibaum06, Galitski06, Tserkovnyak07, Zyuzin07].

Das transistor [Datta90] and a more advanced proposal [Schliemann03] utilize the modulation of the SO-induced-spin splitting [Nitta97] by electric gates. Appropriate switching of such gates allows one to tune the precession frequency of spins in internal fields such that an initial polarized spin can be rotated in the 'on-state' and is left unchanged in the 'off-state' of the transistor.

Full coherent control of the spin is typically achieved by paramagnetic electron spin resonance(ESR) [Abragam61, Bloch57]. In ESR high-frequency magnetic fields are tuned to resonance with the precession frequency of the spin in a static magnetic field. With suitably chosen pulses of such high-frequency fields arbitrary spin rotations can be obtained. Similar to ESR, electric-dipole-induced spin resonance (EDSR) [Bell62, Dobrowolska84] is a technique to control the spin but utilizes electric instead of magnetic driving fields. EDSR therefore allows for fully coherent spin control, has the advantage, however, that it can be integrated in electrically contacted nanostructures, avoiding magnetic rf coils.

The orbital transport processes involved in the MEE, EDSR and the spin-Hall effect are affected by the presence of imperfections -impurities or defects- in the crystal lattice of the conduction channel of the semiconductor and in the surrounding substrate and doping layers. These impurities give rise to a static and random potential from which the electrons moving through the semiconductor scatter and which determines the electrical resistance of the system. In large systems these transport processes are sufficiently described as diffusive, i. e., by assuming that the disorder potential leads to a near-to-complete randomization of the electron motion after a single scattering from an impurity. In systems with SOI diffusive drift which is generated by electric fields and diffusive random motion give rise to effective magnetic fields [cf. Sec. 1.2] and fluctuations of them, respectively. Qualitatively different phenomena occur when the orbital transport processes are phase coherent; since scattering from impurities is static, it leads only to a randomization of the momentum but not of the quantum mechanical phase of the electron. An important example of such coherence effects are mesoscopic fluctuations revealing a dependence of macroscopic sample properties, e.g. its conductivity, on microscopic differences in the spatial distribution of the impurities. These fluctuations can be traced back to phase correlations and are well known in charge transport [Altshuler85, Altshuler91, Lee87, Zumbühl05, Aleiner01, Miller03]. In the presence of SOI, such fluctuations can also be found in the spin. The MEE, for instance, shows mesoscopic fluctuations in the spin polarization that is induced by an electric field.

These effects concern the coherent manipulation of ensembles of spins. On the other hand, the Loss-DiVincenzo proposal [Loss98] puts particular emphasis on the coherence and the entanglement of single spins. These spins serve

as qubits, the basic building blocks of a solid-state based quantum computer. The quantum mechanical entanglement between a higher number of spins allows to implement algorithms [Nielsen00, Mermin07] with higher parallelism. For some tasks such algorithms would therefore outperform the best algorithms that are available on a classical computer for the same task. Registers of qubits and qubit gates can moreover serve to simulate general quantum systems in a controllable environment. The implementation of the quantum computer requires the fulfillment of a number of criteria [DiVincenzo00] concerning the controlled operation, readout, and initialization of spin states towards which the last decade has witnessed enormous progress [Coish07, Hanson07].

1.2 Spin and Spin-orbit interaction

The spin-$\frac{1}{2}$ of the electron is the most elementary quantum mechanical system. Due to the algebraic properties required by the Dirac equation of relativistic quantum mechanics the spin, $\hat{\mathbf{S}}$, can be described as an internal angular momentum of the electron. This "spin" is associated with a magnetic moment $\boldsymbol{\mu} = 2g\mu_B\hat{\mathbf{S}}/\hbar$ where g is the g-factor ($g \approx 2$ for free electrons) and $\mu_B = e\hbar/2m = 5.8 \times 10^{-5}\mathrm{eVT}^{-1}$ is the Bohr magneton. Measurement of $\boldsymbol{\mu}$ along a quantization axis (defined by a magnetic field) yields either of two discrete outcomes, $\pm g\mu_B/2$ corresponding to the spin up- and the spin down-state. The spin is therefore referred to as a two-level system which is described by a superposition of the up and the down state. These two states may serve to encode a classical bit of information by defining spin-up (spin-down) as the logical "1" ("0"). Exploiting, moreover, the coherence property of the spin, quantum mechanical superpositions of these states can be encoded forming a quantum-bit (qubit). The prospect of using the electron spin as a carrier of classical or quantum information has triggered intense research efforts in spintronics and solid-state based quantum computing.

Developing robust schemes to coherently control non-equilibrium spin polarization is therefore a central objective of spintronics. For this purpose electrical instead of magnetic control is desirable since electric fields allow for easier on-chip generation and time-dependent switching by local gates. The spin of free, non-relativistic electrons, however, reacts only weakly to electric fields such that direct electric operation of the spin is not possible. In semiconductor environments, however, the relativistic effects responsible for the coupling between spin and orbital motion can be strongly enhanced with zinc-blend III-V semiconductors showing a particularly strong spin-orbit interaction (SOI). Such enhanced SOI provides the pivotal mechanism enabling (indirect) electrical control of the spin: Indeed, in addition to shaping the

band structure, effective mass, and g-factor, SOI has important consequences for the one-electron energy levels leading to momentum-dependent spin splittings in the absence of magnetic fields. The momentum-dependence of such SO-splittings whose strengths can be varied over a wide range [Nitta97, Papadakis99, Koga06] enables electrical spin operation via the electrical control of the momentum [Kato04a, Mishchenko04, Rashba03b, Duckheim06].

A complete description of the electron and its spin in the non-relativistic limit is given by the the Pauli equation [Schwabl05] including a term describing SOI, known as Thomas term,

$$H_{SO} = \lambda_{SO} \boldsymbol{\sigma} \cdot \mathbf{p} \times \nabla (V_0 + \tilde{V}) \tag{1.1}$$

where $\mathbf{p}$ is the momentum operator and $\boldsymbol{\sigma} = (\sigma^1, \sigma^2, \sigma^3)$ denote the Pauli matrices. V_0 is the lattice-periodic potential of the crystal and $\tilde{V}$ the potential due to impurities, confinement, external fields, etc. Setting $V_0 = 0$ Eq. (1.1) describes SOI of electrons in vacuum (subject to a potential $\tilde{V}$) with $\hbar\lambda_{SO} = -\hbar^2/4m_0^2c^2 = -3.7 \times 10^{-6}\text{Å}^2$ where c is the velocity of light and m_0 the free electron mass. In direct-gap semiconductors such as GaAs, a description of the conduction band electrons by an effective-mass Hamiltonian that includes SOI is obtained in the framework of $\mathbf{k}\cdot\mathbf{p}$-theory [Winkler03]. The SOI mechanisms obtained can be (roughly) classified in two categories. The first is the extrinsic SOI present in the proximity of impurities only, which leads to spin-dependent scattering including Mott-skew scattering [Mott65]. The second type, the intrinsic SOI is an inherent band-structure effect present also in a perfect crystal, i. e. remote from impurities, which leads to (spatially uniform) spin-splittings in the single-electron energy levels.

In GaAs a SOI of the form [Eq. (1.1)] (with $V_0 \to 0$ absorbed in the band structure, $\tilde{V}$ being the impurity potential) arises due to the coupling of s-type conduction band and p-type valence band wave functions. Within the framework of $\mathbf{k} \cdot \mathbf{p}$-theory the prefactor is found [Winkler03, Engel06] to be $\hbar\lambda_{SO} = +5.3\text{Å}^2$, and, therefore, drastically enhanced with respect to its vacuum counterpart. Extrinsic SOI has been identified [D'yakonov72,Engel05,Engel06] as the mechanism for the spin-Hall effect in bulk semiconductors.

For structures with a particular symmetry group, e.g. T_d for bulk zinc-blend crystals, specific intrinsic SO-mechanisms can be described [Dresselhaus55, Rashba60, deAndradaeSilva94, Winkler03]. For instance, in a heterostructure of Zinc-blend materials two SO-mechanisms, the Rashba and the Dresselhaus SOI due to structure inversion asymmetry and bulk inversion asymmetry, respectively, exist. Here, we focus on semiconductor heterostructures forming a two-dimensional electron gas (2DEG). The Rashba SOI for

such a 2DEG is described by the Hamiltonian

$$H_R = \alpha(\boldsymbol{\sigma} \times \mathbf{p}) \cdot \mathbf{e}_z = \boldsymbol{\Omega}_R(\mathbf{p}) \cdot \boldsymbol{\sigma} \tag{1.2}$$

where $\mathbf{e}_z$ is the confinement axis and $\mathbf{p} = (p_1, p_2, 0)$ is the in-plane momentum. The strength of the Rashba coefficient α is given [Winkler03, deAndradaeSilva94] in terms of the band gap E_g, effective mass m, valence band spin-orbit splitting Δ, and the confinement potential $\tilde{V}(z)$ as

$$\alpha = \frac{\hbar^2}{2m} \frac{\Delta}{E_g} \frac{2E_g + \Delta}{(E_g + \Delta)(3E_g + 2\Delta)} e\nabla\tilde{V}(z)\,. \tag{1.3}$$

The Dresselhaus term [Winkler03] for a bulk zinc-blend crystal is of the form $\beta_3 p_x(p_y^2 - p_z^2)\sigma^1$ and cyclic permutations of it[3].

When the electrons are confined in a 2DEG the expectation value $\langle . \rangle_z$ of the momenta in the confinement direction (here, always assumed along the z-direction.) should be taken. While, in this case, the first moment $\langle p_z \rangle = 0$ vanishes, the terms $\langle p_z^2 \rangle_z \equiv \beta/\beta_3$ are finite[4]. The dominant Dresselhaus SOI contribution in a 2DEG (grown in the [001] direction) is therefore

$$\begin{aligned} H_D &= \beta[p_x\sigma^1 - p_y\sigma^2] = \boldsymbol{\Omega}_D(\mathbf{p}) \cdot \boldsymbol{\sigma} \\ H_{D,3} &= \beta_3[p_x^2 p_y \sigma^2 - p_y^2 p_x \sigma^1]. \end{aligned} \tag{1.4}$$

While the Dresselhaus SOI is essentially a material property the strength of the Rashba SOI depends on the asymmetry of the confinement potential in the structure. By an appropriate change of the design parameters of the structure and the confinement potential the Rashba SOI can therefore be tuned while keeping the Fermi energy constant [Papadakis99]. Tab. A.1 gives some typical values for the SO coupling constants α and β which were found by measurement of Shubnikov-de-Haas oscillations [Nitta97], weak localization [Miller03] and and Faraday rotation measurements [Meier07].

Intrinsic spin-orbit interaction and effective magnetic fields

The presence of SOI leads to a combined coherent evolution of the spin and the orbital motion. In general, this interplay of spin and momentum is rather intricate and leads to a number of effects such as zitterbewegung [Schliemann05],

[3] In the presence of a magnetic field the symmetrized form of the kinetic momenta must be used.

[4] A qualitative argument predicts that in strictly 2d systems the cubic terms in Eq. (1.4) often play a minor role: With an effective width δz of the quantum well the ratio of cubic to linear Dresselhaus can be estimated to be on the order of $(\delta z/\lambda_F)^2 \ll 1$, where $\lambda_F = h/p_F$ is the Fermi wavelength in the 2DEG.

Exp.	$\alpha[10^{-12}\text{eVm}]$	$\beta[10^{-12}\text{eVm}]$
Nitta *et al.* [Nitta97] (GaInAs-QW)	$6\ldots10$	n.n.
Miller *et al.* [Miller03]	-0.4 ± 0.1	0.5 ± 0.1
Meier *et al.* [Meier07]	-0.15	0.12

Table 1.1: Numerical values for the SOI strengths.

the spin-Hall effect [Sih05], spin relaxation in quantum dots [Elzerman04, Kroutvar04, Golovach04] and extended structures [D'yakonov72, Averkiev02], current-induced spin polarization [Edelstein90,Silov04,Kato05], and weak antilocalization [Hikami80, Bergmann84, Miller03], of which many have attracted significant interest in the field of spintronics. In systems with weak SOI, however, it is instructive (and an appropriate description for many SO-related effects) to assume that the orbital motion depends only weakly on the state of the spin, i. e. that there is no back action of the spin on the orbital motion which is then governed by external electric fields, scattering, etc. only. This assumption is equivalent to approximating the SO-induced spin splitting $\mathbf{\Omega}(\mathbf{p})$ by an effective field $\mathbf{\Omega}_{eff} \equiv \langle\mathbf{\Omega}(\mathbf{p})\rangle$ obtained by averaging $\mathbf{\Omega}(\mathbf{p})$ over the momentum distribution: Indeed, consider an electron subject to a time-dependent electric field in a disordered conductor. Under the assumption of weak SOI the electron acquires a finite average momentum $\langle\mathbf{p}\rangle(t)$ which is determined (entirely) by $\mathbf{E}(t)$ and momentum scattering. As a consequence, the spin dynamics are equal to those of an electron in a time-dependent magnetic field $\mathbf{\Omega}(\langle\mathbf{p}\rangle(t))$, which the internal field generated by SOI and the momentum. The interpretation of Eqs. (1.2-1.4) in terms of effective magnetic fields illustrates the principle of electrical spin control and enables an easy understanding of SO-related effects such as current induced spin polarization [Edelstein90, Kato05], EDSR and spin relaxation [cf. Sec. 2.2] due to the D'yakonov-Perel mechanism [D'yakonov72, Averkiev02]. Effective fields, however, fail to account for effects based on the full coherent coupling of spin and momentum such as Zitterbewegung [Schliemann05], oscillations of a non-equilibrium out-of-plane polarization [Stich07] and mesoscopic spin fluctuations [Duckheim08].

1.3 Electric-dipole-induced spin resonance

Electric-dipole-induced spin resonance [Bell62, Dobrowolska84, Kato04a] is an efficient scheme to control the electron spin with electric fields [Rashba03b, Schulte05, Wilamowski07, Duckheim06, Duckheim07, Meier07]. Similar to para-

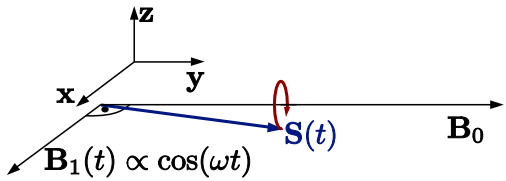

Figure 1.1: Geometry of the magnetic fields in paramagnetic electron spin resonance(ESR) which requires a time dependent magnetic field $\mathbf{B}_1(t) \propto \cos\omega t$ perpendicular to a static magnetic field $\mathbf{B}_0$. With ESR pulses chosen accordingly arbitrary spin rotations can be achieved. In EDSR the external field $B_1(t)$ is replaced by an internal field generated by SOI and ac. orbital transport.

magnetic electron spin resonance (ESR) [Abragam61, Edelstein93] EDSR uses a combination of a static and an oscillating field to drive spin rotations. To illustrate the principle of EDSR we briefly discuss ESR [Abragam61, Slichter96, Edelstein93] which occurs when a spin in a constant magnetic field $\mathbf{B}_0$ is subject to an additional oscillating magnetic field whose frequency ω matches the Larmor frequency $\omega_L = g\mu_B B_0/\hbar$ of B_0. The time dependence of the spin $S^i(t) = \langle\sigma^i\rangle(t)\,; i = 1,2,3$ (brackets denote expectation values) due to ESR is described by Bloch [Bloch57] equations

$$\frac{d}{dt}\mathbf{S} = 2[\mathbf{b}_0 + \mathbf{b}_1(t)] \times \mathbf{S} - \mathbf{\Gamma}[\mathbf{S} - \mathbf{S}_{eq}], \tag{1.5}$$

where $\mathbf{b}_0 = g\mu_B B_0/2$ is the static magnetic field (chosen along the y-axis, see Fig. 1.1) and $\mathbf{b}_1(t) = \mathbf{b}_1 \cos(\omega t)$ is the oscillating field with frequency ω and amplitude b_1 which is perpendicular to $\mathbf{b}_0$. In the first term both fields $\mathbf{b}_0$ and $\mathbf{b}_1(1)$ couple to the spin leading to precession and Rabi oscillations, respectively, while the second term describes relaxation ($\mathbf{\Gamma}$ being the relaxation tensor) towards an equilibrium polarization $\mathbf{S}_{eq}$. Eq. (1.5) can be solved approximately by transformation to the rotating frame [see e.g. [Slichter96]] in the regime $|\Gamma|, |\Gamma\mathbf{S}_{eq}| \ll b_1 \ll b_0$ and $\omega \approx \omega_L$. The resulting solutions $\mathbf{S}(t)$ are Rabi oscillations of the spin between the states of parallel and antiparallel alignment with $\mathbf{b}_0$ with frequency $\omega_R = 2b_1$. These oscillations are superimposed by the precession about $\mathbf{b}_0$ and relaxation towards $\mathbf{S}_{eq}$. Fig. 1.2 shows 3 snapshots of this motion (with negligible relaxation). After the driving field $b_1(t)$ is applied for a time $t = \pi/\omega_R$ the spin is switched from its initial 'up-state' along the y-axis to the 'down-state' [see Fig. 1.2 c]. Moreover, if relaxation is small compared to the driving, arbitrary azimuthal angles of the

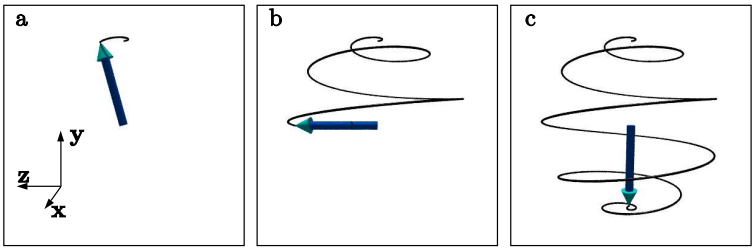

Figure 1.2: Rabi oscillations and precession due to ESR. The images show the time-dependence of the spin $\mathbf{S}(t)$ (dark arrow) which initially (at $t = 0$) points along the y-axis. The black line is the orbit of the tip of $\mathbf{S}(t)$. **a**) Spin at time $\omega_R t \gtrsim 0$, **b**) $\omega_R t = \pi/2$, and **c**) $\omega_R t = \pi$.

spin can be achieved by applying pulses $b_1(t)$ with appropriate duration.

Unlike in paramagnetic ESR, the driving fields in EDSR are electric, coupling to the spin via ac orbital transport and spin-orbit interaction. These electric fields allow thus for easy on-chip generation by applying ac voltages to local electrical contacts or gates. Similar to ESR, in EDSR suitably chosen pulses achieve arbitrary spin rotations. With the orbital motion coupling to the spin, however, scattering from impurities leads to a randomization of the electron momentum and, through SOI, of the electron spin. To leading order in $1/p_F l \ll 1$ where p_F is the Fermi wave length and l the mean free path [cf. Sec. 1.5] the orbital motion can be described by sequences of piecewise (free) linear motion with typical length l interrupted by scattering from impurities (cf. Fig. 1.3) into random directions. Although the scattering along these so-called Boltzmannian paths can be assumed spin independent[5] the random component in momentum gives rise to fluctuating internal magnetic fields due to the intrinsic SOI. These fields cause spin relaxation due to the D'yakonov-Perel mechanism [D'yakonov72, Dyakonov84] and lead to a finite line-width Γ in EDSR. The spin polarization S^{res} that can be achieved at resonance is limited by this line-width like $S^{\text{res}} \propto 1/\Gamma$. In Chaps. 2- 3 we study the broadening and suppression of the resonance using a microscopic model of disorder and intrinsic SOI. There, we find that the suppression of S^{res} results from inter-

[5] Extrinsic effects, i. e., spin-dependent scattering leads to rich physics in charge transport [Feng89, Bergmann84, Akkermans07] and in the spin-Hall effect [Engel06, Engel05] in bulk structures. In strictly 2D systems, however, models based on intrinsic (band-structure dependent) SOI [Aleiner01, Cremers03] explain transport measurements, that are sensitive to the breaking of spin-symmetries [Zumbühl05, Miller03], rather well, and will be the focus of this work.

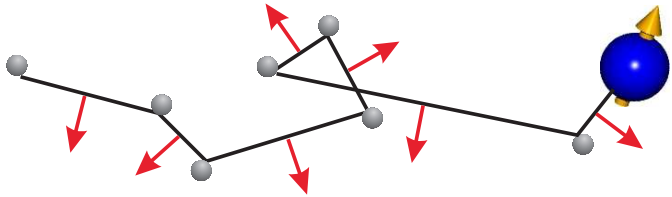

Figure 1.3: Sketch of a Boltzmannian path. Due to scattering from impurities the electron (dark sphere) undergoes a random sequence of free linear motions (solid lines) and scattering events [cf. Sec. 1.5 and Fig. 1.5]. This leads to a random component in the internal spin-orbit field (small arrows) acting on the spin and gives rise to a finite line-width of EDSR.

nal field fluctuations in different directions with respect to $\mathbf{B}_0$ which can be reduced by an optimal field configuration exploiting the interference between Rashba and Dresselhaus SOI.

1.4 Mesoscopic effects

A fascinating aspect of quantum mechanics is the manifestation of coherence effects on mesoscopic scales such as conductance corrections [Anderson79, Gorkov79, Bergmann84, Chakravarty86, Loss93] and conductance fluctuations [Altshuler85, Larkin86, Skocpol86, Lee85, Lee87, Altshuler91, Maslov93] in small nano- to micrometer sized devices.

In the following we give a brief introduction to mesoscopic fluctuations and their relation to quantum mechanical phase coherence. First, we note that the macroscopic properties of a system such as electric and thermal conductivity, magnetic susceptibility etc., are a function of the (random) microscopic structure of the system. As a consequence, these macroscopic properties are random variables as well. A meaningful description of systems by averages of these macroscopic properties is therefore based on the assumption that these properties are very narrowly distributed around their averages. This is the case when the system can be viewed as consisting of statistically independent subsystems. By the law of large numbers, the individual microscopic differences of these subsystems average out and yield well-defined macroscopic properties. The conductivity of a semiconductor sample, for instance, is rendered finite due to scattering from impurities [Drude00, Akkermans07]. These impurities are distributed randomly in each individual sample and differ in detail, e.g., in position or its electrostatic potential. Despite these differences two samples can

have equal conductivities if on average their impurity configurations have the same impurity distance and strength. These samples are called self-averaging, i.e., their measured conductivity coincides with a probability very close to 1 with each other and with the value of any other impurity configuration with the same average strength and distance. In other words, in a self-averaging system the conductivity, given as a random variable of the precise impurity positions, has vanishing variance.

The transition to the mesoscopic regime is marked by the absence of self-averaging occurring at the length scale L_ϕ [Anderson79] over which electrons maintain quantum mechanical phase coherence. For systems of linear dimension $L \approx L_\phi$ the statistical assumption of independent subsystems breaks down since quantum mechanical correlations extend over the full sample length, which for low temperatures may reach up to orders of $1...10\mu$m [Beenakker91]. As a consequence, the conductivity of mesoscopic devices shows sample-to-sample fluctuations, which, since their discovery, have triggered intense theoretical efforts [Altshuler85, Larkin86, Lee85, Lee87, Altshuler91, Loss93] and proven an important experimental tool to study coherence effects in transport processes [Skocpol86, Benoit87, Webb88, Schäfer96, Zumbühl05].

Mesoscopic fluctuations result from the interference of the many scattering trajectories the electrons can take through a disordered conductor. This can be made plausible by a qualitative argument: In the semiclassical approximation, the conductivity can be expressed in terms of the square of two Feynman [Feynman65, Chakravarty86] propagators $G \approx KK^* \approx \sum_{\gamma\gamma'} A_\gamma A_{\gamma'} e^{i(S_\gamma - S_{\gamma'})}$, where the sum runs over the set of classical paths γ in the given sample and S and A are the classical action and the fluctuation determinant of the path γ, respectively. First, we consider the average conductivity $\overline{G}$. A change in the impurity configuration leads to a change in the possible classical trajectories γ and, thus, in the associated action S_γ. Therefore, upon averaging, the phase factors $e^{i(S_\gamma - S_{\gamma'})}$ become randomized and vanish except for the diagonal terms[6] with $\gamma = \gamma'$. These diagonal contributions to $\overline{G}$ are captured by the Diffuson approximation which describes classical diffusion (cf. [Akkermans07]). Next we consider the variance $\mathrm{var}G \approx \overline{|K|^2|K|^2} - \overline{|K|^2}^2$. Here, the phase factor in $\overline{|K|^2|K|^2}$ is $\exp\{i(S_{\gamma_1} - S_{\gamma_1'} + S_{\gamma_2} - S_{\gamma_2'})\}$ where γ_1, γ_1' belong to the first Factor $|K|^2$ and γ_2, γ_2' to the second one. Again, upon averaging only terms with pairwise equal paths survive. Out of these pairs the ones with $\gamma_1 = \gamma_1'$, $\gamma_2 = \gamma_2'$ get subtracted by the second term $\overline{|K|^2}^2$. The terms with $\gamma_1 = \gamma_2'$, $\gamma_2 = \gamma_1'$, however, give rise to a finite variance. On the other hand, for paths longer than L_ϕ, in the phase difference $S_{\gamma_1} - S_{\gamma_2'}$ each term becomes

[6] Also the contribution $\gamma' = \gamma^*$, where γ^* is the time-reversed path, give rise to the weak localization contribution [Gorkov79].

random individually such that the phase factor averages to zero. Therefore, large (incoherent) samples have vanishing variance whereas phase coherence leads to fluctuations in mesoscopic samples. The interfering trajectories, responsible for these fluctuations, are also sensitive to changes in the magnetic field or the chemical potential, which alter the phases acquired by propagation through the sample with a given disorder configuration. An ergodic hypothesis [Altshuler85, Lee85] states that the variance of the fluctuations due to changes in the impurity configuration and due to changes in the magnetic field or the Fermi energy are equal[7]. This hypothesis links the experimental observation [Umbach84, Skocpol86, Benoit87, Webb88, Schäfer96, Zumbühl05] of non-periodic, reproducible fluctuations as a function of external parameters to the theoretical predictions obtained from ensemble impurity averaging.

Conductance fluctuations are moreover sensitive to the coupling to other degrees of freedom which introduce additional phases. In the presence of strong SOI, for instance, conductance fluctuation are suppressed by a factor of 1/4 [Feng89, Chandrasekhar90, Beenakker97] while a magnetic field leads to a factor of 1/2. These suppression factors are well described by the fundamental symmetry classes in random matrix theory [Imry86, Macedo92, Beenakker97] but have also been described [Feng89, Chandrasekhar90] in diagrammatic approaches.

In mesoscopic samples with SOI not only the conductance but also the spin shows qualitatively different behavior than in macroscopic samples. The spin polarization due to transport through a disordered conductor with spin-orbit scattering, for instance, is zero in an incoherent sample, but is predicted to fluctuate locally [Zyuzin90, Nazarov90] due to extrinsic spin-orbit scattering and orbital phase coherence. Similar coherence effects are found for spin-spin correlations [Jagannathan88, Zyuzin92, Lerner93], the fluctuations of the density of states in quantum corrals [Walls07] and the spin-Hall conductivity in general nano-structures [Bardarson07, Nazarov07] and chaotic quantum dots [Bardarson07, Krich08]. In Chap. 4 we investigate mesoscopic fluctuations of the spin polarization in a 2DEG with intrinsic Rashba SOI. We find that such fluctuations exist for all spin components -including the out-of-plane component perpendicular to the 2DEG which is zero in self-averaging samples. These spin fluctuations exceed in magnitude the polarization due to the MEE in self-averaging samples, and since the latter has been observed in Faraday rotation measurements [Kato04b, Kato05], are also within experimental reach.

[7] This hypothesis is based on the assumption that changing interference patterns by changing impurity positions and e.g. the magnetic field is statistically equivalent which is true for sampling sufficiently large magnetic field ranges. If the range over which the field is sweeped is not sufficiently large, non-universal, sample-specific corrections to the ergodicity hypothesis occur [Tsyplyatyev03, Mohanty02]

1.5 Diagrammatic description of disordered transport

Spin- and charge transport in systems with disorder can conveniently be described by diagrammatic techniques. In this section we give a short introduction to the relevant diagrams, Feynman rules and definitions which are used in these techniques. Comprehensive treatments are found in the relevant textbooks [Akkermans07, Rammer98].

Green functions are a calculational tool to treat a perturbation V (for instance a disorder potential) to the diagonalizable part of a system described by a Hamiltonian H. The bare and full retarded Green function G_0^R and G^R solve equations of the form $[i(\hbar)\partial/\partial t - H + (V)]G^R(\mathbf{x}, t, \mathbf{x}', t') = \delta(\mathbf{x} - \mathbf{x}')\delta(t - t')$ for $t > t'$ and $G^R = 0$ for $t < t'$. Equivalently, $G^R_{(0)}$ can be defined in terms of the time evolution operator $U(t)$ of H by $G^R_{(0)}(\mathbf{x}, t, \mathbf{x}', t') = -i\theta(t-t')\langle\mathbf{x}|U(t-t')|\mathbf{x}'\rangle$.

The associated Feynman diagrams for $G^{R/A}$ in the position/time and, for a time-independent and spatially homogeneous system, in the momentum-frequency representation, respectively, are denoted by solid lines

$$G^R_{\alpha\alpha'}(\mathbf{x}, t, \mathbf{x}', t') = \quad \mathbf{x}, t, \alpha \longleftarrow \mathbf{x}', t', \alpha' \quad \mathsf{R} \tag{1.6}$$

$$G^A_{\alpha\alpha'}(\mathbf{x}, t, \mathbf{x}', t') = \quad \mathbf{x}', t', \alpha' \longrightarrow \mathbf{x}, t, \alpha \quad \mathsf{A}$$

$$G^R_{\alpha\alpha'}(\mathbf{p}, E) = \quad \alpha \longleftarrow \mathbf{p}, E \longleftarrow \alpha' \quad \mathsf{R} \tag{1.7}$$

$$G^A_{\alpha\alpha'}(\mathbf{p}, E) = \quad \alpha' \longrightarrow \mathbf{p}, E \longrightarrow \alpha \quad \mathsf{A} \quad ,$$

where $\alpha, \alpha' = \pm 1$ denote spin indices, $\mathbf{p}$ and E momentum and energy, and $\mathbf{x}, \mathbf{x}'$ and t, t' position and time, respectively.

When charge is transported through a disordered semiconductor the charge carriers scatter from a large number (N) of impurities which are randomly distributed in the sample at positions $\mathbf{x}_i, i = 1, \ldots, N$. The scattering renders the conductivity finite by randomizing the carrier motion and determines other system properties such as the spin-electric susceptibility. The potential generated by the impurities is described by $V(\mathbf{x}) = \sum_{i=1}^{N} u(\mathbf{x} - \mathbf{x}_i)$ in a model first introduced by Edwards [Edwards58] where the individual impurity potential u is assumed to be the same at all $\mathbf{x}_i$ which are random and homogeneously distributed in over the sample[8] [cf. Fig. 1.4].

[8] Other models of disorder allow for more general potentials with a probability density

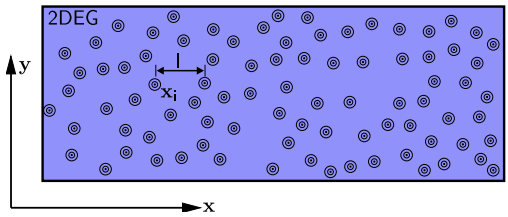

Figure 1.4: Disordered sample. Impurity positions $\mathbf{x}_i$ are randomly and homogeneously distributed over the sample with average distance l.

Observables such as the conductivity or spin-electric susceptibility are therefore random variables of the N positions $\mathbf{x}_i$. In self-averaging systems (cf. Sec.1.4) these observables are then given as an average over the distribution of the impurities which is obtained in two steps. First, the observable is expressed, e.g. by a Kubo formula, in terms of the full Green functions. Treating the disorder potential V perturbatively the full Green functions are given by the Dyson series $G = G_{(0)} + G_{(0)}VG_{(0)} + G_{(0)}VG_{(0)}VG_{(0)} + \dots$. Note that in these expression G is still a random variable of the impurity positions $\mathbf{x}_i$. In the second step, the averaged susceptibility is obtained by homogeneously averaging over the positions $\mathbf{x}_i$ of the impurities. This procedure is referred to as the impurity average or disorder average and can be quite intricate since the perturbation expansion of G contains infinitely many factors of the random potential V. Therefore exact analytical expressions for the impurity averaged observables are usually not available. Instead a class of diagrams is typically identified that yields the leading order contribution to this average in the small parameter $1/p_F l$ where l is the mean distance between impurities and p_F is the Fermi momentum.

In the following we introduce the impurity correlator, the self-energy, and the Diffuson of which disorder averages of susceptibilities and variances are composed and define their Feynman rules.

$P[V]$ given in terms of a functional P of V, but do not explicitly include the microscopic impurity potential. Averages with respect to P are denoted by overbars $\overline{\dots}$, e.g. correlation functions of the form $\overline{V(\mathbf{r}_1)V(\mathbf{r}_2)\dots}$. A simplified assumption is used in Gaussian disorder models where only the correlation function $\overline{V(\mathbf{r})V(\mathbf{r}')} \neq 0$ is assumed to be finite. The Edwards model and the Gaussian model become equivalent for short-ranged impurities.

The impurity correlator is given by

$V_2(\mathbf{p}_1, \mathbf{p}_1', \mathbf{p}_2, \mathbf{p}_2') =$ 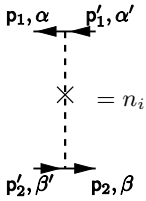

$= n_i \delta(\mathbf{p}_1 + \mathbf{p}_2 - (\mathbf{p}_1' + \mathbf{p}_2'))|u(\mathbf{p}_1 - \mathbf{p}_1')|^2 \delta_{\alpha\alpha'}\delta_{\beta\beta'},$ (1.8)

where $u(\mathbf{p})$ is the Fourier transform of $u(\mathbf{x})$ and $n_i = N/\mathcal{V}$ the impurity density (with $\mathcal{V}$ standing for the volume/area of the sample). In the case of short-ranged impurities, which will be assumed in the following, the potential $u(\mathbf{p}) = u_0$ in Eq. (1.8) becomes constant and the impurity correlator simplifies to $V_2 = (m\tau)^{-1}\delta(\mathbf{p}_1 + \mathbf{p}_2 - (\mathbf{p}_1' + \mathbf{p}_2'))\delta_{\alpha\alpha'}\delta_{\beta\beta'}$ where τ is the average time between scatterings. This is equivalent to

$$\overline{V(\mathbf{x})V(\mathbf{x}')} = \delta(\mathbf{x} - \mathbf{x}')\frac{1}{m\tau}. \tag{1.9}$$

An important quantity to partially sum sub-diagrams within larger diagrams is the full Green function $\overline{G}$ averaged over the impurity positions. The full averaged Green function is given by a Dyson equation $\overline{G} = G_{(0)} + G_{(0)}\overline{\Sigma}\overline{G}$ and is calculated by identifying the leading order irreducible diagrams [Akkermans07, Rammer98] contributing to the self-energy $\overline{\Sigma}$. In the self-consistent Born approximation and for $1/p_F l \ll 1$ the imaginary part of the self-energy is given by

$\mathrm{Im}\overline{\Sigma}^{R/A}_{\alpha,\alpha'}(\mathbf{p}, E_F) = \mathrm{Im}$ 

$=$ (1.10)

$$= \mathrm{Im}\, n_i \int \frac{d^2p'}{(2\pi)^2}|u(\mathbf{p} - \mathbf{p}')|^2 \overline{G}^{R/A}_{\alpha\alpha'}(\mathbf{p}', E_F) = \mp\frac{1}{2\tau}\delta_{\alpha\alpha'},$$

where the last equality is true for a potential due to short-ranged scatterers with the property Eq. (1.9)[9]. The averaged Green function $\overline{G}(\mathbf{x}, \mathbf{x}') = G_{(0)}(\mathbf{x}, \mathbf{x}')e^{-|\mathbf{x}-\mathbf{x}'|/2l}$ describes the transition amplitude for a collisionless propagation from $\mathbf{x}$ to $\mathbf{x}'$ and therefore decays exponentially as a function of the spatial variable on the scale of the mean free path l.

[9] Eq. (1.10) remains valid in the presence of other terms in H than the kinetic energy $p^2/2m$ such as SOI, magnetic fields, etc., as long as the typical energy scales of these terms evaluated at the Fermi momentum are much smaller than the Fermi energy E_F.

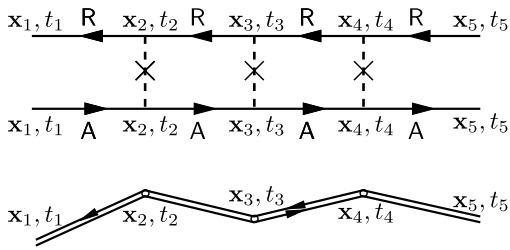

Figure 1.5: Relation of the Diffuson to classical diffusion. Upper panel: Term in the infinite series of ladder diagrams in the Diffuson. The diagram describes the probability to reach $\mathbf{x}_1$ from $\mathbf{x}_5$ after a sequence of free linear motions and scattering from impurities at the intermediate positions $\mathbf{x}_4 \dots \mathbf{x}_2$. The upper Green function between two rungs of the ladder corresponds to a factor $G^R(\mathbf{x}_i, t_i, \mathbf{x}_{i+1}, t_{i+1},)$ which (for $t_i > t_{i+1}$) equals the quantum mechanical amplitude $-i\langle \mathbf{x}_i | U(t_i - t_{i+1}) | \mathbf{x}_{i+1} \rangle$ for propagation from $\mathbf{x}_{i+1}$ to $\mathbf{x}_i$. Similarly, the lower segment yields the complex conjugate of this amplitude. Therefore, one segment of the ladder between two rungs corresponds to the classical probability for free motion from $\mathbf{x}_{i+1}$ to $\mathbf{x}_i$. Summation over the number of segments and integration over all intermediate points describes therefore a classical diffusion process. Lower panel: Real-time trajectory as described by the ladder diagram.

In the remainder of this text we identify $G^{R/A} = \overline{G}^{R/A}$ if no confusion is possible implying partial summation of all impurity correlators connecting only to one single Green function.

More complex diagrams, e.g. the spin susceptibility in Eq. (1.18) (see below) contain a larger number of Green functions which become correlated in the procedure of averaging over impurity positions. The impurity average of a product of two Green functions, for instance, is not equal to the product of the individually averaged Green functions. To understand the origin of this inequality we consider the modulus square $P(\mathbf{x}, t|\mathbf{x}', t')$ of the quantum mechanical transition amplitude $\langle \mathbf{x}|U(t-t')|\mathbf{x}'\rangle$ for a particle in a disordered system. For times $t > t'$ this quantity is given by the impurity average $P(\mathbf{x}, t|\mathbf{x}', t') = \overline{G^R(\mathbf{x}, t, \mathbf{x}', t')G^A(\mathbf{x}', t', \mathbf{x}, t)}$ of two Green functions. P can thus be understood as the conditional probability to find the particle at $\mathbf{x}$ at time t given that it was at $\mathbf{x}'$ at time t'. To leading order in $1/p_F l$ the average $P(\mathbf{x}, t|\mathbf{x}', t')$ is given by two terms. The first term $\overline{G}^R(\mathbf{x}, t, \mathbf{x}', t')\overline{G}^A(\mathbf{x}', t', \mathbf{x}, t) \propto e^{-|\mathbf{x}-\mathbf{x}'|/l}$ is the classical probability for a collisionless propagation from $\mathbf{x}$ to $\mathbf{x}'$. The

second term is the Diffuson $D(\mathbf{x}, t, \mathbf{x}', t')$ which is the summed probability to reach $\mathbf{x}$ from $\mathbf{x}'$ after a sequence of scattering events. The Diffuson $D(\mathbf{x}, \mathbf{x}')$ is, therefore, interpreted as the classical probability for diffusion from $\mathbf{x}'$ to $\mathbf{x}$ [cf. Fig. 1.5 for this interpretation][10]. Moreover, a sub-leading contribution to P, relevant at $\mathbf{x} \approx \mathbf{x}'$, exists, which contains the Cooperon C [Akkermans07,Rammer98] and can be linked to quantum mechanical interference processes [Akkermans07,Rammer98] between clockwise and anticlockwise propagation through closed diffusive loops.

Here we give the Diffuson in the position representation to further familiarize the Feynman rules and to motivate the Hikami notation used in Chap. 4. The Diffuson is determined by the diagrammatic equation

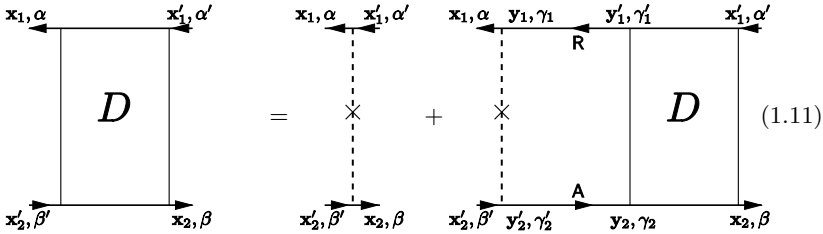

(1.11)

which when reiterated becomes an infinite sum of diagrams with non-crossing impurity lines between the upper and the lower Green functions, so-called ladder diagrams. Using the Feynman rules in Eq. (1.6) and Eq. (1.8) for the impurity correlator and the Green functions, respectively, the analytical form of the Diffuson (Eq. (1.11)) is found as

$$\begin{aligned} D^{\alpha\alpha'}_{\beta\beta'}(\mathbf{x}_1, \mathbf{x}_1', \mathbf{x}_2, \mathbf{x}_2'|E, \omega) &= \frac{1}{m\tau}\delta(\mathbf{x}_1 - \mathbf{x}_1')\delta(\mathbf{x}_2 - \mathbf{x}_2')\delta(\mathbf{x}_1 - \mathbf{x}_2')\delta_{\alpha\alpha'}\delta_{\beta\beta'} \\ &+ \frac{1}{m\tau}\int d^2y_1' d^2y_2 \delta_{\alpha\gamma_1}\delta_{\beta'\gamma_2'} \\ &\times G^R_{\gamma_1,\gamma_1'}(\mathbf{y}_1, \mathbf{y}_1', E+\omega) G^A_{\gamma_2,\gamma_2'}(\mathbf{y}_2, \mathbf{y}_2', E) D^{\gamma_1'\alpha'}_{\beta,\gamma_2}(\mathbf{y}_1', \mathbf{x}_1', \mathbf{x}_2, \mathbf{y}_2). \end{aligned} \tag{1.12}$$

The equation can be simplified by the ansatz

$$D^{\alpha\alpha'}_{\beta\beta'}(\mathbf{x}_1, \mathbf{x}_1', \mathbf{x}_2, \mathbf{x}_2') = D^{\mu\nu}(\mathbf{x}_1, \mathbf{x}_1')\delta(\mathbf{x}_1 - \mathbf{x}_2')\delta(\mathbf{x}_1 - \mathbf{x}_2')\sigma^{\mu}_{\alpha\beta'}\sigma^{\nu}_{\beta\alpha'}. \tag{1.13}$$

[10] Indeed, for free spin-less particles in a disordered conductor the Diffuson has the same functional form as the Wiener measure describing Brownian motion [Chaichian01,Rammer98]. In Appendix C a partial differential equation, Eq. (C.6) for the spin density $\boldsymbol{\rho}(\mathbf{r})$ is derived starting from the expression Eq. (1.14) for the Diffuson. This equation has the form $[i\omega - D\Delta]\boldsymbol{\rho}(\mathbf{r}) =$ rhs of a diffusion or heat flow equation where rhs stands for additional precession terms due to SOI.

where $\sigma^i, i = 1,2,3$ are the Pauli matrices ($\sigma^0 = \mathbb{1}_2$) and summation over $\mu,\nu = 0,1,2,3$ is implied. Inserting Eq. (1.13) into Eq. (1.11) yields

$$D^{\mu\nu}(\mathbf{x},\mathbf{x}') = \frac{1}{2m\tau}\delta^{\mu\nu}\delta(\mathbf{x}-\mathbf{x}') + \int d^2y X^{\mu\rho}(\mathbf{x},\mathbf{y}) D^{\rho\nu}(\mathbf{y},\mathbf{x}') \tag{1.14}$$

which is a 4×4 matrix and where the integral kernel $X^{\mu\rho}(\mathbf{x},\mathbf{y})$ is given by

$$X^{\mu\rho}(\mathbf{x},\mathbf{y}) = \frac{1}{2m\tau}\mathrm{tr}_S\left\{\sigma^\mu G^R(\mathbf{x},\mathbf{y})\sigma^\rho G^A(\mathbf{y},\mathbf{x})\right\}. \tag{1.15}$$

and tr_S is the trace over spin. The definition of D in Eq. (1.13) is represented by a new diagram

$D^{\mu\nu}(\mathbf{x},\mathbf{x}') =$ 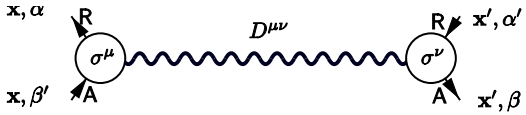

(1.16)

which makes explicit the dependence of D on two spatial arguments only. Due to the property $\overline{V(\mathbf{x})V(\mathbf{x}')} \propto \delta(\mathbf{x}-\mathbf{x}')$ of the impurity correlator the upper and lower position arguments on the left and on the right side can be set equal. An interpretation of the Diffuson in the position representation is given in Fig. 1.5. In view of the short range of the averaged Green functions $\overline{G^{R,A}}(\mathbf{x},\mathbf{x}') \propto e^{-|\mathbf{x}-\mathbf{x}'|/2l}$, one would expect the Diffuson to vanish if its arguments are separated by more than a mean free path. However, concatenating infinitely many $G^{R/A}$s , $D(\mathbf{x},\mathbf{x}')$ remains finite for $|\mathbf{x}-\mathbf{x}'| > l$. This long range is a property of diffusion with multiple scatterings and is represented by the long wavy line in Eq. (1.16). The diagrammatic notation of Eq. (1.16) is due to [Hikami81].

In Sec. C a diffusion equation for the spin density is derived using Eq. (1.14) as a starting point.

1.6 Kubo formula

Experiments in condensed matter physics often probe the response of observables of a physical system such as current or magnetization to a weak perturbation. This procedure is mapped on a theoretical description in the framework of linear response theory.

The response $s^i(\omega) = \langle\sigma^i\rangle(\omega)$ of the spin σ^i to a (spatially constant) electric field $\mathbf{E}(\omega) = -i\omega\mathbf{A}(\omega)/c$ with frequency ω is given by

$$s^i(\omega) = -i\int\frac{dE}{2\pi}\int\frac{d^2p}{(2\pi)^2}\mathrm{tr}_S\{\sigma^i G^<(\mathbf{p},E,\mathbf{p},E+\omega)\} \tag{1.17}$$

in terms of the lesser Green function $G^< = [G^K - (G^R - G^A)]/2$. Here, G^K is the Keldysh Green function [Rammer86] and G^R and G^A denote the retarded and advanced Green function, respectively, and the the trace tr_S is over spin states. Expanding the $G^<$ to linear order in the electric field yields the Kubo formula

$$\begin{aligned}\chi^{ij}(\omega) = \frac{-e}{2\pi\omega}\int dE[f(E+\omega)-f(E)]\int \frac{d^2p}{(2\pi)^2}\mathrm{tr}_S\left\{\sigma^i G^R_{E+\omega}(\mathbf{p})v_j G^A_E(\mathbf{p})\right\}\\ + f(E)\int \frac{d^2p}{(2\pi)^2}\mathrm{tr}_S\left\{\sigma^i G^R_{E+\omega}(\mathbf{p})v_j G^R_E(\mathbf{p})\right\}\\ - f(E)\int \frac{d^2p}{(2\pi)^2}\mathrm{tr}_S\left\{\sigma^i G^A_E(\mathbf{p})v_j G^A_{E-\omega}(\mathbf{p})\right\}, \qquad (1.18)\end{aligned}$$

where v_j is the velocity operator and f the Fermi distribution function. Eq. (1.18) is the starting point[11] for the diagrammatic calculation of the disorder average of the spin polarization $s^i = \chi^{ij}E_j$, $i = 1,2,3$ given in terms of a linear susceptibility χ^{ij}, and its variance $\overline{(\delta\chi^{ij})^2}$, where $\delta\chi^{ij} = \chi^{ij} - \overline{\chi^{ij}}$ and the overbar denotes impurity averaging.

1.7 Outline

In Chap. 2 we investigate EDSR in disordered semiconductors using a diagrammatic approach. We use a microscopic model of linear Rashba SOI and δ-correlated impurities to demonstrate the viability of EDSR in such a system and show that the resonance acquires a line-shape determined by disorder and SOI. In Sec. 2.2 we show that the spin dynamics due to EDSR are captured by a phenomenological model to the lowest order in the SOI strength. This model, however, fails to describe the generation of spin currents due to EDSR which we infer from the diagrammatic approach in higher order in the SOI strength in Sec. 2.3.

The presence of disorder limits the amount of spin polarization that can be achieved by EDSR. In Chap. 3 we show that such limitations can be overcome by exploiting the interference of linear Rashba and Dresselhaus SOI. Using the equation of motion for the spin we relate spin polarization and spin current and give a geometric interpretation of the spin current in terms polarization components [cf. Sec. 3.3].

While the orbital motion in EDSR is well described by classical diffusion, in in Chap. 4 we consider effects of orbital phase coherence on the spin dynamics

[11] The two last terms in Eq. (1.18) contribute negligibly to s^i if averaged over impurities, but are retained here, since their contribution to the fluctuations has to be discussed later, see footnote to Eq. (4.2).

and investigate mesoscopic fluctuations of the spin polarization generated by the magneto-electric effect. We thereby focus on the spin-electric susceptibility which characterizes the polarization due to the MEE and calculate its variance averaged over disorder as a function of SOI strength, magnetic field and difference in gate voltages.

2

Electric dipole-induced spin resonance in disordered semiconductors

In this chapter, we present a theoretical study of EDSR for a two-dimensional electron gas in the presence of disorder where random impurities not only determine the electric resistance but also the spin dynamics via the Rashba SOI. Considering a specific geometry with the electric and magnetic fields parallel and in-plane, we show that the magnetization develops an out-of - plane component at resonance which survives the presence of disorder. These results are derived in a diagrammatic approach with the dominant effects coming from the spin vertex correction, and the optimal parameter regime for observation is identified.

2.1 Electric-dipole induced spin resonance

The field of spintronics [Awschalom02, Zutic04] focusses on the interplay between spin and charge degrees of freedom of the electron. The relativistic effects responsible for the coupling between spin and orbital motion can be strongly enhanced in solids due to band structure effects, with zinc-blend III-V semiconductors showing a particularly strong spin-orbit interaction (SOI) resulting in zero-field spin splittings. For instance, the bulk inversion asymmetry gives rise to Dresselhaus SOI [Dresselhaus55], while structural inversion asymmetry occurring in heterostructures gives rise to Rashba SOI [Rashba60]. The strength of such SOIs can be varied over a wide range which offers the advantage to control the magnetic moments with electric fields. A well-known and particularly powerful way of manipulating spins in such structures is electric dipole induced spin resonance (EDSR) [Bell62, Dobrowolska84, Kato04a, Rashba03b,Schulte05,Wilamowski07,Duckheim06,Duckheim07,Meier07] where the radiofrequency (rf) fields coherently driving the spins are electric, and not magnetic like in standard paramagnetic resonance. The advent of materials with tailored SOI [Awschalom02] has sparked intense interest in a va-

riety of spin orbit effects such as the spin-Hall effect [D'yakonov71, Sinova04, Hirsch99, Kato04c, Wunderlich05, Sih05, Valenzuela06, Stern06], zitterbewegung [Schliemann05], spin-based quantum information processing [Awschalom02, Loss98], and, in particular, EDSR [Bell62, Dobrowolska84, Kato04a, Rashba03b, Schulte05, Wilamowski07, Duckheim06, Duckheim07, Meier07], which is the focus of this work.

Experimental indication for electric dipole transitions was earliest reported for conduction band and donor bound electron spins in cavity resonance experiments with InSb [Bell62] and $Cd_{1-x}Mn_xSe$ [Dobrowolska84], respectively. In these experiments the resonance signal increased upon positioning the sample in the cavity away from the maximum of the magnetic field (node of the electric field), thus demonstrating electrical instead of magnetic coupling to the spin. More recently, EDSR was detected optically [Kato04a, Meier07] and in cavity experiments [Schulte05, Wilamowski07] for conduction band electrons in semiconductors. EDSR was also described theoretically for 2DEGs [Rashba03b], 2D hole gases [Bulaev07] and for single electrons in quantum dots [Golovach06] where it was recently measured using spin blockade in a double quantum dot [Nowack07].

We consider a semiconductor heterostructure forming a two-dimensional electron gas (2DEG). Inversion asymmetry of the structure, due to an asymmetric confinement potential, gives rise [Rashba60, Bychkov84] to the Rashba SOI which is linear in momentum and provides an effective internal magnetic field about which the spin precesses. In realistic 2DEGs, moreover, disorder leads to momentum scattering which is responsible not only for the finite electric resistance but also for spin relaxation due the randomization of the internal field [D'yakonov72, Dyakonov84]. The interplay of SOI and the orbital motion can be quite subtle as it has been appreciated for instance in the context of the spin-Hall effect where universal spin currents predicted in clean systems [Sinova04] were found to be cancelled in the presence of disorder [Inoue04, Mishchenko04, Chalaev05, Dimitrova05], which, technically speaking, results from an unusual cancellation of vertex corrections. Spin currents in these systems are dominated by other (extrinsic) effects [D'yakonov71, Engel06, Engel05]. Similar concerns, for instance, apply to conclusions reached for EDSR in clean systems [Rashba03b]. Therefore the role of disorder in EDSR needs to be examined carefully. In doing so in this chapter, we show that EDSR survives impurity scattering but acquires a line shape that is determined by disorder and SOI.

We consider a geometry as shown in Fig. 2.1, where the electric rf field and the static external magnetic field are parallel and both in the plane of the 2DEG. At resonance, the magnetization acquires a non-zero out-of-plane component. This we show first for a clean 2DEG by deriving an effective Bloch

equation. Turning then to 2DEGs with disorder we treat the electric rf field in linear response and obtain for the magnetization a Lorentzian resonance whose width is given by a generalized D'yakonov-Perel spin relaxation rate. In addition, we find a shift of the resonance due to disorder and SOI which gives rise to an effective g-factor that depends on the magnetic field. Using a standard diagrammatic approach to treat SOI and disorder systematically, we find that it is the spin vertex correction (coming from disorder) that leads to the resonance, in stark contrast to zero frequencies where the spin vertex vanishes [Edelstein90]. Assuming realistic system parameters we identify the most promising regime for the experimental observation of EDSR. The 2DEG consists of non-interacting electrons of mass m and charge e which are subject to a random impurity potential V. In addition, we allow for a general SOI $\mathbf{\Omega}(\mathbf{p})\cdot\boldsymbol{\sigma} = \Omega_{ij}p_j\sigma^i$ linear in momentum $\mathbf{p}$ and a static external magnetic field $\mathbf{B}_0$ applied in-plane, as well as a time-dependent electric field $\mathbf{E}(t)$ applied as a bias along $\mathbf{B}_0$, see Fig. 2.1. The Hamiltonian for this system reads

$$H = \frac{1}{2m}\left(\mathbf{p} - \frac{e}{c}\mathbf{A}\right)^2 + \mathbf{\Omega}(\mathbf{p})\cdot\boldsymbol{\sigma} + (\mathbf{b}_0 + \mathbf{b}_1(t))\cdot\boldsymbol{\sigma} + V, \tag{2.1}$$

where $\mathbf{b}_1(t) = -\frac{e}{c}\mathbf{\Omega}\left(\mathbf{A}(t)\right)$ is the rf part of the internal 'magnetic' field induced by the electric field via SOI, and $\mathbf{A}(t) = -c\int^t dt'\mathbf{E}(t')$ is the associated vector potential, c being the speed of light. The Zeeman term contains $\boldsymbol{b}_0 = g\mu_B\mathbf{B}_0/2$ and the Pauli matrices σ^i, $i = 1,2,3$ ($\sigma^0 = \mathbb{1}$), while $\mathbf{\Omega}(\mathbf{p})$ is the 'zero-field spin splitting' due to the internal SOI field.

We show now that for the described setup the dynamics of the electron spin exhibits resonant behavior (EDSR) generated by the electric rf field $\mathbf{E}(t)$. Starting with the simple case of no disorder ($V = 0$), we derive a Bloch equation for the spin dynamics (for weak SOI), from which the EDSR property immediately follows.

We begin by noting that the density matrix $\rho(t)$ is diagonal in momentum space, and its elements can be expanded in the spin basis as $\rho(\mathbf{p},t) = \sum_{\nu=0}^{3} s^\nu(\mathbf{p},t)\sigma^\nu$, where $\sigma^0 = 1$. The expectation value of the spin is then $\langle\sigma^i(t)\rangle = \int d^2p\ s^i(\mathbf{p},t)/(2\pi)^2 \equiv S^i(t)$, where $\int s^0 d^2p/(2\pi)^2 = 1$ due to normalization. In momentum space the symmetry is broken by the small SOI term such that the coefficients decompose into an isotropic and a small anisotropic part, $s^i(\mathbf{p},t) = \overline{s}^i(p,t) + \Delta s^i(\mathbf{p},t)$. Averaging the von Neumann equation for $\rho(\mathbf{p},t)$ over directions of $\mathbf{p}$ we obtain

$$\dot{\overline{\mathbf{s}}}(p,t) = \frac{2}{\hbar}(\mathbf{b}_0 + \mathbf{b}_1(t)) \times \overline{\mathbf{s}}(p,t), \tag{2.2}$$

where we have dropped the angular average of $\mathbf{\Omega}(\mathbf{p}) \times (\overline{\mathbf{s}}(p,t) + \Delta\mathbf{s}(\mathbf{p},t))$ since it is higher order in the SOI. Eq. (2.2) is now recognized as a Bloch equation describing spin resonance.

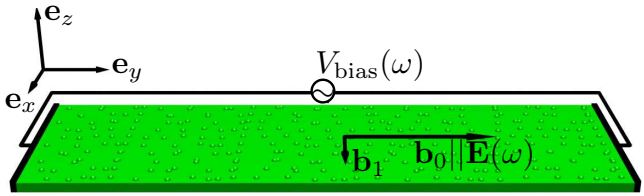

Figure 2.1: Geometry of the setup with the disordered 2DEG in the xy-plane. An oscillating bias $V_{\rm bias}(\omega)$ generates an electric field ($\mathbf{E}(\omega)$) parallel to the magnetic field $\mathbf{b}_0 = g\mu_B\mathbf{B}_0/2$ along the y-axis. At resonance an out-of-plane magnetization $S^3(\omega)$ is generated.

Indeed, specifying henceforth to Rashba SOI $\mathbf{\Omega}(\mathbf{p}) = \mathbf{\Omega}_R(\mathbf{p}) = \alpha\mathbf{p}\times\mathbf{e}_z$, where $\mathbf{e}_z$ is a unit vector along the confinement axis, and taking $\mathbf{E}$ in the plane along $\mathbf{b}_0||\mathbf{e}_y$ results in the standard resonance setup [Cohen-Tannoudji77] with an oscillating internal field $\mathbf{b}_1(t) \propto \mathbf{E}\times\mathbf{e}_z \perp \mathbf{B}_0$. Tuning $\mathbf{E}(\omega)$ to resonance, i. e. $\omega = \omega_L$, with $\omega_L = g\mu_B B_0$ being the Larmor frequency, the spin starts to precess around the x-axis (in the yz-plane) with a Rabi frequency given by $\omega_R = b_1/\hbar = eE\alpha/\hbar\omega_L$ (see Appendix A.4 for an estimate).

Having established the existence of EDSR for the clean system we turn now to the realistic case of a disordered 2DEG. For this we assume a dilute random distribution of short- ranged scatterers with the disorder average $\overline{V(\mathbf{x})V(\mathbf{x}')} = (m\tau)^{-1}\delta(\mathbf{x}-\mathbf{x}')$ taken to be δ - correlated and proportional to the mean free time τ between elastic scattering events. For $A = 0$ and $V = 0$ the eigenenergies of H become $E_s(\mathbf{p}) = p^2/2m + s\ b_{\rm eff}(\mathbf{p})$, with $s = \pm 1$ and the effective magnetic field $\mathbf{b}_{\rm eff}(\mathbf{p}) = \mathbf{\Omega}_R(\mathbf{p}) + \mathbf{b}_0$. In the corresponding retarded (advanced) Green functions

$$G^{R/A}(\mathbf{p}, E) = \frac{1}{2}\sum_{s=\pm 1}\frac{1 + s\hat{\mathbf{b}}_{\rm eff}(\mathbf{p})\cdot\boldsymbol{\sigma}}{E - E_s(\mathbf{p}) \pm i/2\tau}, \tag{2.3}$$

where $\hat{\mathbf{b}}_{\rm eff} = \mathbf{b}_{\rm eff}/b_{\rm eff}$, the disorder manifests itself as a finite self-energy term $i/2\tau$ generated by the disorder average [1].

We turn now to the explicit calculation of the magnetization $S^i(\omega)$ (per unit area) at frequency ω, induced by $\mathbf{E}(\omega)$. Working in the linear response

[1] In the self-consistent Born approximation τ is independent of momentum due to the short range nature of V. We have also checked that a renormalization of the Zeeman splitting, i. e. matrix valued corrections, are of order b_0/E_F and can be neglected as the Fermi energy E_F is taken to be the largest energy scale. Thus, the averaged Green function is given by (2.3) with the standard isotropic and spin independent term $i/2\tau$ [Rammer98].

regime we start from the Kubo formula for $S^i(\omega)$ averaged over disorder and evaluate it using standard diagrammatic techniques. In Ref. [Edelstein90] such a calculation was performed for the static ($\omega = 0$) and zero field ($\mathbf{B}_0 = 0$) case, where, as a simplifying feature, the spin vertex correction turned out to vanish. For finite frequencies, however, this is no longer the case, and, as we shall sketch now, it is this vertex correction which leads to a finite out-of-plane magnetization $S^z(\omega)$ at resonance $\omega = \omega_L$. To be specific, for $\hbar\omega \ll E_F$ $S^i(\omega)$ becomes

$$S^i(\omega) = \frac{-eE_j(\omega)}{2\pi} \mathrm{Tr}\left\{ G^A(q, E_F)\ \Sigma^i(\omega)\ G^R(q, E_F + \omega)\ v_j \right\}, \tag{2.4}$$

where summation over repeated indices is implied. Here, the velocity operator $v_j = i/\hbar[H, x_j] = p_j/m + \Omega_{kj}\sigma^k$ contains a spin-dependent term, and $\mathrm{Tr} \to \int d^2q/(2\pi)^2\,\mathrm{tr}$ denotes momentum integration and tracing over spin states. In Eq.(2.4) we introduced the impurity renormalized spin vertex $\Sigma(\omega)$ determined by the diagrammatic equation Fig. 2.2, where the cross denotes the insertion

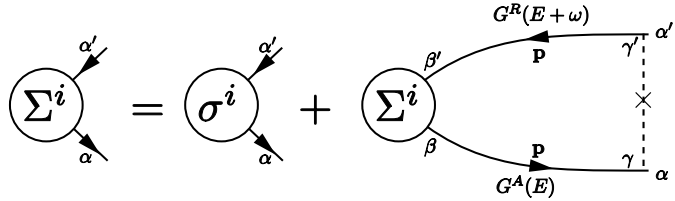

Figure 2.2: Renormalized spin vertex

of a factor $1/m\tau$. Analytically this can be written as

$$\Sigma^i_{\alpha\alpha'}(\omega) = \sigma^i_{\alpha\alpha'} + \frac{1}{m\tau}\int \frac{d^2p}{(2\pi)^2}\delta_{\alpha\gamma}G^A_{\gamma\beta}(\mathbf{p})\Sigma^i_{\beta\beta'}(\omega)G^R_{\beta'\gamma'}(\mathbf{p})\delta_{\gamma'\alpha'}. \tag{2.5}$$

The class of diagrams included in Σ corresponds to the ladder approximation, the leading order contribution in $1/p_F l$. Thus, weak localization corrections [Edelstein95, Chalaev05], being higher order in $1/p_F l$, are not considered here.

For further evaluation of Eq. (2.4) we introduce the spin-spin ($X^{\mu\nu}$) and the spin-momentum ($Y^{\mu j}$) terms, $\mu, \nu = 0, 1, 2, 3$ resulting from the spin and the normal part of v_j, respectively,

$$\begin{aligned} X^{\mu\nu}(\omega) &= \frac{1}{2m\tau}\int \frac{d^2p}{(2\pi)^2}\mathrm{tr}\left\{ G^A(\mathbf{p}, E_F)\ \sigma^\mu\ G^R(\mathbf{p}, E_F + \hbar\omega)\ \sigma^\nu \right\} \\ Y^{\mu j}(\omega) &= \frac{1}{2m\tau}\int \frac{d^2p}{(2\pi)^2}\mathrm{tr}\left\{ G^A(\mathbf{p}, E_F)\ \sigma^\mu\ G^R(\mathbf{p}, E_F + \hbar\omega)\ \frac{p_j}{m} \right\}. \end{aligned} \tag{2.6}$$

The renormalized spin vertex is expanded in terms of Pauli matrices, $\Sigma^i(\omega) = \Sigma^{i\nu}(\omega)\sigma^\nu$. Using the identity $\delta^{\alpha\alpha'}\delta^{\beta\beta'} = 1/2\sum_{\mu=0}^{3}\sigma^\mu_{\alpha\beta}\sigma^\mu_{\beta'\alpha'}$ the diagrammatic equation in Fig. 2.2 factorizes to

$$\Sigma^{\mu\nu}(\omega) = \delta^{\mu\nu} + \Sigma^{\mu\rho}(\omega)X^{\rho\nu}(\omega) \tag{2.7}$$

and can be solved. The matrix elements of the vertex correction are obtained in the form $\Sigma(\omega) = (\mathbf{1} - X(\omega))^{-1}$. With this result we then obtain from Eq. (2.4) for the magnetization

$$S^i(\omega) = \frac{-eE_j(\omega)m\tau}{\pi\hbar^2}\Sigma^{i\mu}(\omega)\left(\alpha X^{\mu\nu}(\omega)\epsilon_{\nu j3} + Y^{\mu j}(\omega)\right), \tag{2.8}$$

where ϵ_{ijk} is the Levy-Civita tensor. Thus, $S^i(\omega)$ is expressed in terms of the 4×4-matrices Y, X, and Σ, which we proceed to evaluate for two limiting cases, first for $\mathbf{b}_0 = 0$, and then for $b_0 \gg \alpha p_F$.

First we consider the simpler case without magnetic field, i.e. $\mathbf{B}_0 = 0$. Performing the integrals in Eq. (2.6) we find $X^{00}(\omega) = 1/\lambda$ and $X^{33}(\omega) = \lambda/(\lambda^2 + x^2)$, while the in-plane components are equal, $X^{11} = X^{22} = (X^{00} + X^{33})/2$[2]. Here, we introduced $\lambda(\omega) = 1 - i\omega\tau$, and the dimensionless parameter $x = 2p_F\alpha\tau/\hbar$ which is a measures of the precession angle around the internal field $2p_F\alpha/g\mu_B$ between scatterings. The off-diagonal components $X^{\mu\nu}$ vanish so that the spin vertex follows simply as $\Sigma^{\mu\mu} = (1 - X^{\mu\mu})^{-1}$. The spin-momentum matrix is found as $Y^{\mu j} = -\alpha\epsilon_{\mu j3}/\lambda$. Hence, the magnetization becomes

$$S^i(\omega) = \frac{eE_j(\omega)m\tau\alpha}{\pi\hbar^2}\epsilon_{\mu j3}\left[\delta^{i\mu} - \Sigma^{i\mu}(\omega)\left(1 - \frac{1}{\lambda}\right)\right]. \tag{2.9}$$

Thus, since the spin vertex is diagonal for $\mathbf{B}_0 = 0$, we see that $\mathbf{S}(\omega)$ lies in-plane and perpendicular to $\mathbf{E}(\omega)$, i.e. $S^3(\omega)$ vanishes identically for all ω in this case. Further, for $\omega \to 0$ the factor $1 - 1/\lambda$ vanishes and thus the spin vertex $\Sigma^{i\mu}(0)$ drops out from Eq. (2.9) and the result of [Edelstein90] is recovered. [Below we will see that Eq. (2.9) remains valid also for finite $\mathbf{B}_0$ but with a different $\Sigma^{i\mu}(\omega)$ which is then no longer diagonal (see Eq. (2.10) below).]

Next we consider the opposite case of a magnetic field $\mathbf{B}_0$ that is large compared to the internal SOI field. We characterize this regime by the small expansion parameter $a = \alpha p_F/2b_0 = x/2\omega_L\tau \ll 1$, being the ratio of precession angles around the internal and external magnetic fields, resp., between

[2] These results have already been obtained in [Chalaev05] in the evaluation of the spin Hall conductivity.

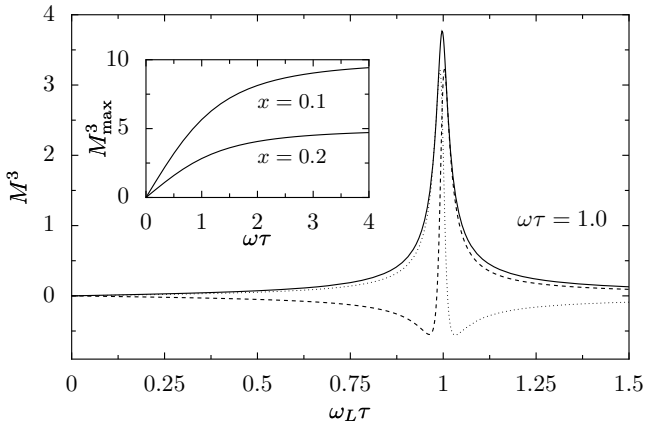

Figure 2.3: Reduced magnetization $M^3 = x(1-1/\lambda)\Sigma^{31}$ (cf. Eqs.(2.9), (2.12)) plotted as a function of the Larmor frequency $\omega_L = g\mu_B B_0$, with resonance peak at $\omega_L = \omega$ of width Γ given in Eq. (2.13). Modulus (full line), real (dashed) and imaginary part (dotted) are shown for $\omega\tau = 1$ and $x = 0.15$. Inset: Peak height of M^3 at resonance as function of $\omega\tau$ for $x = 0.2$ and $x = 0.1$.

scatterings. The field $\mathbf{B}_0$ leads to an equilibrium in-plane polarization[3], which, as we shall see, is dynamically modulated by the electric rf field $\mathbf{E}(\omega)$, giving eventually rise to an EDSR response.

With both, the internal and external magnetic fields present, the dispersion relation $E_s(\mathbf{p})$ is no longer isotropic as b_{eff} depends on the direction of $\mathbf{p}$. This complicates the momentum integrations considerably, and as a further complication, the matrices X, Y, and Σ become off-diagonal through the additional spin terms in X and Y. Fortunately, for $a \ll 1$ analytical progress is still possible, and $\Sigma(\omega)$ can be evaluated explicitly as we outline in Sec. A.1.

[3]Note that in the Kubo formula the equilibrium polarization due to $\mathbf{B}_0$ is only indirectly accounted for since Eq.(2.4) characterizes the *deviation* from equilibrium in response to the electric bias.

As a result, we obtain for the spin vertex correction

$$\Sigma(\omega) = \begin{pmatrix} \frac{\lambda}{\lambda-1} & 0 & 0 & 0 \\ 0 & \frac{\lambda^2+(\omega_L\tau)^2-\lambda}{\tau^2(\omega_L^2-\omega^2)+x^2\gamma} & 0 & \frac{\omega_L\tau}{\tau^2(\omega_L^2-\omega^2)+x^2\gamma} \\ 0 & 0 & \frac{\lambda}{\lambda-1+x^2\gamma_{22}} & 0 \\ 0 & \frac{-\omega_L\tau}{\tau^2(\omega_L^2-\omega^2)+x^2\gamma} & 0 & \frac{\lambda^2+(\omega_L\tau)^2-\lambda}{\tau^2(\omega_L^2-\omega^2)+x^2\gamma} \end{pmatrix}, \quad (2.10)$$

where $\gamma_{22} = 1/2\lambda(\lambda^2+y^2)$ and we have neglected terms of order $\mathcal{O}(x^2)$ in the numerators of $\Sigma^{\mu\nu}$. The imaginary part of the complex function

$$\gamma(\omega) = \frac{3(\lambda-1)\lambda^3 - (\omega_L\tau)^2\lambda(6\lambda-1) - (\omega_L\tau)^4}{2\lambda(\lambda^2+(\omega_L\tau)^2)^2} \quad (2.11)$$

characterizes the line-width induced by the impurity scattering via the SOI, as described below. The spin-momentum term keeps the same form as for $\mathbf{B}_0 = 0$, i.e. $Y^{\mu j} = -\alpha\epsilon_{\mu j 3}/\lambda$. The magnetization $S^i(\omega)$ is then again given by Eq. (2.9) but now with above spin vertex (2.10). Accordingly, the out-of-plane component S^3 is proportional to the reduced magnetization $M^3 \equiv x\Sigma^{31}(1-1/\lambda)$ which is plotted in Fig. 2.3 as function of the Larmor frequency ω_L, exhibiting a pronounced peak at the resonance $\omega_L = \omega$ (up to a small shift, see below). This clearly shows that the EDSR resonance found in the clean case survives weak disorder, and, technically speaking, stems from the spin vertex correction.

Let us now analyze the line-shape of the peaks close to the two resonances $\pm\omega_L$ in more detail, i.e. for $|\omega_L \pm \omega| \gg |\omega_L \mp \omega|$. In this case and to order x^2 Eq. (2.9) can be rewritten as a sum of two Lorentzians, with the transverse components ($i = 1, 3$) becoming

$$S^i(\omega) = \frac{eE_y(\omega)m\alpha}{2\pi\hbar^2}\frac{\omega_i\tau}{1-i\omega\tau} \times \left(\frac{1}{\omega_L - \omega + \delta\omega - i\Gamma} + \frac{1}{\omega_L + \omega - \delta\omega + i\Gamma}\right), \quad (2.12)$$

where $\omega_1 = \omega_L$ and $\omega_3 = i\omega$, resp. Eq. (2.12) is the main result of this work. Here, Γ is the line-width of the resonance peak and is explicitly given by the imaginary part of the damping function (2.11) evaluated at the (bare) resonance,

$$\Gamma = \frac{x^2}{2\omega_L\tau^2}\,\mathrm{Im}\,\gamma(\omega=\omega_L) = \frac{x^2}{2\tau}\left(1 + \frac{1}{2[1+(\omega_L\tau)^2]}\right). \quad (2.13)$$

Here, the prefactor $x^2/2\tau$ is the familiar D'yakonov-Perel spin relaxation rate [D'yakonov72, Dyakonov84] coming from internal random fields induced by disorder and we find that two terms contribute to the width in Eq. (2.13). By comparison to a phenomenological model(cf. Sec. 2.2) we will see that the first term in Eq. (2.13) comes from disorder-induced fluctuations of the internal field parallel to $\mathbf{b}_0$ while the second term is due to fluctuations perpendicular to $\mathbf{b}_0$ and gets suppressed with increasing $\omega_L\tau$. Remarkably, the resonance polarization[4] $S_{\rm res} \propto \alpha/\Gamma$ due to EDSR with Γ given by Eq. (2.13) is proportional to α^{-1}. This results from the simultaneous dependence of the driving and the relaxation mechanism on the SOI such that, for instance, doubling α doubles the driving field while the width increases by a factor 4.

Next, the bare location ω_L of the resonance gets renormalized by the disorder leading to a small shift $\delta\omega \ll \omega_L$, determined by the real part of (2.11),

$$\delta\omega = \frac{x^2}{2\omega_L\tau^2}\mathrm{Re}\;\gamma(\omega=\omega_L) = \frac{\omega_L x^2/4}{1+(\omega_L\tau)^2}. \tag{2.14}$$

We note that for $\omega_L\tau \sim 1$ we get $\Gamma \sim 5\delta\omega$. Also, the shift $\delta\omega$ depends non-monotonically on the magnetic field (ω_L), giving rise to an effective g-factor, $g_{eff} = g(1 + x^2/4(1 + (\omega_L\tau)^2))$, which is B-field dependent. Experimental Observation of this effect would provide useful additional evidence for EDSR.

Finally, the longitudinal component (i.e. along $\mathbf{B_0}$) of the magnetization vanishes identically, i.e., $S^2(\omega) = 0$. This is not quite unexpected in linear response approximation, since it is known from conventional paramagnetic resonance [Cohen-Tannoudji77] that changes in the occupation probability are nonlinear in the driving field.

Let us now give some numbers to illustrate the EDSR effects discussed here (for details see Sec. A.4). To quantify the amount of spins resonantly excited, we introduce the polarization $P = (N_\uparrow - N_\downarrow)/(N_\uparrow + N_\downarrow)$ given by the ratio of S^3 and the electron sheet density. Here $N_\uparrow$ and $N_\downarrow$ denote the average number of spins pointing up and down along the $z-$axis, resp. Choosing now parameter values typical for a GaAs 2DEG sample of a few hundred micrometers in lateral size, a magnetic field of one Tesla, and an ac bias of 0.1 Volt and 8 GHz we get $P = 10^{-4}$ at resonance. This corresponds to $N_\uparrow - N_\downarrow = 200$ excess spins in the laser spot of a typical optical measurement scheme [Sih05], and although being small, this is within reach of detection. Further we note that the polarization P increases at resonance with increasing frequency ω (cf. inset in Fig. 2.3 and Eqs. (2.13) and (2.12)). Thus, the higher the resonance frequency (and the magnetic field) the larger the EDSR signal.

[4] However, $S_{\rm res}$ does not diverge for $\alpha \to 0$ since the next-to-leading order relaxation mechanism, e.g. due to spin-orbit scattering from impurities, keeps Γ finite while the amplitude of the driving field vanishes.

2.2 Phenomenological description

The spin polarization Eq. (2.12) can be interpreted in terms of an internal driving field $\mathbf{b}_1(\omega)$ and spin relaxation due to fluctuating internal fields. To illustrate this interpretation we show that the spin dynamics due to EDSR in can be described in a simplified model which does not involve the orbital degree of freedom. This model is described by the Hamiltonian

$$H = [\mathbf{b}_0 + \mathbf{b}_1(t)] \cdot \boldsymbol{\sigma} + \mathbf{h}(t) \cdot \boldsymbol{\sigma}. \tag{2.15}$$

where, the effective driving field

$$b_1(t) = \alpha \frac{eE_0\tau}{1+(\omega_0\tau)^2}[\cos(\omega_0 t) - \omega_0\tau \sin(\omega_0 t)]\,. \tag{2.16}$$

is given as the Fourier transform of the internal field $\mathbf{b}_1(\omega) = \boldsymbol{\Omega}(\langle \mathbf{p} \rangle_{Drude}(\omega))$ due to the ac Drude drift momentum $\langle \mathbf{p} \rangle_{Drude}(\omega) = eE\tau/(1 - i\omega\tau)$. Note that in the ballistic limit $\omega\tau \gg 1$ the Rabi frequency ω_R found in Eq. (2.2) is recovered.

Scattering from impurities leads to a fluctuating component of the momentum $\delta p(t)$ which varies on the time scale of the mean free scattering time τ. In the phenomenological approach of this section we take δp to be an external stochastic process with vanishing average $\langle \delta p_i(t) \rangle = 0$ where $\langle\rangle$ denotes expectation values of the process. We also assume the correlation function to be $\langle p_i(t) p_j(t') \rangle = \frac{1}{2}\delta_{ij} p_F^2 e^{-|t-t'|/\tau}$. The obvious choice for the fluctuations in the field h, which are generated by the momentum fluctuations and SOI, is then [5]

$$\langle h(t) \rangle = \Omega_{ij} \langle \delta p_j(t) \rangle = 0 \tag{2.17}$$

$$\langle h_i(t) h_j(t') \rangle = \Omega_{ik}\Omega_{jl} \langle \delta p_k(t) \delta p_l(t') \rangle = \frac{1}{2} p_F^2 e^{-|t-t'|/\tau} \Omega_{ik}\Omega_{jk} \equiv \chi^{ij}(t-t'). \tag{2.18}$$

Starting from the statistical properties of Eqs. (2.17) we find an effective Bloch equation for the spin polarization $\mathbf{S}(t)$ in Bloch-Redfield theory [Bloch57, Slichter96] given by

$$\dot{\mathbf{S}} = 2[\mathbf{b}_0 + \mathbf{b}_1(t)] \times \mathbf{S} - \boldsymbol{\Gamma}[\mathbf{S} - \mathbf{S}_{eq}], \tag{2.19}$$

where $\mathbf{S}_{eq} || \mathbf{b}_0$ is the equilibrium polarization due to the magnetic field and the spin relaxation tensor is given by

$$\Gamma^{\mu\nu} = -4 \int_0^\infty d\bar{t} \chi^{\kappa\rho}(\bar{t}) R^{j\rho}(\bar{t}) [\delta_{j\mu}\delta_{\nu\kappa} - \delta_{j\kappa}\delta_{\mu\nu}], \tag{2.20}$$

[5] A similar analysis was made in Ref. [Tahan05] for relaxation rates in paramagnetic spin resonance.

where $R(t)$ is a rotation around $\mathbf{b}_0$ with frequency $\omega_L = 2b_0/\hbar$. Specifying to Rashba SOI and choosing the magnetic field along the y-direction Γ we find the components

$$\begin{aligned}
\Gamma^{11} &= 2\mathrm{Re}[\chi^{33}(\omega_L) + \chi^{22}(0)] = \Gamma_{DP} \\
\Gamma^{22} &= 2\mathrm{Re}[\chi^{11}(\omega_L) + \chi^{33}(\omega_L)] = \Gamma_{DP}\left[\frac{1}{1+(\omega_L\tau)^2}\right] \\
\Gamma^{33} &= 2\mathrm{Re}[\chi^{11}(\omega_L) + \chi^{22}(0)] = \Gamma_{DP}\left[1+\frac{1}{1+(\omega_L\tau)^2}\right],
\end{aligned} \tag{2.21}$$

where $\chi(\omega) = \int dt e^{i\omega t}\chi(t)$, in particular $\chi^{33} = 0$ since internal fields are in-plane, and $\Gamma_{DP} = x^2/2\tau$. Here, we subtracted the antisymmetric part of Γ and interpreted it as a renormalization of the magnetic field given by $\delta\omega = \Gamma_{DP}y/(2(1+y^2))$ which agrees with Eq. (2.14).

We solve the Fourier transform of Eq. (2.19) to linear order(cf. Chap.13, [Cohen-Tannoudji77]) in the driving field b_1 for $S(\omega) = \int_{-\infty}^{\infty} dt e^{i\omega t}\mathrm{S}(t)/2\pi$. Explicitly, we find $S^2 = S_{eq}$ for the longitudinal component and

$$\begin{aligned}
\begin{pmatrix} S^1(\omega) \\ S^3_{(1)}(\omega) \end{pmatrix} &= S_{\mathrm{eq}} b_1 \frac{1}{2}[\delta(\omega-\omega_0)+\delta(\omega+\omega_0)] \begin{pmatrix} 1 \\ \frac{-i\omega}{\omega_L} \end{pmatrix} \\
&\times \left(\frac{1}{\omega_L - \omega + \delta\omega - i\Gamma} + \frac{1}{\omega_L + \omega - \delta\omega + i\Gamma}\right).
\end{aligned} \tag{2.22}$$

for the transverse components. In agreement with Eq. (2.13), the width is found to be $\Gamma = (\Gamma^{11}+\Gamma^{33})/2 = \Gamma_{DP}\left(1+1/2[1+(\omega_L\tau)^2]\right) = \mathrm{Re}\chi^{11}(\omega_L) + 2\chi^{22}(0)$. The latter identity allows us to distinguish two contributions to the width Γ coming from internal field fluctuations along the magnetic field $\mathbf{b}_0$ ($\chi^{22}(0)$) and perpendicular ($\chi^{11}(\omega_L)$).

2.3 Spin-Hall current

We finally turn to a brief discussion of the associated spin Hall current for a homogeneous infinite 2DEG (for details see Sec. A.5). Using the Heisenberg equation of motion we can express the spin Hall current, defined as $I^3_x = \{\sigma^3, v_x\}/2$ [Sinova04], in terms of the magnetization components S^1 and S^3, see Eq. (19) in SI. This relation allows one to access the spin current via a measurement of the magnetization. From the ratio $\hbar I^3_x/2E_y$ the associated ac spin Hall conductivity follows, which, at resonance, is explicitly given by (see Sec. A.5) $\sigma^{3,res}_{xy} = e\omega_L^2\tau/4\pi\Gamma(1-i\omega_L\tau)$. Thus, for $\omega_L\tau \sim 1$ we see that $|\sigma^{3,res}_{xy}| \gg e/4\pi$ (since $\omega_L \gg \Gamma$), which indicates a sizable spin Hall current.

2.4 Conclusion

We have investigated the magnetization of a 2DEG in the presence of spin-orbit interaction and disorder. We have shown that carrier spins in a specific field configuration with an electric rf field give rise to EDSR with a line-width coming from spin relaxation due to disorder and spin orbit interaction. Our results emphasize the importance of tunable SOI for coherent spin manipulation by electric means in semiconductors.

3

Resonant spin polarization and spin current

In this chapter we study the spin polarization and its associated spin-Hall current due to electric-dipole-induced spin resonance in a disordered two-dimensional electron system with Rashba- and Dresselhaus spin-orbit interaction. We show that the disorder induced damping of the spin polarization at resonance can be strongly reduced by an optimal field configuration that exploits the interference between Rashba and Dresselhaus spin-orbit interaction. This leads to a striking enhancement of the spin susceptibility while the spin-Hall current vanishes at the same time. We give an interpretation of the spin current in geometrical terms which are associated with the trajectories the polarization describes in spin space.

3.1 Resonant spin polarization and spin current

In a two-dimensional electron gas (2DEG) with pure Rashba SOI the amount of spin polarization which can be achieved by EDSR is limited by disorder (cf. Chap. 2 and [Duckheim06]) . Similar limitations are found for pure Dresselhaus SOI. However, if both Dresselhaus and Rashba SOI are present interference between the two SOI mechanisms can occur and qualitatively new behavior emerges, such as anisotropy in spin relaxation [Averkiev02, Golovach04, Li06] and transport [Schliemann04, Ganichev04, Trushin07]. For spin relaxation this anisotropy is most pronounced if both SOIs have equal strength. In this case, the spin along the $[1\bar{1}0]$ direction [see Fig. 3.1] is conserved [Schliemann03, Averkiev02], and the associated spin relaxation rates vanish, whereas they become maximal along the perpendicular direction [110]. For the driven system considered here we show that similar interference effects occur and that not only the internal rf field but also the EDSR line-width becomes dependent on the direction of the magnetic field. In a microscopic approach we show then that due to this dependence an optimal configuration exists where the

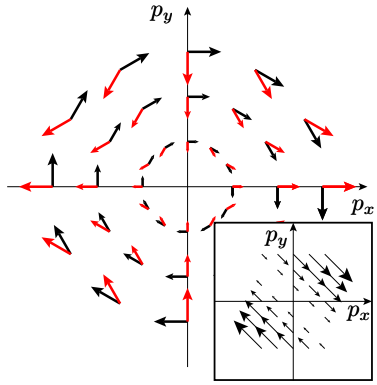

Figure 3.1: Momentum dependent magnetic fields induced by Rashba- (black arrows) and Dresselhaus SOI (red arrows) $\mathbf{\Omega}_R(\mathbf{p}) = \alpha(p_y, -p_x)$ and $\mathbf{\Omega}_D(\mathbf{p}) = \beta(p_x, -p_y)$, respectively. Inset: The sum $\mathbf{\Omega}_R + \mathbf{\Omega}_D$ for equal strength of the SOI ($\alpha = \beta$) is shown. The interference of the two types of SOI leads to a suppression or enhancement of the spin splitting in certain crystallographic directions.

line-width and the internal field simultaneously become minimal and maximal, resp., and that, as a consequence, the spin susceptibility gets enhanced. In other words, this optimal configuration allows one to obtain a high spin polarization with relatively small electric fields and thus making the power consumption for spin polarization minimal.

Due to spin-orbit interaction angular momentum can be transferred between spin and orbital degrees of freedom. This fact leads, in particular, to a dynamical coupling between spin and spin current described by the Heisenberg equation of motion [Erlingsson05b, Chalaev05, Duckheim06]. Exploiting this coupling we show that the spin current can be interpreted in geometrical terms: the spin dynamics generated by the rf fields describes an elliptical trajectory. The spin-Hall conductivity can then be expressed entirely in terms of the semi-minor and semi-major axis and the tilt angle of this ellipse. Since the spin dynamics (trajectories) is experimentally accessible, for instance with optical methods [Kato04c, Sih05], this opens up the possibility for a direct measurement of the spin-Hall current. Finally, we find that for the optimal configuration the spin current vanishes, in contrast to the spin polarization which, as mentioned, becomes maximal.

We consider a non-interacting 2DEG consisting of electrons with mass m

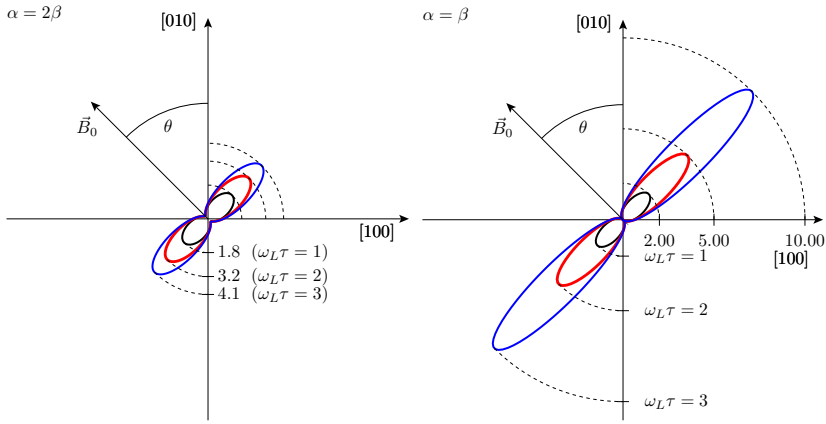

Figure 3.2: Polar plot of the resonance susceptibility $\bar{\chi}^{\text{res}}$ (in arbitrary units) as a function of θ for $\beta = \alpha/2$ (left panel), $\beta = \alpha$ (right panel), and $\omega_L\tau = 1$ (black curve), $\omega_L\tau = 2$(red), and $\omega_L\tau = 3$(blue). The configuration of the external magnetic and electric field $\mathbf{B}_0$ and $\mathbf{E}_0$ is shown. For $\mathbf{B}_0||\mathbf{E}_0||[110]$ both SOI contributions add constructively in the direction perpendicular to $\mathbf{B}_0$ leading to an enlarged Rabi field.

and charge e which are subject to a random impurity potential V. We take into account linear SOI $\sum_{ij} \mathbf{\Omega}_{ij} p_j \sigma^i$ of the Rashba - and Dresselhaus type where $\sigma^i, i = 1, 2, 3$, are the Pauli matrices and $\mathbf{p}$ is the canonical momentum. Taking the coordinate axes along the [100], [010], [001] crystallographic directions, the internal magnetic field $\mathbf{\Omega}$ is then given by (cf. Fig.3.1) $\mathbf{\Omega}(\mathbf{p}) = \alpha(p_y, -p_x, 0) + \beta(p_x, -p_y, 0)$ where α and β is the strength of the Rashba and Dresselhaus SOI, respectively. Additionally, the external static magnetic field is given by $\mathbf{B}_0 = B_0 \mathbf{e}_{||}$ with $\mathbf{e}_{||} = (-\sin\theta, \cos\theta, 0)$, and the external electric rf field by $\mathbf{E}(t) = E(t)(-\sin\theta', \cos\theta', 0)$, where θ, θ' are the angles enclosed with the [010] direction. The system is described by the Hamiltonian

$$H = \frac{1}{2m} (\mathbf{p} - e\mathbf{A})^2 + (\mathbf{\Omega}(\mathbf{p} - e\mathbf{A}) + \mathbf{b}_0) \cdot \boldsymbol{\sigma} + V, \tag{3.1}$$

where $\mathbf{A}(t) = -\int^t dt' \mathbf{E}(t')$ is the vector potential associated with $\mathbf{E}$ and $\boldsymbol{b}_0 = g\mu_B \mathbf{B}_0/2$ with g the electron g-factor and μ_B the Bohr magneton.

3.2 Spin polarization.

We turn now to the calculation of the spin polarization (magnetization/μ_B) per unit area, $\mathbf{S}(\omega) = \int_{-\infty}^{\infty} dt e^{i\omega t}\langle \boldsymbol{\sigma}(t)\rangle/2\pi$, evaluated in linear response to an applied electric field $\mathbf{E}(\omega) = \mathbf{E}_0[\delta(\omega-\omega_0)+\delta(\omega+\omega_0)]/2$ and in the presence of both Rashba and Dresselhaus SOI. Due to the interference between these two SOI mechanisms we need to extend the calculations of Chap. 2 , which were carried out for the simpler Rashba model only, to this new situation. We will then be able to identify a configuration that allows one to obtain a maximum degree of spin polarization due to this interference.

Working in the linear response regime, $S^i(\omega)$ is obtained from a Kubo formula averaged over the random distribution of impurities in the 2DEG. We evaluate this average with standard diagrammatic techniques assuming the impurities to be short-ranged, isotropic and uniformly distributed. In this case, the impurity average $\overline{V(\mathbf{x})V(\mathbf{x}')} \equiv (m\tau)^{-1}\delta(\mathbf{x}-\mathbf{x}')$ is δ - correlated and proportional to the momentum relaxation time τ. We further take the Fermi energy $E_F = p_F^2/2m$ to be the largest energy scale in the problem. Then, to leading order in $1/p_F l$ with $l = p_F/m\tau$ the mean free path, the averaged spin polarization is given by the the diffuson diagram, giving rise [Akkermans07, Rammer98] to a correction $\sigma^i \to \Sigma^i \equiv \Sigma^{ij}\sigma^j$ of the spin vertex (cf. Sec. 2.1) in the Kubo formula. Thus, the spin susceptibility defined by $S^i(\omega) = \chi^{ij}(\omega)E_j(\omega)$ is given by

$$\chi^{ij}(\omega) = \sum_{k=1}^{k=3} 2e\nu\tau\left[\delta^{ik} - \left(1-\frac{1}{\lambda}\right)\Sigma^{ik}\right]\Omega_{kj}\,, \tag{3.2}$$

where $\nu = m/2\pi\hbar^2$ is the two-dimensional density of states and $\lambda(\omega) = 1-i\omega\tau$.

We evaluate the vertex correction Σ of Eq.(3.2) for the case of a magnetic field B_0 that is large compared to the internal fields induced by SOI. This regime is characterized by $a_R \equiv \alpha p_F/2b_0 \ll 1$ and $a_D \equiv \beta p_F/2b_0 \ll 1$. The components Σ^{ij} with $i,j = 1,2,3$ of the vertex correction are then found to be given by

$$\Sigma = \frac{1}{(\omega_L^2-\omega^2)\tau^2+q} \tag{3.3}$$
$$\times \begin{pmatrix} y^2\frac{\lambda-\cos^2(\theta)}{\lambda-1}+\lambda(\lambda-1)+q_{11} & \frac{-y^2}{2(\lambda-1)}\sin(2\theta)+q_{12} & y\cos(\theta)+q_{13} \\ \frac{-y^2}{2(\lambda-1)}\sin(2\theta)+q_{12} & y^2\frac{\lambda-\sin^2(\theta)}{\lambda-1}+\lambda(\lambda-1)+q_{22} & y\sin(\theta)+q_{23} \\ -y\cos(\theta)-q_{13} & -y\sin(\theta)-q_{23} & y^2+\lambda(\lambda-1)+q_{33} \end{pmatrix},$$

where $y = 2b_0\tau/\hbar = \omega_L\tau$. Here, the functions q_{ij} and q are second order in a_R and a_D, and depend on the frequency ω, the Larmor frequency ω_L, and

the angle θ[1].

We discuss now the different components of χ –which we derive from Eq. (3.3)– along and transverse to $\mathbf{B}_0$. In the 2DEG the constant field gives rise to a constant equilibrium polarization due to Pauli paramagnetism. This polarization is given by $\mathbf{S}_{\rm eq} = \nu\hbar\omega_L \mathbf{e}_{||}$ along $\mathbf{B}_0$ and is independent of the electric field. The polarization dynamically generated by $\mathbf{E}(\omega)$, however, depends on the amplitude of the oscillating internal field perpendicular to $\mathbf{B}_0$. It is thus instructive to consider the longitudinal (along $\mathbf{B}_0||\mathbf{e}_{||}$) and the transverse (along $\mathbf{e}_\perp \equiv \mathbf{e}_{||} \times \mathbf{e}_3$ and $\mathbf{e}_3$) polarization components given by $S'^2 = \mathbf{e}_{||} \cdot \mathbf{S}$ and $S'^1 = \mathbf{e}_\perp \cdot \mathbf{S}$, $S'^3 = S^3$, resp.

As a result, we find the polarization $S'^i(\omega) = \bar{\chi}^i(\omega, \theta')E(\omega)$ in terms of the transformed susceptibility $\bar{\chi}$. To lowest order in a_R, a_D only the transverse components ($i = 1, 3$) are finite. They are given by

$$\begin{aligned}\bar{\chi}^i(\omega, \theta') &= S_{\rm eq}\, l(\omega) \left[\alpha \cos(\theta' - \theta) - \beta \sin(\theta' + \theta)\right] \\ &\times w_i \left(\frac{1}{\omega_L - \omega + \delta\omega - i\Gamma} + \frac{1}{\omega_L + \omega - \delta\omega + i\Gamma} \right), \end{aligned} \tag{3.4}$$

where $w_1 = 1$ for the in-plane ($i = 1$) and $w_3 = -i\omega/\omega_L$ for the out-of-plane component ($i = 3$), and $l(\omega) = e\tau/\hbar(1 - i\omega\tau)$ is proportional to the Drude conductivity[2].

Close to resonance the scattering from disorder leads to a renormalization of the magnetic field dependence. The resonance is shifted by a term

$$\begin{aligned}\delta\omega &= \mathrm{Re}\, q(\omega = \omega_L)/2\omega_L\tau^2 \\ &= \frac{p_F^2\tau}{\hbar^2}[\alpha^2 + \beta^2 - 2\beta\alpha \sin(2\theta)] \frac{\omega_L\tau}{1 + (\omega_L\tau)^2}, \end{aligned} \tag{3.5}$$

corresponding to an effective g-factor which depends both on the amplitude and the orientation of the magnetic field. The line-width Γ of the resonance

[1] The q_{ij} and q are given in Sec. A.2. In the following, only $\mathrm{Im}\, q$, $\mathrm{Re}\, q$ and the linear combination $\sqrt{2}(q_{13} - q_{23})y + (q_{11} - 2q_{12} + q_{22})(\lambda - 1) - 2\lambda q$ are relevant for the line-width and the spin-Hall conductivity, resp., which are explicitly given below in Eqs. (3.6) and (3.9).

[2] From Eq.(3.4) we can identify the component of the internal rf field $b_1(\omega)$ (which effectively drives the spin dynamics) in terms of the electrically induced momentum drift $\langle \mathbf{p} \rangle(\omega) = \hbar l(\omega)\mathbf{E}(\omega)$. We find it to be given by the projection of the internal rf field (induced by $\langle \mathbf{p} \rangle(\omega)$) on the transverse direction $\mathbf{e}_\perp$ in the form $b_1(\omega) = \mathbf{e}_\perp \cdot \mathbf{\Omega}(\langle \mathbf{p} \rangle(\omega))$. Due to disorder scattering the Fourier transform $\langle \mathbf{p} \rangle(t)$ and $b_1(t)$ are phase-lagged with respect to $\mathbf{E}(t)$.

peak is given by

$$\Gamma = -\mathrm{Im}\, q(\omega = \omega_L)/2\omega_L\tau^2 = 2p_F^2\tau/\hbar^2 \qquad (3.6)$$
$$\times \left[\left(\alpha^2 + \beta^2 + 2\alpha\beta\sin(2\theta)\right) + \frac{(\alpha^2+\beta^2) - 2\alpha\beta\sin(2\theta)}{2[1+(\omega_L\tau)^2]} \right].$$

Note that in Γ the Rashba and Dresselhaus SOI do not simply add up but can interfere with each other, enabling a strong enhancement of the susceptibility as we will see next. In Fig. 3.2 we plot the spin susceptibility at resonance, $\bar{\chi}^{\mathrm{res}} \propto [\cos(\theta' - \theta) - \sin(\theta' + \theta)\rho]/\Gamma$ for the case $\rho = \beta/\alpha = 0.5$ measured in [Ganichev04]. The angle θ' has been tuned to maximize $\bar{\chi}^{\mathrm{res}}$ which displays a pronounced dependence on the magnetic field direction. In Eq. (3.6) we note that Γ scales with the mean square fluctuations of the internal magnetic fields $\langle(\mathbf{e}_{||}\cdot\mathbf{\Omega}(p_F\hat{\mathbf{n}}))^2\rangle_{\hat{\mathbf{n}}}$ and $\langle(\mathbf{e}_{\perp}\cdot\mathbf{\Omega}(p_F\hat{\mathbf{n}}))^2\rangle_{\hat{\mathbf{n}}}$, where $\langle.\rangle_{\hat{\mathbf{n}}}$ denotes a uniform average over all (in-plane) directions $\hat{\mathbf{n}}$. Comparison with a simple model [Bloch57, Tahan05] of spin relaxation (Bloch equation) shows that the first term in Eq. (3.6) comes from pure dephasing, i.e. from disorder induced fluctuations of the internal fields along $\mathbf{B}_0$, while the second term is due to fluctuations along $\mathbf{e}_{\perp}$. Choosing a configuration with $\theta = \theta' = -\pi/4$ and tuning the SOI strengths to $\alpha = \beta$ the first term vanishes while the second is subject to narrowing due to the magnetic field. The width becomes $\Gamma_{\mathrm{DP}}/[1 + (\omega\tau)^2]$ where $\Gamma_{DP} = 2(\alpha p_F)^2\tau/\hbar^2$ is the D'yakonov - Perel spin relaxation rate for Rashba SOI. Increasing the frequency such that (at resonance) $\omega_L\tau = \omega\tau \gg 1$ will lead to an increase of the inverse width Γ^{-1} and, hence, of the susceptibility at resonance, given by

$$|\bar{\chi}^{\mathrm{res}}_{\alpha=\beta}| = S_{\mathrm{eq}}\frac{e\alpha\tau}{\hbar\Gamma_{DP}}\sqrt{1+(\omega_L\tau)^2}. \qquad (3.7)$$

For comparison, we find the ratio to the resonance susceptibility $\bar{\chi}^{\mathrm{res}}_{\beta=0}$ in the pure Rashba case as $|\bar{\chi}^{\mathrm{res}}_{\alpha=\beta}/\bar{\chi}^{\mathrm{res}}_{\beta=0}| = (1+y^2)[1+1/(2(1+y^2))]$ growing quadratically with $y = \omega_L\tau$. Thus, the spin polarization can be substantially enhanced by tuning the SOIs to equal strengths and by increasing the magnetic field. Finally, the range of validity for the linear response regime can be estimated as follows. Assuming full polarization ($|S'^{3,\mathrm{res}}_{\alpha=\beta}|/S_{\mathrm{eq}} \approx 1$) and parameters for a GaAs 2DEG [Sih05] with spin-orbit splitting $\Delta_{\mathrm{SO}} = \alpha p_F = 60\,\mu\mathrm{eV}$, Fermi wavelength $\lambda_F = 180\,\mathrm{nm}$ and $\omega_L\tau = 10$, we find from Eq. (3.7) that the linear response is valid for electric fields with amplitudes up to $E_0 = 2\pi\Delta_{\mathrm{SO}}/\lambda_F\omega_L\tau \approx 200\,\mathrm{eV m^{-1}}$.

3.3 Polarization and Spin current.

We consider the spin current defined by $\mathbf{I}^3 = \langle\{\sigma^3, \mathbf{v}\}\rangle/2$. Using the Heisenberg equation of motion the spin current components $I^3_{x'}$ and $I^3_{y'}$ along $\mathbf{e}_\perp$ and $\mathbf{e}_{||}$ can be expressed in terms of the polarization at frequency ω as

$$\begin{pmatrix} I^3_{x'} \\ I^3_{y'} \end{pmatrix} = \frac{\hbar}{2m(\alpha^2-\beta^2)} \times \begin{pmatrix} [\alpha - \beta\sin(2\theta)](i\omega S'^1 + \omega_L S'^3) - i\omega\beta\cos(2\theta)S'^2 \\ (\alpha + \beta\sin(2\theta))i\omega S'^2 - \beta\cos(2\theta)(i\omega S'^1 + \omega_L S'^3) \end{pmatrix}. \tag{3.8}$$

We consider the configuration $\theta = \theta' = -\pi/4$ such that the SOI induced internal rf field is perpendicular to $\mathbf{B}_0$ and the longitudinal component $S'^2(t) = S_{\rm eq}$ is not altered in linear response in E. Note that in this case Eq.(3.8) simplifies such that $I^3_{x'} = \hbar(i\omega S'^1 + \omega_L S'^3)/(2m(\alpha-\beta))$. This relation differs from the naive model of an average spin-orbit field equating the internal field $\mathbf{\Omega}(\mathbf{p}(t))$ with its average $\mathbf{\Omega}(\langle\mathbf{p}\rangle(t))$. Contrary to Eq.(3.8), we then find $i\omega S'^1 + \omega_L S'^3 = \Gamma^1 S'^1$ where Γ^1 is a phenomenological transverse relaxation rate. Discrepancies to the model of an averaged spin-orbit field occur similarly for other effects such as the generation of an out-of plane polarization [Engel06] and Zitterbewegung [Schliemann05].

We proceed by evaluating the spin-Hall current $I^3_{x'}$ in terms of the vertex correction Eq.(3.3) which was obtained in the diagrammatic approach and is valid up to second order in a_R, a_D. The linear combination $i\omega S'^1 + \omega_L S'^3$ cancels in lowest order (cf. Eq.(3.4)) such that $I^3_{x'}$ is given by the second order terms q_{ij}, q. From Eq.(3.2) and Eq.(3.8) we find the spin-Hall conductivity, defined as $\sigma^{3,\rm res}_{x'y'} = \hbar I^3_{x'}/2E(\omega)$, to be given by

$$\sigma^{3,\rm res}_{x'y'} = \frac{e}{4\pi}\frac{i\omega_L\tau(\alpha^2-\beta^2)}{(3\alpha^2 - 2\alpha\beta + 3\beta^2) - i2\omega_L\tau(\alpha-\beta)^2}. \tag{3.9}$$

Remarkably, for high frequencies $\omega_L\tau(\alpha-\beta)^2 \gg (\alpha+\beta)^2$ and $\alpha \neq \beta$ Eq.(3.9) reaches the universal limit $\sigma^{3,\rm res}_{x'y'} = |e|(\alpha+\beta)/8\pi(\alpha-\beta)$ (independent of the absolute SOI strengths and disorder details) which was also obtained in the clean limit in [Mishchenko04]. Indeed, for the condition $\omega_L\tau \gg 1$ ($\omega_L = \omega$), many cycles of the electric rf field pass through between subsequent scattering events such that the system effectively behaves as ballistic. This regime can be exploited to achieve high spin polarizations as described above. Moreover,

the singularity in Eq.(3.8) for $\alpha = \beta$ is removed in Eq.(3.9) up to the accuracy $\mathcal{O}(a_R^2, a_D^2, a_D a_R)$ considered here and we find that $\sigma^{3,\mathrm{res}}_{x'y'}$ vanishes in the configuration where $\bar{\chi}$ is maximal, i.e. for $\alpha = \beta$ and $\theta = \theta' = -\pi/4$.

We turn now to a geometrical interpretation of the spin Hall current relating it to the trajectories $\boldsymbol{\mathcal{S}} = \{(S'^1(t), S'^3(t)) | t \in \mathbb{R}\}$ followed by the tip of the polarization vector. For an applied electric field $\mathbf{E}(\omega) = E_0 \mathbf{e}_{||}[\delta(\omega - \omega_0) + \delta(\omega + \omega_0)]/2$ with frequency ω_0 this trajectory is given by the polarization (as a function of time)

$$\begin{pmatrix} S'^1(t) \\ S'^3(t) \end{pmatrix} = \Lambda(\omega_0) \begin{pmatrix} \cos\omega_0 t \\ \sin\omega_0 t \end{pmatrix} \tag{3.10}$$

with the matrix

$$\Lambda(\omega_0) = E_0 \begin{pmatrix} \mathrm{Re}\bar{\chi}^1(\omega_0) & -\mathrm{Im}\bar{\chi}^1(\omega_0) \\ \mathrm{Re}\bar{\chi}^3(\omega_0) & -\mathrm{Im}\bar{\chi}^3(\omega_0) \end{pmatrix} \tag{3.11}$$

containing the Fourier components $\bar{\chi}^{1,3}(\omega)$ of the susceptibility evaluated at $\omega = \omega_0$. Eq. (3.10) constitutes a quadratic form for the trajectory given by $\boldsymbol{\mathcal{S}} = \{(S'^1, S'^3) | \mathbf{S}'^{\mathrm{t}} \cdot \Lambda_2 \mathbf{S}' = 1\}$ with real, positive eigenvalues $\lambda_{1,2}$ (say $\lambda_1 < \lambda_2$) of the defining matrix $\Lambda_2 = (\Lambda^{-1})^{\mathrm{t}} \Lambda^{-1}$. Thus, $\boldsymbol{\mathcal{S}}$ is of elliptic shape with semi-major and semi-minor axis $a = 1/\sqrt{\lambda_1}$ and $b = 1/\sqrt{\lambda_2}$, resp. We can further determine the angle δ enclosed by the semi-major axis of $\boldsymbol{\mathcal{S}}$ and the S'^1 direction since the matrix Λ_2 is diagonalized by a rotation δ around S'^2. The polarization of Eq. (3.10) can thus be written as

$$\begin{pmatrix} S'^1(t) \\ S'^3(t) \end{pmatrix} = \begin{pmatrix} \cos\delta & -\sin\delta \\ \sin\delta & \cos\delta \end{pmatrix} \begin{pmatrix} a\cos(\omega_0 t + \varphi) \\ b\sin(\omega_0 t + \varphi) \end{pmatrix}. \tag{3.12}$$

Here, φ is a phase shift between the electric field and the polarization. From Eqs. (3.10) and (3.12), we can relate the real and imaginary part of the susceptibilities $\bar{\chi}^1$ and $\bar{\chi}^3$ to the parameters a, b, φ, and δ. In particular, we obtain the spin Hall current (Eq.(3.8)) at resonance ($\omega_L = \omega$) as

$$I^3_{x'}(\omega) = \frac{\hbar E(\omega) e^{i(\varphi - \delta)}}{2m(\alpha - \beta)E_0} i\omega_L (a - b)\,. \tag{3.13}$$

Eq. (3.13) provides a remarkable interpretation of the spin Hall current in terms of the geometric properties of the orbit $\boldsymbol{\mathcal{S}}$. The component $I^3_{x'}$ is given by a complex phase depending on the rotation angle δ and the difference between

the semi-minor and semi-major axis $a - b$. In the linear response regime, the spin Hall current characterizes the deviation from a circular orbit with $a = b$ to an elliptic shape (with $a \neq b$). Therefore, $I^3_{x'}$ becomes accessible in terms of simple geometric properties of $\boldsymbol{\mathcal{S}}$ in experiments capable of resolving individual polarization components.

3.4 Conclusion

We predict a substantially enhanced spin polarization due to interference effects of Rashba and Dresselhaus SOI. The spin Hall current associated with this polarization can be interpreted in terms of the trajectory in spin space and vanishes if the polarization is maximal.

4

Mesoscopic fluctuations in the spin-electric susceptibility due to Rashba spin-orbit interaction

We investigate mesoscopic fluctuations in the spin polarization generated by a static electric field and by Rashba spin-orbit interaction in a disordered 2D electron gas. In a diagrammatic approach we find that the out-of-plane polarization – while being zero for self-averaging systems – exhibits large sample-to-sample fluctuations which are shown to be well within experimental reach. We evaluate the disorder-averaged variance of the susceptibility and find its dependence on magnetic field, spin-orbit interaction, dephasing, and chemical potential difference.

4.1 Mesoscopic fluctuations in the spin-electric susceptibility

A primary goal in semiconductor spin physics is the control of magnetic moments by electric fields [Awschalom02, Awschalom07]. One way to achieve this is to make use of the magnetoelectric effect (MEE) [Levitov85, Edelstein90], a spin polarized steady state which emerges from intrinsic 'magnetic' fields generated by spin-orbit interactions (SOI) and transport. While this MEE has been observed e.g. in n-InGaAs epilayers [Kato04b, Kato04a, Kato05] and hole gases [Silov04], the resulting net polarization is below percent for electron systems [Kato04b, Kato05], and thus much smaller than what has been achieved by optical pumping [Kato04a, Stich07, Meier07]. Moreover, in a standard two-dimensional electron gas (2DEG), with typical Rashba SOI [Bychkov84], the MEE generates only in-plane spin polarization but no out-of-plane components [Edelstein90, Engel07, Milletarì08]. The latter would be desirable, also since they can be detected more easily e.g. by optical means.

However, these observations apply only to disordered phase-incoherent systems with self-averaging [Akkermans07]. On the other hand, it is well-known

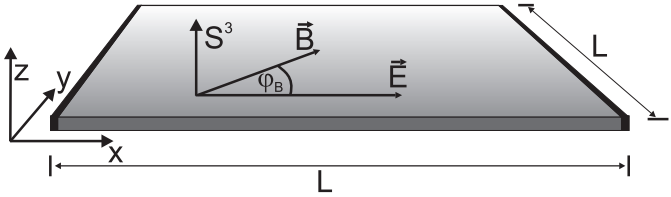

Figure 4.1: Disordered two-dimensional electron gas with spin-orbit interaction and electric contacts at $x = 0$ and $x = L$. Mesoscopic fluctuations of the magnetoelectrical spin susceptibility χ^{31} allow for a finite out-of-plane polarization S^3 in response to an in-plane electric field $\mathbf{E}$.

that phase-coherence in mesoscopic systems leads to new quantum effects such as conductance fluctuations or weak antilocalization, especially due to intrinsic SOI [Altshuler85, Altshuler91, Lee87, Zumbühl05, Aleiner01, Miller03].

Similarly, mesoscopic spin effects emerge for the MEE when the system becomes phase-coherent. Indeed, focussing on 2DEGs with Rashba SOI, we will show here that the spin-electric susceptibility is subject to strong sample-to-sample fluctuations, and thus individual mesoscopic samples with phase coherence can exhibit a large net spin polarization. Quite remarkably, these strong fluctuations show up not only in the in-plane but also in the out-of-plane spin components. We find that these fluctuations considerably exceed the polarization obtained in self-averaging samples, and since the latter has been successfully measured by optical means [Kato04b, Kato05], the spin fluctuations predicted here should be well within experimental reach. We will see that this strong enhancement is special for Rashba (or Dresselhaus [1]) SOI, and, diagrammatically, it results from a spin vertex renormalization typical for such intrinsic SOI [Edelstein90, Chalaev05, Duckheim06].

Related effects studied before are local spin fluctuations in metallic conductors due to the extrinsic spin-orbit effect [Zyuzin90] (as opposed to the intrinsic Rashba SOI [Engel06]), density of states fluctuations of quantum corrals [Walls07], and fluctuations of spin currents in general nanostructures [Bardarson07] and chaotic quantum dots [Bardarson07, Krich08]. While thermal spin fluctuations have been observed [Oestreich05], we are not aware of studies of mesoscopic spin fluctuations due to the MEE as described here.

We consider a disordered mesoscopic square-shaped 2DEG of size L^2 (cf. Fig. 4.1) containing non-interacting electrons of mass m and charge e and

[1] We note that Dresselhaus and Rashba SOI give the same results since the corresponding Hamiltonians are unitarily related [Chalaev05].

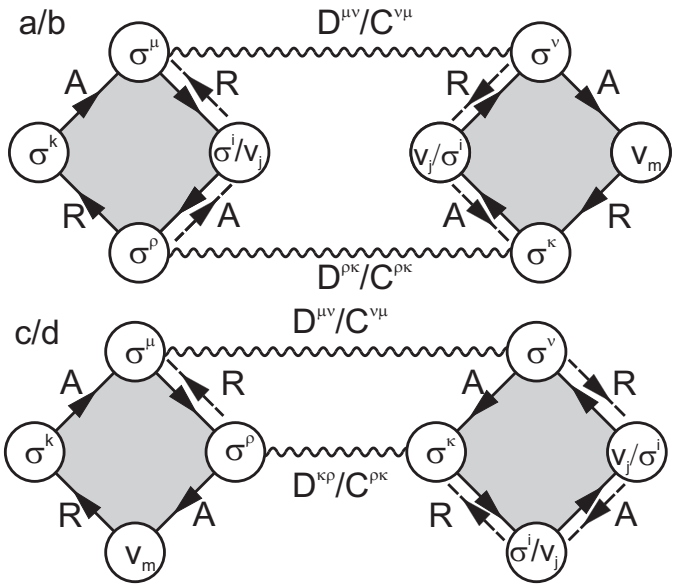

Figure 4.2: Dominant diagrams (for $1/p_F l \ll 1$) leading to the variance $\overline{\delta\chi^{ij}\delta\chi^{km}}$ given in Eq. (4.3), see also Fig. 4.3. The upper diagrams a and b contain the Hikami boxes (HB) V_{La}, V_{Ra}(with solid arrows) and two Diffusons (D) and V_{Lb}, V_{Rb} (with dashed arrows) and two Cooperons (C), *resp.* The lower diagram contains the HBs V_{Lc}, V_{Rc} (solid arrows, two Diffusons) and V_{Ld}, V_{Rd} (dashed arrows, two Cooperons).

described by the Hamiltonian

$$H = \frac{\mathbf{p}^2}{2m} + \alpha(p_1\sigma^2 - p_2\sigma^1) + \mathbf{b}\cdot\boldsymbol{\sigma} + V. \tag{4.1}$$

Here, $\mathbf{p} = (p_1, p_2, 0)$ is the in-plane momentum, α the Rashba SOI constant [Bychkov84], $2b = g\mu_B B(\cos\varphi_B, \sin\varphi_B, 0)$ an external in-plane magnetic field, and $\boldsymbol{\sigma} = (\sigma^1, \sigma^2, \sigma^3)$ the Pauli matrices (and $\sigma^0 = \mathbb{1}$). The disorder potential V is due to static, short-ranged and randomly distributed impurities[2] leading to a mean free path $l = \tau p_F/m$, where τ is the scattering time and p_F the Fermi

[2] We want to note that randomness in other microscopic properties, e.g., the SOI strength [Melnikov72, Glazov05] might lead to mesoscopic effects as well, but is beyond the scope of the present work.

momentum. We, moreover, define the parameter $x = 2\alpha p_F \tau$ characterizing the interplay of disorder and SOI and the D'yakonov-Perel [D'yakonov72] spin relaxation rate $\tau_{DP}^{-1} = x^2/2\tau$.

The spin polarization due to the MEE is given in linear response by $\langle \sigma^i \rangle = \chi^{ij} E_j$, $i = 1, 2, 3$, where E_j is a static electric field applied along the j-direction and χ^{ij} the (zero-frequency) spin-electric susceptibility (per unit area). Here, we focus on the mesoscopic fluctuations of χ^{ij} due to disorder, described by the variance $\overline{(\delta\chi^{ij})^2}$, where $\delta\chi^{ij} = \chi^{ij} - \overline{\chi^{ij}}$ and where the overbar denotes disorder averaging. We start from the Kubo formula for χ^{ij} expressed in terms of retarded/advanced Green functions $G^{R/A}_{E_F}$ at the Fermi energy E_F [Duckheim06]

$$\chi^{ij}(E_F) = \frac{e}{4\pi} \mathrm{Tr} \sigma^i (G^R_{E_F} - G^A_{E_F}) v_j (G^R_{E_F} - G^A_{E_F}) \,, \tag{4.2}$$

where $\mathrm{Tr} \to \int d^2p/(2\pi)^2 \mathrm{tr}_S$ denotes momentum integration and spin trace, and $v_j = i[H, x_j]/\hbar$ is the SOI-dependent velocity operator. In Eq. (4.2) we have used time reversal invariance [3] to make the symmetry $\chi^{ij} = \chi^{ji}$ explicit[4].

The variance $\overline{(\delta\chi^{ij})^2}$ is obtained as the impurity average over the product of two susceptibilities given in Eq. (4.2). Extending the diagrammatic approach of [Altshuler91,Edelstein90,Akkermans07] to include SOI and spin vertices, we obtain the diagrams shown in Fig. 4.2 which give the dominant contribution to the variance for $1/p_F l \ll 1$. Explicitly, we find

$$\begin{aligned}
\overline{\delta\chi^{ij}(E_F + \Delta E)\delta\chi^{km}(E_F)} = \Big(\frac{e}{2\pi L}\Big)^2 \int \frac{d^2q}{(2\pi)^2} \Big[& V^{\mu\rho}_{La} V^{\nu\kappa}_{Ra} D^{\mu\nu}_{-q}(\Delta E) D^{\rho\kappa}_{q}(-\Delta E) \\
& + V^{\mu\rho}_{Lb} V^{\nu\kappa}_{Rb} C^{\nu\mu}_{q}(\Delta E) C^{\rho\kappa}_{q}(-\Delta E) \\
& + V^{\mu\rho}_{Lc} V^{\nu\kappa}_{Rc} \big\{ D^{\mu\nu}_{q}(\Delta E) D^{\kappa\rho}_{q}(\Delta E) + D^{\mu\nu}_{q}(-\Delta E) D^{\kappa\rho}_{q}(-\Delta E) \big\} \\
& + V^{\mu\rho}_{Ld} V^{\nu\kappa}_{Rd} \big\{ C^{\nu\mu}_{q}(\Delta E) C^{\rho\kappa}(q, \Delta E) + C^{\nu\mu}_{q}(-\Delta E) C^{\rho\kappa}_{q}(-\Delta E) \big\} \Big] \,,
\end{aligned} \tag{4.3}$$

where ΔE is the difference in chemical potentials of χ^{ij} and χ^{km}, D_q and C_q are the Diffuson and Cooperon matrices, respectively, and $\int d^2q$ stands for the summation over Diffuson/Cooperon modes (see Sec.B.1.2).

The V_{La}'s (V_{Ra}'s) are Hikami boxes (HBs) shown in Fig. 4.3 and on the left (right) in Fig. 4.2. Since $\chi^{ij} = \chi^{ji}$ (see Eq. (4.2)), each product $V^{\mu\rho}_L V^{\kappa\nu}_R$ in Eq. (4.3) turns into a sum with 4 terms. These terms are obtained by

[3] The B-field breaks time-reversal invariance and leads to additional terms in Eq. (4.2). However, their contribution to $\overline{(\delta\chi^{ij})^2}$ is negligible for the small B-fields $b \approx \sqrt{x^2/\tau\tau_\phi}$ relevant for C, see Eq. (4.7).

[4] Note that $G^R G^R$ ($G^A G^A$) drops out in Eq. (4.2) due to the identity $G^{R/A}_E v_j G^{R/A}_E = -i[x_j, G^{R/A}_E]/\hbar$.

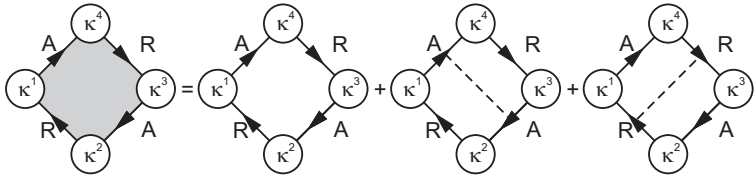

Figure 4.3: General Hikami box (HB): shaded area represents the correction to the 'empty' box $V_{(a)}$ by $V_{(b)}, V_{(c)}$ containing a single impurity line (dashed). The vertices are denoted by $\kappa^i \in \{\sigma^\mu, v_1, v_2\}$, and R/A stands for the averaged $G^{R/A}_{E_F,b}$.

exchanging spin and velocity vertices in the $V's$ such as e.g. $V^{\mu\rho}_{La}V^{\kappa\nu}_{Ra} \equiv V^{\mu\rho}_{La}[\sigma^k,\sigma^i]V^{\kappa\nu}_{Ra}[v_j,v_m] + (\sigma^k \leftrightarrow v_m) + (\sigma^i \leftrightarrow v_j) + (\sigma^k \leftrightarrow v_m, \sigma^i \leftrightarrow v_j)$. Additionally, the vertices have to be dressed with non-crossing impurity lines ([Duckheim06, Chalaev05]). In contrast to conductance fluctuations [Altshuler91, Akkermans07], such vertex corrections are crucial here as they give the dominant dependence on the SOI (see below).

Let us now evaluate Eq. (4.3) by calculating first $V_{L/R}$, given in Fig. 4.2, and then C/D[5]. From now on, we restrict ourselves to the diffusive regime $l/L \ll x = 2\alpha p_F \tau \ll 1$, which allows us to neglect the q-dependence in $V_{L/R}$ and to expand in x. Additionally, we may neglect b and ΔE in $V_{L/R}$. Indeed, we first note that $V_{b\neq 0}/V_{b=0} \propto b\tau$ and $V_{\Delta E\neq 0}/V_{\Delta E=0} \propto \Delta E\tau$ for small b and ΔE, and second, that the suppression of C/D with increasing b and ΔE sets in on a much smaller scale $b \approx \sqrt{x^2/\tau\tau_\phi}$ and $\Delta E \approx 1/\tau_\phi$ (dephasing, see below). As a result, we can unify the calculation of the $2\times 4\times 4$ HBs in Fig. 4.2 by relating them to the general HB $V = V_{(a)} + V_{(b)} + V_{(c)}$ in Fig. 4.3.

Next, we evaluate the Diffuson D and Cooperon C in Eq. (4.3), given by $D_q = (1/2m\tau)(1 - X_+)^{-1}$ and $C_q = (1/2m\tau)k(1 - X_-)^{-1}k$, where $k^{\mu l} = \mathrm{tr}\{\sigma^2\sigma^\mu\sigma^l\}/2$. Expanding $X^{\mu\nu}_\pm = \mathrm{Tr}\{\sigma^\mu G^R_{E_F,b}(\mathbf{p})\sigma^\nu G^A_{E_F,\pm b}(\mathbf{p}-\mathbf{q})\}/2m\tau$ in $\bar{q} = ql \ll 1$, $2b\tau \ll 1$, and x we find D/C by matrix inversion. To account for orbital dephasing we introduce a corresponding dephasing time τ_ϕ in D and C by the standard replacement (see e.g. Eq.(3.15) in [Bergmann84] and [Altshuler81]) $\Delta E \to \Delta E + i/\tau_\phi$. This defines the length scale $L_\phi = l\sqrt{\tau_\phi/2\tau}$ describing the transition from the mesoscopic to the macroscopic regime.

Although generalized to include spin vertices, the method presented so far involves the calculation of similar diagrams as for the conductance fluctuations [Altshuler85, Akkermans07]. An important difference, however, is the inclusion

[5] For a more detailed description see Appendix B

of the vertex corrections for spin and spin-dependent velocity which we discuss now. For the velocity vertex this leads to $v_j \to p_j/m$, i.e. the spin part of the velocity is cancelled in the dc limit [Chalaev05]. For the spin vertex this leads to the replacement $\sigma^i \to \Sigma^{i\mu}\sigma^\mu$ where Σ is diagonal given by $\Sigma = (1 - X_+)^{-1}$ at $\bar{q} = 0$, with the relevant entries $\Sigma^{11} = \Sigma^{22} = 2/x^2$ and $\Sigma^{33} = 1/x^2$. These expressions are valid in the regime $l/L \ll x$ and will be used here. For general x, L, the finite size form of the vertex correction has to be taken into account, giving e.g. $\Sigma^{22} = (2/x^2)(1 - \tanh(xL/2l)/(xL/2l))$, which then renders Eq. (4.6) given below finite for $x \to 0$.

As a result, in the regime $D/L^2, \tau_\phi^{-1} \ll \tau_{DP}^{-1}$ considered here ($D = v_F^2\tau/2$ being the diffusion constant), we find for the in-plane ($i = 1, 2$) and out-of-plane ($i = 3$) components of the variance

$$\overline{(\delta\chi^{ij})^2} = \left(\frac{e\delta\bar{q}^2}{8\pi^3 v_F}\right)^2 \sum_{n_x=1,n_y=0}^{\infty} s^{ij}(\bar{q}_{n_x}, \bar{q}_{n_y}) \,, \tag{4.4}$$

where $v_F = p_F/m$ is the Fermi velocity, $\delta\bar{q} = \pi l/L$, and the sum over the $\bar{q}_n \equiv \delta\bar{q}n$ satisfies the mixed boundary conditions for the Diffuson [Akkermans07] in a finite sample of square size L with two opposite sides attached to the leads. Here, s^{ij} in Eq. (4.4) are rational functions in $\bar{q}_{n_x}, \bar{q}_{n_y}$ depending parametrically on $x = 2\alpha p_F\tau$, $\mathbf{b}$, ΔE, and the orbital dephasing rate $\tau/\tau_\phi = l^2/2L_\phi^2$.

Evaluating s^{ij} for $D/L^2, \tau_\phi^{-1} \ll \tau_{DP}^{-1}$ first for $b = \Delta E = 0$, and choosing the E-field along x (i.e. $j = 1$) we find that the singlet component D^{00}, and C^{22} are dominant, and thus

$$s^{i1} = \frac{a_i \left(4x\Sigma^{ii}\right)^2}{\left(\bar{q}^2 + 2\frac{\tau}{\tau_\phi}\right)^2} \,, \tag{4.5}$$

where $a_1 = a_2 = 1$ and $a_3 = 2$. From Eqs. (4.4), (4.5) we then obtain $\overline{(\delta\chi^{i1})^2} = (ex\Sigma^{ii}/2\pi^3 v_F)^2 c_2 a_i$, where $c_2 = \sum_{n_x,n_y} 1/[(n_x^2 + n_y^2) + (L/\pi L_\phi)^2]^2$. To assess the magnitude of this result we compare it to the average of the in-plane susceptibility $\overline{\chi^{21}} = ex/2\pi v_F$ [Edelstein90]. For the out-of-plane component of the spin fluctuations this yields

$$\frac{\overline{(\delta\chi^{31})^2}}{(\overline{\chi^{21}})^2} = \frac{2c_2}{\pi^4 x^4} = \frac{c_2}{2\pi^4}\frac{\tau_{DP}^2}{\tau^2} \,, \tag{4.6}$$

and similarly for the in-plane components. Thus, we see that the relative fluctuations grow with increasing τ_{DP}.

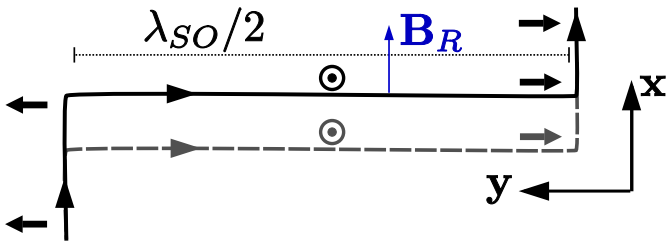

Figure 4.4: Example of a path along which an initially y-polarized spin rotates exclusively into the positive out-of-plane direction (circled dots). The spin directions are denoted by small arrows at the left of each path segment and result from precession about the Rashba spin-orbit field $\mathbf{B}_R$ that is generated by the propagation along the path. The length of the horizontal segment is chosen half the spin-orbit length $\lambda_{SO}/2 = 1/4m\alpha$ so that the spin rotates about $\mathbf{B}_R$ by an angle π. An interfering path is shown (dashed line) generating the same spin rotations.

The suppression of $\overline{\chi^2}$ in a macroscopic sample ($L \gg L_\phi$) is described by $c_2 \approx (L_\phi/L)^2$, whereas for negligible dephasing, i.e. $L_\phi \gg L$, one obtains $c_2 \approx 1.51$, and the spin fluctuations $\overline{(\delta\chi^{ij})^2}$ become independent of the sample size. Taking typical GaAs parameters, $(\hbar)\alpha = 2\ldots20\times10^{-13}$eVm, $l = 250$nm, and $L = 2L_\phi = 40l$, we get $x = 0.1\ldots1$, and, thus, from Eq. (4.6) large relative fluctuations, $\sqrt{\overline{(\delta\chi^{ij})^2}}/\overline{\chi^{21}} \approx 20\ldots0.2$. To obtain an estimate for the out-of-plane polarization $P_\perp = (N_\uparrow - N_\downarrow)/(N_\uparrow + N_\downarrow)$, where $N_\uparrow$ ($N_\downarrow$) is the number of up- (down-) spins, we choose the electric field $E = 1\text{mV}/\mu\text{m}$. This yields $\text{rms}(P_\perp) = 0.1\%$ which in absolute numbers becomes $\text{rms}(P_\perp)nL^2 = \text{rms}(N_\uparrow - N_\downarrow) = 274\ldots27$ and $\overline{P_\parallel}nL^2 = 16\ldots160$ for a sheet density $n = 4\times10^{15}\text{m}^{-2}$. Since the average in-plane polarization $\overline{P_\parallel}$ has been measured [Kato04b] and since $\text{rms}(P_\perp) \approx 20\ldots0.2\overline{P_\parallel}$, we can expect the out-of-plane fluctuations to be within experimental reach as well.

To gain physical insight into this result, we consider an electron with spin initially pointing along the y-axis, see Fig. 4.4. While the electron propagates coherently through the sample, its spin precesses about the intrinsic Rashba SOI field $\mathbf{B}_R$ which is in-plane and perpendicular to the propagation direction. Averaged over impurity configurations its motion is diffusive and follows different random paths such that no spin polarization is found out-of-plane. However, in a mesoscopic sample ($L_\phi \gtrsim L$) with a given impurity configuration the electron propagates along paths that are preferred by constructive

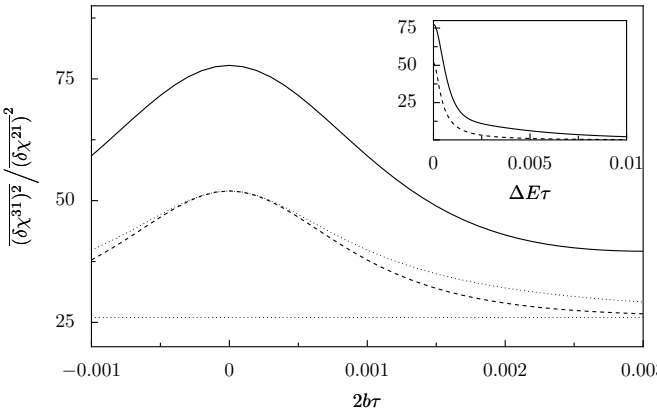

Figure 4.5: The relative variance of the out-of-plane spin susceptibility $\overline{(\delta\chi^{31})^2}/\overline{\delta\chi^{21}}^2$ is shown as a function of the in-plane magnetic field $2b\tau$ for $x = 0.1$, $L_\phi = 100l$, and sample sizes $L = 100\pi l$ (solid line) and $L = 200\pi l$ (dashed line), *resp.* The low field approximation, Eq. (4.7), (curved dotted line) and half of the $b = 0$-value (straight dotted line) are shown for $L = \pi l 100$. Inset: Variance as a function of ΔE for $x = 0.1$, $L_\phi = 100l$, and $L = 100\pi l$ (solid line) and $L = 200\pi l$ (dashed line). The suppression of $\overline{\delta\chi^{31}}$ with increasing b and ΔE is described by Eqs. (4.7) and (4.8).

interference. Fig. 4.4 shows a particular example of such a path and the associated spin directions [6]. Along this entire path the spin can only point up ($+z$-direction), but never down. Now, if initially the electrons were unpolarized, the net out-of-plane polarization in this case would be cancelled by spins that are initially pointing along the negative y-direction. However, due to the (in-plane) MEE, which itself is subject to strong fluctuations, e.g. due to conductance fluctuations, there is a finite in-plane polarization to begin with. The cancellation is therefore incomplete. These considerations make plausible that disorder configurations exist that give rise to strong out-of-plane spin polarizations.

[6] Note that along each segment the electron undergoes many scatterings for $x = l/\lambda_{SO} \ll 1$.

4.1.1 Dependence on gate voltage and magnetic field

We next consider the effect of an in-plane magnetic field [7]. For $b = 0$ we see that the diagrams a) and b) in Eq. (4.3) contribute equally to the variance. However, for $b \neq 0$ the main contribution from the Cooperon is cut off, leading to a suppression of $\overline{\delta\chi^2}$ (see Fig. 4.5), and we can approximate Eq. (4.4) by making use of

$$s_b^{ij} \approx s_{b=0}^{ij} \frac{1}{2} \left[1 + 1 \Big/ \left(1 + \frac{32(b\tau)^2}{\left(\bar{q}^2 + 2\frac{\tau}{\tau_\phi} \right) x^2} \right) \right] , \tag{4.7}$$

where the first term in Eq. (4.7) results from the Diffuson contribution (diagram a) in Fig. 4.2) which is not affected by (moderate) magnetic fields.

Unlike the magnetic field, a difference in energies ΔE (e.g. induced by gate voltages) leads to a suppression of all terms contributing to $\overline{\delta\chi^2}$ (see Fig. 4.5). This is described by

$$s_{\Delta E}^{ij} \approx s_{\Delta E=0}^{ij} \Big/ \left(1 + \frac{4(\Delta E\tau)^2}{\left(\bar{q}^2 + 2\frac{\tau}{\tau_\phi} \right)^2} \right) , \tag{4.8}$$

which gives rise to a correlation scale for susceptibilities at different gate voltages. Indeed, according to Eq. (4.8), we can regard $\chi(E_F)$ and $\chi(E_F + \Delta E)$ as uncorrelated for $\Delta E \geq \max\{1/\tau_\phi, (\pi l/L)^2/\tau\}$.

4.2 Conclusion

From a diagrammatic calculation we find strong mesoscopic fluctuations of the spin-electric susceptibility in a disordered 2DEG due to Rashba SOI, manifesting as large out-of-plane polarizations in individual mesoscopic samples. The predicted values and dependences on the SOI strength, B-field, dephasing rate, and Fermi energy are well within experimental reach. Such spin-dependent coherence effects, besides being of fundamental interest, might prove useful in spintronics applications aiming at the electrical control of spin polarization.

[7] Here, we consider isotropic scattering. For anisotropic scattering even an average out-of-plane polarization can result for $b \neq 0$ [Engel07, Milletarì08].

A

Calculation of the spin polarization due to EDSR

A.1 Calculation of the spin vertex correction

In this appendix we describe the calculation of the magnetization $S^i(\omega)$ due to EDSR, Eq. (2.8), in terms of the spin-spin and the spin-momentum terms, X, Y, respectively, and the spin vertex correction Σ. The simultaneous presence of the internal and external fields, $\mathbf{\Omega}(\mathbf{p}) \cdot \boldsymbol{\sigma}$ and $\mathbf{b}_0$, respectively, breaks the symmetry in orbital space such that no analytical expression[1] for the integrals in Eq. (2.6) can be obtained.

However, in the typical regime for EDSR the amplitude of the internal (driving) field is much smaller than the (perpendicular) static external magnetic field. This is analogous to standard paramagnetic resonance. Thus, without any essential restriction we can concentrate on the regime with the SOI being small compared to $\mathbf{b}_0$, i.e. $a = \alpha p_F/2b_0 = x/2\omega_L\tau \ll 1$. First, upon inspection of Eq. (2.6) we note that the contribution of Y to the magnetization is due to the momentum-part of the velocity and thus must vanish in the absence of SOI. Thus, the leading order term in Eq. (2.8) coming from Y is at least linear in a. More precisely, with a calculation similar to the one outlined below for X, we obtain for the spin-momentum diagram

$$Y^{\mu j} = -\epsilon_{\mu j 3} \frac{\alpha}{\lambda(\omega)} \tag{A.1}$$

i.e. the same result as before for $b_0 = 0$. Thus, the expression Eq. (2.9) has an overall prefactor linear in the SOI α. In order to obtain $S^i(\omega)$ to the lowest non-vanishing order in $\alpha \propto a$ it is therefore sufficient to calculate the spin-spin diagram with setting α to zero and retaining only the $\mathbf{b}_0$ dependence. However, this way, the spin vertex correction $\Sigma(\omega)$ becomes singular at resonance, i.e.

[1] An exact result for $X^{\mu\nu}$ is available [Pletyukhov07] in the simpler Rashba model.

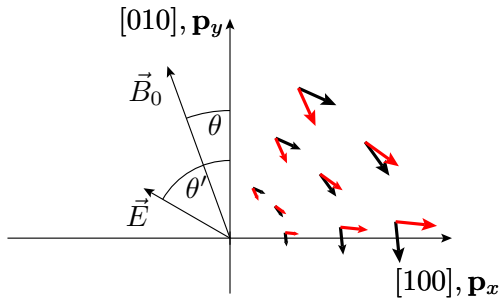

Figure A.1: Geometry of $\mathbf{\Omega}(\mathbf{p})$ and $\mathbf{b}_0 = b_0(-\sin\theta, \cos\theta, 0)$ and the electric field $\mathbf{E}$. The x-axis is chosen along the [100] axis. The internal fields $\mathbf{\Omega}_R(\mathbf{p})$(black) and $\mathbf{\Omega}_D(\mathbf{p})$(red arrows) are shown.

when $\omega = \omega_L$ (Larmor frequency). This shows that at resonance the next-to-leading order contributions of the spin-spin diagram $X = X_{(0)} + a^2 X_{(2)}$ become relevant[2] in $\Sigma(\omega) = (\mathbf{1} - X_{(0)}(\omega) - a^2 X_{(2)}(\omega))^{-1}$ and must be kept. Indeed, they represent the dominant contribution if the determinant of the first term $\mathbf{1} - X_{(0)}$ vanishes. Obviously, at resonance the dominant a dependence becomes $1/a$. Hence, we concentrate on the evaluation of the spin-spin diagram up to order of a^2, with $X_{(2)}$ characterizing the behavior of the magnetization around the resonance where the present analysis is valid.

A.1.1 Calculation of the spin-spin diagram

We calculate now the spin-spin diagram $X^{\mu\nu}$ in the presence of linear Rashba- and Dresselhaus SOI $\mathbf{\Omega}(\mathbf{p}) = \mathbf{\Omega}_R(\mathbf{p}) + \mathbf{\Omega}_D(\mathbf{p})$ and an in-plane external magnetic field $\mathbf{b}_0 = b_0(-\sin\theta, \cos\theta, 0)$ enclosing an angle θ with the y-axis(cf. Fig. A.1). In this case, the effective magnetic field in the Green functions Eq. (2.3) is given by

$$\bar{\mathbf{B}}(\mathbf{P}) = \frac{\mathbf{b}_{\text{eff}}(\mathbf{P}\, p_F)}{E_F} = \bar{\mathbf{B}}_0 + 2a_R \bar{B}_0 \bar{\mathbf{\Omega}}_R(\mathbf{P}) + 2a_D \bar{B}_0 \bar{\mathbf{\Omega}}_D(\mathbf{P}) \,, \tag{A.2}$$

with the expansion parameters $a_R = \alpha p_F / 2b_0 \ll 1$ and $a_D = \beta p_F / 2b_0 \ll 1$ and where we introduced the dimensionless internal fields $\bar{\mathbf{\Omega}}_{R/D}$ defined by

[2] For linear SOI the first order in a vanishes due to the symmetry in the angular integration. Indeed, we note that the angular dependence (in the integrals in Eq. (2.6)) comes from the magnetic field $\mathbf{\Omega}(p(\cos\varphi, \sin\varphi))$ where φ always occurs in terms of a trigonometric function simultaneously with a factor a. Expanded in a the linear terms thus vanish upon angular integration.

$\bar{\mathbf{\Omega}}_{R/D}(\mathbf{P}) = \mathbf{\Omega}_{R/D}(p_F\mathbf{P})/E_F$. To order $\mathcal{O}(a_R^2, a_D^2)$ the modulus $\bar{B} = |\bar{\mathbf{B}}|$ and the unit vector $\hat{\mathbf{B}} = \mathbf{B}/B$ of the effective field are then given by

$$\begin{aligned}\bar{B}(\mathbf{P}) &= \bar{B}_0\left[1 - 2Pa_1(\varphi) + 2P^2 a_2(\varphi)\right]\\ \hat{\mathbf{B}}(\mathbf{P}) &= \hat{\mathbf{B}}_0 + 2P[\mathbf{a}(\varphi) + a_1\hat{\mathbf{B}}_0] + 2P^2[2a_1\mathbf{a} + \hat{\mathbf{B}}_0(2a_1^2 - a_2)]\end{aligned} \tag{A.3}$$

in terms of the auxiliary quantities

$$\begin{aligned}a_1(\varphi) &= a_R\cos(\varphi-\theta) + a_D\sin(\varphi+\theta)\\ a_2(\varphi) &= a_D^2 + a_R^2 + a_D a_R\sin(\varphi) - (a_R\cos(\varphi-\theta) + a_D\sin(\varphi+\theta))^2\\ \mathbf{a} &= a_R\hat{\mathbf{\Omega}}_R(\hat{\mathbf{P}}) + a_D\hat{\mathbf{\Omega}}_D(\hat{\mathbf{P}})\ .\end{aligned} \tag{A.4}$$

where φ is the polar angle of the momentum $\mathbf{P}$. After insertion of Eqs. (A.2, A.3) into the Green functions (Eq. (2.3)) in the spin-spin diagram (Eq. (2.6)) is found as

$$X^{\mu\nu} = \frac{r}{4}\sum_{s,s'=\pm1}\left\langle\int_0^{+\infty}\frac{dP\,P}{2\pi}\frac{T^{\mu\nu}_{s,s'}(P)}{(P-Q_1)\ldots(P-Q_4)c_\varphi}\right\rangle_\varphi\ , \tag{A.5}$$

where $\langle ...\rangle_\varphi$ denotes integration over the φ (normalized by 2π), $c_\varphi \approx 1$ and the poles Q_i are given by

$$\begin{aligned}Q_1 &= +1 + k_1 + i\frac{r}{2}\ , & k_1 &= \bar{B}_0 s(a_1 - a_2) + \frac{1}{2}(w - s\bar{B}_0)\\ Q_2 &= -1 + k_2 - i\frac{r}{2}\ , & k_2 &= \bar{B}_0 s(a_1 + a_2) - \frac{1}{2}(w - s\bar{B}_0)\\ Q_3 &= +1 + k_3 - i\frac{r}{2}\ , & k_3 &= \bar{B}_0 s'(a_1 - a_2) - \frac{s'\bar{B}_0}{2}\\ Q_4 &= -1 + k_4 + i\frac{r}{2}\ , & k_4 &= \bar{B}_0 s'(a_1 + a_2) + \frac{s'\bar{B}_0}{2}\varphi\ .\end{aligned} \tag{A.6}$$

in terms of the dimensionless frequency $w = \hbar\omega/E_F$, scattering rate $r = \hbar/E_F\tau$, and momentum $P = p/p_F$.

Trace. In Eq. (A.5) we introduced the trace over spin states

$$\begin{aligned}T^{\mu\nu}_{s,s'}(\mathbf{P}) &= \mathrm{tr}\{\sigma^\mu(1 + s\,\hat{\mathbf{B}}(\mathbf{P})\cdot\boldsymbol{\sigma})\sigma^\nu(1 + s'\,\hat{\mathbf{B}}(\mathbf{P})\cdot\boldsymbol{\sigma})\}\\ &= 4\,\delta^{\mu\nu}[\delta^{\mu0}\delta_{s,s'} + \delta^{\mu\neq0}\delta_{s,-s'}]\\ &+ 4\,[\delta^{\mu\neq0}\delta^{\nu0}\hat{B}_\mu(\mathbf{P}) + \delta^{\mu0}\delta^{\nu\neq0}\hat{B}_\nu(\mathbf{P})]s\delta_{s,s'}\\ &+ 4\,(-i)\epsilon_{\mu\nu k}\hat{B}_k(\mathbf{P})\delta^{\mu\neq0}\delta^{\nu\neq0}s\delta_{s,-s'}\\ &+ 4\,s\,s'\hat{B}_\mu(\mathbf{P})\hat{B}_\nu(\mathbf{P})\delta^{\mu\neq0}\delta^{\nu\neq0}\ ,\end{aligned} \tag{A.7}$$

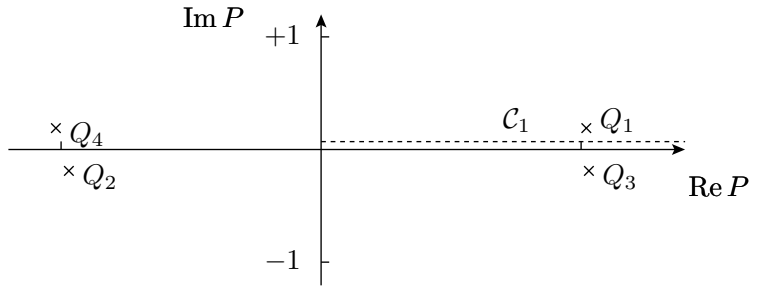

Figure A.2: View of the poles Q_i of the retarded and advanced Green functions in the complex plane (cf. Eq. (A.6)). The contour $\mathcal{C}_1$ of the momentum integral (Eq. (A.5)) running from 0 to $+\infty$ is shown.

where $\delta^{\mu\neq 0} = 1 - \delta^{\mu 0}$ etc., and where summation over repeated indices is implied. The trace $T^{\mu\nu}_{s,s'}(\mathbf{P})$ and the direction of $\hat{\mathbf{B}}_0 \equiv \mathbf{B}_0/B_0$ determine which components of $X^{\mu\nu}$ are nonzero.

Momentum integration. The poles in Eq. (A.6) have been approximated to second order in $a_{R,D}$ and to linear order in $w, r, \bar{B}_0 \ll 1$. They are approximately located at $Q_i \approx \pm 1$ with small corrections k_i and imaginary part $\pm r/2 = \pm\hbar/2E_F\tau$(cf. Fig. A.2). Integration over P is straightforward[3] but lengthy since the various terms in Eq. (A.5) contain products of $\hat{B}_0$ whose P-dependence has to be taken into account. The subsequent angular integrations become simple when expanding in the small parameter a_R, a_D.

[3]Note that the P-dependence of $1/B(P)$ in $T^{\mu\nu}_{s,s'}$ for $a \neq 0$ generates additional singularities at $Q_{5/6} = \exp(\pm i\varphi)/2a$ when analytically continued into the complex plane away from the real axis. The application of complex contour integration is thus non-trivial. A direct calculation, however, shows that these poles do not contribute to X within the accuracy $O(w, B_0, r)$.

This way we obtain

$$R_z(-\theta)XR_z(\theta) = \begin{pmatrix} \frac{1}{\lambda} & 0 & 0 & 0 \\ 0 & \frac{\lambda}{y^2+\lambda^2} & 0 & \frac{y}{y^2+\lambda^2} \\ 0 & 0 & \frac{1}{\lambda} & 0 \\ 0 & \frac{-y}{y^2+\lambda^2} & 0 & \frac{\lambda}{y^2+\lambda^2} \end{pmatrix} \tag{A.8}$$

$$+ x^2 \begin{pmatrix} 0 & 0 & 0 & 0 \\ 0 & \frac{y^4+4\lambda^2y^2-\lambda^4}{2\lambda(y^2+\lambda^2)^3} & 0 & \frac{-2y\lambda^2}{(y^2+\lambda^2)^3} \\ 0 & 0 & \frac{-1}{2\lambda(\lambda^2+2y^2)} & 0 \\ 0 & \frac{2y\lambda^2}{(y^2+\lambda^2)^3} & 0 & \frac{(y^2-\lambda^2)\lambda}{(y^2+\lambda^2)^3} \end{pmatrix}$$

$$+ gx^2 \begin{pmatrix} 0 & 0 & 0 & 0 \\ 0 & \frac{g\left(y^4+4\lambda^2y^2-\lambda^4\right)-2\left(y^2-\lambda^2\right)^2\sin(2\theta)}{2\lambda\left(y^2+\lambda^2\right)^3} & \frac{(y^2-\lambda^2)\cos(2\theta)}{\lambda\left(y^2+\lambda^2\right)^2} & \frac{2y\left((y^2-\lambda^2)\sin(2\theta)-g\lambda^2\right)}{\left(y^2+\lambda^2\right)^3} \\ 0 & \frac{(y^2-\lambda^2)\cos(2\theta)}{\lambda\left(y^2+\lambda^2\right)^2} & \frac{-g+2\sin(2\theta)}{2\lambda^3+2y^2\lambda} & -\frac{2y\cos(2\theta)}{\left(y^2+\lambda^2\right)^2} \\ 0 & \frac{2y\left(g\lambda^2+\left(\lambda^2-y^2\right)\sin(2\theta)\right)}{\left(y^2+\lambda^2\right)^3} & \frac{2y\cos(2\theta)}{\left(y^2+\lambda^2\right)^2} & \frac{\lambda\left(4\sin(2\theta)y^2+g(y^2-\lambda^2)\right)}{\left(y^2+\lambda^2\right)^3} \end{pmatrix},$$

where $g = \beta/\alpha$ is the ratio of Rashba and Dresselhaus SOI-strength,$y = 2b_0\tau = \omega_L\tau$, and $R_z(\theta)$ is a rotation around the 3-axis by an angle θ keeping X^{00} constant. In the case $y = 2b_0\tau = 0$ (no magnetic field) this turns into

$$R_z\left(\frac{-\pi}{4}\right)XR_z\left(\frac{\pi}{4}\right) = \begin{pmatrix} \frac{1}{\lambda} & 0 & 0 & 0 \\ 0 & \frac{1}{\lambda} - \frac{(g+1)^2x^2}{2\lambda^3} & 0 & 0 \\ 0 & 0 & \frac{1}{\lambda} - \frac{(g-1)^2x^2}{2\lambda^3} & 0 \\ 0 & 0 & 0 & \frac{1}{\lambda} - \frac{\left(g^2+1\right)x^2}{\lambda^3} \end{pmatrix} \tag{A.9}$$

This way, we obtain the components $X^{\mu\nu}$ and via the matrix inversion $\Sigma = (\mathbf{1} - X)^{-1}$ the spin vertex correction in Eq. (2.10). The frequency dependence and resonance behavior of the magnetization for $g = 0$ are discussed in chapter 2. The geometry and the spin current in the simultaneous presence of Rashba and Dresselhaus SOI can be inferred from Eq. (A.8) and are discussed in chapter 3.

A.2 Second order damping functions

In this section we give the relevant functions q and q_{ij} in Eq. (3.3). For $\theta = -\pi/4$ and $\omega = \omega_L$ the functions q and q_{ij} are given by

$$q_{11} = \frac{-2a_R^2(\lambda-1)^2\lambda}{(1-2\lambda)^2}\left[1+6\lambda^2(\rho-1)^2+(\rho-8)\rho-4\lambda(1+(\rho-5)\rho)\right] \tag{A.10}$$

$$q_{12} = \frac{-2a_R^2(\lambda-1)^2}{(1-2\lambda)^2}\left[2\lambda^3(\rho-1)^2+4\lambda^2\rho+(1+\rho)^2-\lambda(3+\rho(4+3\rho))\right] \tag{A.11}$$

$$q_{13} = \frac{i\sqrt{2}a_R^2(\lambda-1)^2}{(1-2\lambda)^2}\big[1+4\lambda^3(\rho-1)^2+\rho(6+\rho) - 4\lambda^2(1+(\rho-4)\rho)-2\lambda(1+\rho(8+\rho))\big] \tag{A.12}$$

$$q_{33} = \frac{-2a_R^2(\lambda-1)^2}{\lambda(1-2\lambda)^2}\big[4\lambda^4(\rho-1)^2-12\lambda^2\rho-(1+\rho)^2 + 3\lambda(1+\rho)^2-4\lambda^3(1+(\rho-4)\rho)\big] \tag{A.13}$$

and $q_{22} = q_{11}$ and $q_{23} = q_{13}$.

A.3 Regime of validity

We now give a summary of the parameters controlling the regime of validity of the present theory.

A first constraint ensures the validity of the linear response approach. For this, we give a heuristic argument based on the analogy to conventional ESR [Cohen-Tannoudji77] expressed by Eq. (2.2) of the paper. For this case, we consider the Bloch equations Eq. (2.19) in Sec. 2.2 where, for simplicity, we assume the relaxation tensor Γ diagonal with two equal transverse rates $\Gamma^{11} = \Gamma^{33} \equiv T_2^{-1}$ and the longitudinal rate $\Gamma^{22} = T_1^{-1}$.

The familiar steady state solutions in the rotating frame for the longitudinal component S^2 and the transverse components S^u and S^v, respectively are

$$\begin{aligned} S^2 &= S_{\rm eq}\frac{1+\Delta\omega^2T_2^2}{1+\Delta\omega^2T_2^2+T_1T_2\omega_1^2} \\ S^u &= S_{\rm eq}\frac{\Delta\omega\omega_1T_2^2}{1+\Delta\omega^2T_2^2+T_1T_2\omega_1^2} \\ S^v &= S_{\rm eq}\frac{\omega_1T_2}{1+\Delta\omega^2T_2^2+T_1T_2\omega_1^2}, \end{aligned} \tag{A.14}$$

where $\omega_1 = \gamma B_1$, $\omega_L = \gamma B_0$, and $\Delta\omega = \omega_L - \omega$.

The resulting transverse polarization close to resonance is, thus, proportional to $\omega_1/[(\omega-\omega_L)^2 + \omega_1^2(T_1/T_2) + 1/T_2^2]$ with the phenomenological relaxation rate $1/T_2$. Thus, two relaxation terms are present, viz. the 'external' damping given by $1/T_2^2$ and an intrinsic term $\omega_1^2(T_1/T_2)$ given by the driving rf field itself.

Similarly, the same intrinsic mechanism should be expected if the driving field B_1 is generated by a SOI-mediated bias like in the case considered in the paper. We thus anticipate a total spin relaxation rate of the form[4] $\sqrt{\omega_R^2 + \Gamma^2}$ with Rabi frequency $\omega_R = eE_0\alpha/\hbar\omega_L$ derived at resonance from Eq. (2.2). Here, E_0 denotes the amplitude of the electric field $\mathbf{E}(t) = E_0\mathbf{e}_y\cos(\omega t)$ and Γ is given by Eq. (2.13). However, the Rabi frequency occurring in the rate $\sqrt{\omega_R^2 + \Gamma^2}$, being E-field dependent, must be negligible for a polarization S^i which is calculated in linear response with respect to $\mathbf{E}(t)$. This imposes the self-consistent condition

$$\omega_R \ll \Gamma \quad \Leftrightarrow \quad \frac{\hbar e E_0}{p_F \omega_L \tau} \ll 2\alpha p_F \left(1 + \frac{1}{2[1+(\omega_L\tau)^2]}\right) \tag{A.15}$$

for the validity of the linear response approach. A more systematic approach for estimating the validity of the linear response regime requires an explicit evaluation of the non-linear response, which, however, is beyond the scope of the present work.

Secondly, in order to carry out the momentum integrals in Eq. (2.6) we introduced a condition limiting the SOI strength

$$a = \frac{\alpha p_F}{\hbar\omega_L} \ll 1. \tag{A.16}$$

This constraint not only simplified our analysis but also defines the most interesting regime for EDSR. Indeed, in order to have a pronounced resonance, the width of the resonance peak needs to be smaller than the resonance frequency, i.e. $\Gamma \ll \omega_L$, which is equivalent to $\alpha p_F x \ll \hbar\omega_L$ (see Eq. (2.13)). For self-consistency we need to assume $x \leq 1$ (see the text before Eq. (2.12)), and thus we see that $a \ll 1$ ensures $\Gamma \ll \omega_L$.

In this context we note the somewhat counterintuitive fact that the height of the resonance decreases with increasing SOI, see Eqs. (2.12,2.13). Indeed, on one hand the polarization is proportional to α via the driving rf field, and thus increases with increasing SOI. On the other hand, at resonance the polarization becomes proportional to $1/\Gamma$ (due to disorder) which gives then rise to a suppression factor $1/\alpha^2$. Thus, in total the polarization decrease as $1/\alpha$ with increasing SOI at resonance.

[4] assuming $T_1 = T_2$ for simplicity

Our last constraints

$$\frac{b_0}{E_F}, \frac{\hbar\omega}{E_F}, \frac{\hbar}{E_F\tau} \ll 1 \tag{A.17}$$

correspond to the physically relevant situation where the Fermi energy E_F is the largest energy in the system. Further, the condition $x = 2\alpha p_F\tau/\hbar \ll 1$ does not restrict the validity of Eqs. (2.10) and (2.11) but permits us to represent Eq. (2.12) in terms of two Lorentzians. In the case $\omega\tau \approx 1$, however, it becomes equivalent to the inequality (A.16).

A.4 Numerical estimates

To illustrate the predicted effects we now evaluate the polarization explicitly using typical GaAs parameters (cf. table A.1), thereby making sure that we stay within the range of validity of our approximations. With a typical sheet density $n_2 = p_F^2/2\pi\hbar^2 = 4 \times 10^{15}$ m^{-2}, effective mass $m^* = 0.067\, m_e$ and a high mobility scattering time $\tau = 2\times10^{-11}$ s taken from [Beenakker91] we can estimate the maximum polarization P as the ratio of the peak polarization per unit area and the sheet density

$$P = \frac{S^3_{max}}{n_2} = \frac{eEm^*}{(2\pi\hbar n_2)^2 2\alpha\tau}\frac{\omega\tau}{\sqrt{1+\omega^2\tau^2}}\left(1+\frac{1}{2(1+\omega^2\tau^2)}\right)^{-1}. \tag{A.18}$$

In order to stay within the condition (3.11) we choose a small Rashba - parameter $\alpha = 10^{-14}$ eVm and find $x = 0.1$. Assuming a realistic microwave frequency $\omega = 50 \times 10^9$ s^{-1} corresponding to $\omega\tau = 1$ and a voltage amplitude of $V = 0.1$ V over a sample length of $l = 600$ μm we find an electric field $E_0 = 166$ Vm^{-1} and a polarization of $P = 10^{-4}$. Note that the size of the chosen $E-$field satisfies the linear response condition (A.15) (and poses no severe limitation for a real experiment).

The corresponding number of excess spins $N_\uparrow - N_\downarrow$ in a laser spot of size $5\mu m \times 5\mu m$ is 200. This number is measurable with state-of-the-art optical detection techniques such as Faraday rotation [Kato04a, Sih05, Sih05].

We can further quantify the peak width Γ and the frequency shift $\delta\omega$. Making use of Eqs. (2.13) and (2.14) we find

$$\begin{aligned}\Gamma &= 0.3 \times 10^9 \text{ s}^{-1}\\ \delta\omega &= 0.06 \times 10^9 \text{ s}^{-1}.\end{aligned} \tag{A.19}$$

As a further characterization of the resonance we estimate the Rabi frequency ω_R, given by the amplitude of $b_1(t)$ in Eq. (2.2) and (2.16). Assuming a bias $\mathbf{E}(t) = E_0\mathbf{e}_y\cos(\omega t)$ we find

$$\omega_R = \frac{eE_0\alpha}{\hbar\omega} = 0.08 \times 10^9 \text{ s}^{-1}, \tag{A.20}$$

evaluated at resonance[5] $\omega_L = \omega$ with the parameters given above. A summary of the above calculation and a check of the constraints Eqs. (3.11,A.15) is given in table A.1.

A.5 Spin current and magnetization

We show now that the obtained magnetization S^i can be related to the spin current (defined below) via an exact relation. More generally, we consider the density associated with the spin

$$\rho^i(\mathbf{x}) = \frac{1}{2}\{\sigma^i, \delta(\mathbf{x} - \hat{\mathbf{x}})\} \tag{A.21}$$

whose homogenous limit $S^i = \int d^2x \rho^i(\mathbf{x})$ equals the magnetization. The spin density is defined as the (symmetrized) product of the spin with the particle density operator $\delta(\mathbf{x}-\hat{\mathbf{x}})$ where $\hat{\mathbf{x}}$ is the quantum mechanical position operator. The spin current associated with ρ^i is defined in the usual way [Sinova04, Schliemann04, Inoue04, Mishchenko04, Dimitrova05, Erlingsson05b, Chalaev05]

$$j^i_k(\mathbf{x}, t) = \frac{1}{2}\{\sigma^i, j_k(\mathbf{x})\} \tag{A.22}$$

in terms of the current operator $j_k(\mathbf{x}, t) = \frac{1}{2}\{\delta(x - \hat{\mathbf{x}}), v_k\}$ where, in contrast to the linear response treatment of the paper, the velocity operator $v_k = i/\hbar[H, x_k] = (p_k - (e/c)A_k)/m + \alpha(\boldsymbol{\sigma} \times \mathbf{e}_z)_k$ contains the kinetic momentum including the (homogenous) vector potential $\mathbf{A}$.

The two operators ρ^i and j^i_k are related via the Heisenberg equation of motion

$$\frac{d}{dt}\rho^\eta(\mathbf{x}, t) = \frac{i}{\hbar}[H, \rho^\eta] \tag{A.23}$$

given by the Hamiltonian Eq. (2.1). Analogous to [Erlingsson05b] where the Rashba- and Dresselhaus SOI has been considered it forms an exact operator identity

$$\frac{d}{dt}\rho^1(\mathbf{x}, t) + \nabla \cdot \mathbf{j}^1(\mathbf{x}, t) = -\frac{2\alpha m}{\hbar} j^3_x(\mathbf{x}, t) - \frac{2}{\hbar}\left[\rho^2(\mathbf{x}, t) b_{0,z} - \rho^3(\mathbf{x}, t) b_{0,y}\right] \tag{A.24}$$

$$\frac{d}{dt}\rho^2(\mathbf{x}, t) + \nabla \cdot \mathbf{j}^2(\mathbf{x}, t) = -\frac{2\alpha m}{\hbar} j^3_y(\mathbf{x}, t) - \frac{2}{\hbar}\left[\rho^3(\mathbf{x}, t) b_{0,x} - \rho^1(\mathbf{x}, t) b_{0,z}\right]$$

$$\frac{d}{dt}\rho^3(\mathbf{x}, t) + \nabla \cdot \mathbf{j}^3(\mathbf{x}, t) = +\frac{2\alpha m}{\hbar}\left[j^1_x(\mathbf{x}, t) + j^2_y(\mathbf{x}, t)\right] - \frac{2}{\hbar}\left[\rho^1(\mathbf{x}, t) b_{0,y} - \rho^2(\mathbf{x}, t) b_{0,x}\right],$$

[5] corresponding to a magnetic field $B \approx 1$ T for $|g| = 0.44$

for the case of an additional static magnetic field with components $b_{0,i}$; $i = x, y, z$ which holds independently of the impurity potential as ρ^i commutes with the position operator.

In deriving Eq. (A.24) the definition of j_k^i arises naturally as a divergence term of a current associated with the spin density. Together with the time derivative $\dot{\rho}^i$ it forms the left-hand side of a continuity equation. The right hand side, however, is nonzero and describes the dynamics of the spin due to the external magnetic field $\mathbf{b}_0$ and the internal SOI field. The definition of Eq.(A.22) as a 'spin current' is thus ambiguous [Rashba03a, Engel05] and it is not clear to what extent the quantity Eq. (A.22) can be identified with actual spin transport, i.e. with spin polarized currents which are experimnetally accessible [Erlingsson05a].

In spite of the above concerns we note that the present theory accesses the spin current as the time derivative of the magnetization. Namely, going over to the homogenous limit $I_k^i = \int d^2x j_k^i(x)$ such that the gradient in Eq.(A.24) vanishes we find the transverse spin current

$$I_x^3(\omega) = \frac{\hbar}{2\alpha m} i\omega S^1(\omega) + \frac{b_{0,y}}{\alpha m} S^3(\omega). \tag{A.25}$$

Since S^3 vanishes for $\omega = 0$ it is obvious from Eq. (A.25) that there is no spin current in the long time limit $\omega \to 0$ for a homogenous infinite sample [Inoue04, Erlingsson05b, Chalaev05]. This means a generalization of the argument given in [Erlingsson05b, Chalaev05] to the case of a finite magnetic field. For finite frequencies, however, Eq. (A.25) predicts a non-vanishing oscillating spin current expressed in terms of the magnetization components perpendicular to the applied electric rf field. With the results for S^i inserted we find the ac spin Hall conductivity

$$\sigma_{xy}^3(\omega) \equiv \frac{I_x^3 \hbar/2}{E_y} = \frac{e}{4\pi} \frac{i\omega\,\omega_L\tau}{1 - i\omega\tau} \left(\frac{1}{\omega_L - \omega + \delta\omega - i\Gamma} + \frac{1}{\omega_L + \omega - \delta\omega + i\Gamma} \right). \tag{A.26}$$

We emphasize that this relation provides a direct link between the experimentally accessible magnetization and the spin current. Evaluated at the resonance $\omega = \omega_L + \delta\omega$ we get

$$\sigma_{xy}^{3,res} = \frac{e}{4\pi} \frac{\omega_L\tau}{1 - i\omega_L\tau} \frac{\omega_L}{\Gamma}, \tag{A.27}$$

where we neglected $\delta\omega$ against ω_L. Thus, we see that for $\omega_L\tau \approx 1$ the modulus of the ac spin Hall conductivity becomes much larger than $e/4\pi$ since $\omega_L \gg \Gamma$.

Description	Parameter	Value
sheet density	n_2	4×10^{11} cm^{-2}
effective mass	m^*	$0.067\, m_e$
scattering time	τ	2×10^{-11} s
frequency	$f = \omega/2\pi$	8 GHz
Larmor frequency	$f = f_L = \omega_L/2\pi$	8 GHz
Rashba Parameter	α	10^{-12} eV cm
electric field	E	1.66 V cm^{-1}
polarization	P	10^{-4}
SOI vs. scattering	x	0.1
spin relaxation rate	$\Gamma/2\pi$	0.05 GHz
resonance shift	$\delta\omega/2\pi$	0.01 GHz
Rabi frequency	$\omega_R/2\pi$	0.012 GHz
validity conditions		
linear response	ω_R/Γ	0.27
relative SOI strength	$a = \alpha p_F/\hbar\omega_L$	0.05

Table A.1: Numerical estimates

B

Calculation of the spin susceptibility fluctuations

B.1 Calculation of the spin susceptibility fluctuations

In this appendix we describe how to calculate the spin-electric susceptibility in Eq. (4.3). A list of symbols is given at the end (Sec. B.2). The analysis consists of two main steps: the calculation of the Diffuson and Cooperon D and C, respectively, and the calculation of the Hikami boxes V_L and V_R.

The variance $\overline{(\delta\chi^{ij})^2}$ is obtained as the impurity average over the product of two susceptibilities given in Eq. (4.2) (in Sec. 4.1. The calculation of this average is similar to the diagrammatic approach of [Altshuler85,Altshuler91,Akkermans07], which is generalized here to include both spin and spin-dependent velocity vertices. An important difference, however, is the vertex correction of the spin which is absent for the momentum vertices in conductance fluctuations. The dominant contributions to the variance for $1/p_F l \ll 1$ are given by Eq. (4.3) and the diagrams shown in Figs. 4.2 and B.1. Let us now evaluate Eq. (4.3) by calculating first $V_{L/R}$, occurring in Fig. B.1 (see Eqs. (B.1-B.5) below), and then C/D in the diffusive regime $l/L \ll x = 2\alpha p_F \tau \ll 1$.

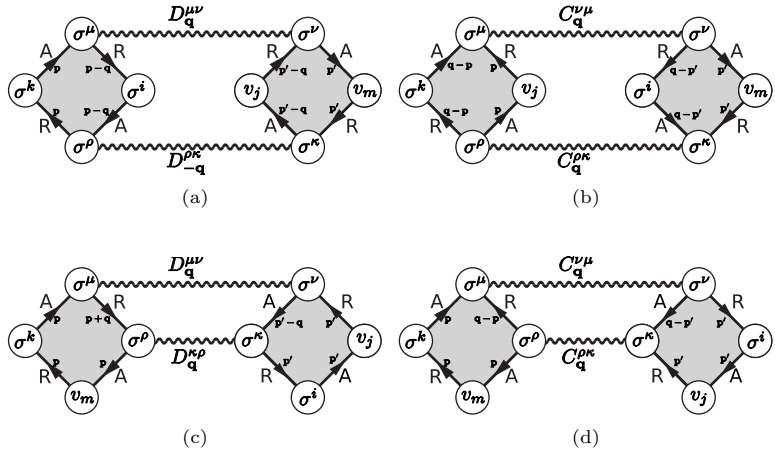

Figure B.1: Dominant diagrams a - d (for $1/p_F l \ll 1$) for the variance $\overline{\delta\chi^{ij}\delta\chi^{km}}$ (cf. Eq. (4.3)). The left and right Hikami boxes V_L and R_R, respectively, are given in Eq. (B.1- B.5).

B.1.1 Calculation of the Hikami boxes

The $2 \times 4 \times 4 \times 3$ Hikami boxes in Fig. B.1 are given by

$$V^{\mu\rho}_{La(a)}[\sigma^k,\sigma^i] = \int \frac{d^2p}{(2\pi)^2} \mathrm{tr}\Big\{\sigma^\mu G^A(p)\sigma^k G^R(p)\sigma^\rho G^A(p-q)\sigma^i G^R(p-q)\Big\} \tag{B.1}$$

$$V^{\nu\kappa}_{Ra(a)}[v_j,v_m] = \int \frac{d^2p'}{(2\pi)^2} \mathrm{tr}\Big\{\sigma^\kappa G^R(p')v_m G^A(p')\sigma^\nu G^R(p'-q)v_j G^A(p'-q)\Big\} \tag{B.2}$$

$$V^{\mu\rho}_{Lb(a)}[\sigma^k,v_j] = \int \frac{d^2p}{(2\pi)^2} \mathrm{tr}\Big\{\sigma^\mu G^R(p)v_j G^A(p)[G^A(q-p)\sigma^k G^R(q-p)\sigma^\rho]^t\Big\} \tag{B.3}$$

$$V^{\nu\kappa}_{Rb(a)}[\sigma^i,v_m] = \int \frac{d^2p'}{(2\pi)^2} \mathrm{tr}\Big\{\sigma^\kappa G^R(p')v_m G^A(p')[G^A(q-p')\sigma^i G^R(q-p')\sigma^\nu]^t\Big\} \tag{B.4}$$

$$V^{\mu\rho}_{Lc(a)}[\sigma^k, v_m] = \int \frac{d^2p}{(2\pi)^2} \mathrm{tr}\Big\{\sigma^\mu G^A(p)\sigma^k G^R(p) v_m G^A(p)\sigma^\rho G^R(p+q)\Big\} \quad \text{(B.5)}$$

$$V^{\nu\kappa}_{Rc(a)}[\sigma^i, v_j] = \int \frac{d^2p'}{(2\pi)^2} \mathrm{tr}\Big\{\sigma^\kappa G^A(p'-q)\sigma^\nu G^R(p') v_j G^A(p')\sigma^i G^R(p')\Big\} \quad \text{(B.6)}$$

$$V^{\mu\rho}_{Ld(a)}[\sigma^k, v_m] = \int \frac{d^2p}{(2\pi)^2} \mathrm{tr}\Big\{\sigma^\mu G^R(q-p)\sigma^\rho [G^A(p)\sigma^k G^R(p) v_m G^A(p)]^t\Big\} \quad \text{(B.7)}$$

$$V^{\nu\kappa}_{Rd(a)}[v_j, \sigma^i] = \int \frac{d^2p'}{(2\pi)^2} \mathrm{tr}\Big\{\sigma^\kappa G^R(p') v_j G^A(p')\sigma^i G^R(p')\sigma^\nu [G^A(q-p')]^t\Big\} \quad \text{(B.8)}$$

and the associated HBs $V_{La(b)}, V_{Ra(b)}, \ldots, V_{Rd(b)}$ and $V_{La(c)}, V_{Ra(c)}, \ldots, V_{Rd(c)}$ generated by the insertion of a single impurity line(cf. Eqs. (B.9-B.11) below). We, moreover, have to take into account the HBs generated by exchange of vertices in Eqs. (B.1-B.5) as described below Eq. (4.3).

The condition $l/L \ll x = 2\alpha p_F \tau \ll 1$ allows us to neglect the q-dependence in $V_{L/R}$ and to expand to second order in x. Additionally, we neglect b and ΔE in $V_{L/R}$ since first $V_{b\neq 0}/V_{b=0} \propto b\tau$ and $V_{\Delta E\neq 0}/V_{\Delta E=0} \propto \Delta E\tau$ for small b and ΔE, and second the suppression of C/D with increasing b and ΔE sets in on a much smaller scale $b\tau \approx \sqrt{\phi x^2}$ and $\Delta E\tau \approx \phi = \tau/\tau_\phi$ (dephasing, see Sec. 4.1).

As a result, we can unify the evaluation of Eqs. (B.1- B.5). Indeed, these HBs can be expressed by a linear relation in terms of a general HB $V = V_{(a)} + V_{(b)} + V_{(c)}$ given in Fig. 3 of the main paper, defined by the 'empty' box

$$V_{(a)}[\kappa^1, \kappa^2, \kappa^3, \kappa^4] = \int \frac{d^2p}{(2\pi)^2} \mathrm{tr}\left\{G^A\kappa^1 G^R\kappa^2 G^A\kappa^3 G^R\kappa^4\right\} \quad \text{(B.9)}$$

and the associated HBs

$$V_{(b)}[\kappa^1, \kappa^2, \kappa^3, \kappa^4] = \frac{1}{2m\tau}\int \frac{d^2p}{(2\pi)^2} \mathrm{tr}\left\{G^A\kappa^1 G^R\kappa^2 G^A\sigma^\delta\right\} \times \int \frac{d^2p'}{(2\pi)^2} \mathrm{tr}\left\{G^A\kappa^3 G^R\kappa^4 G^A\sigma^\delta\right\} \quad \text{(B.10)}$$

and

$$V_{(c)}[\kappa^1, \kappa^2, \kappa^3, \kappa^4] = \frac{1}{2m\tau}\int \frac{d^2p}{(2\pi)^2} \mathrm{tr}\left\{G^R\kappa^2 G^A\kappa^3 G^R\sigma^\delta\right\} \times \int \frac{d^2p'}{(2\pi)^2} \mathrm{tr}\left\{G^R\kappa^4 G^A\kappa^1 G^R\sigma^\delta\right\} \quad \text{(B.11)}$$

with a single impurity line. Here, $\kappa^i \in \{\sigma^\mu, v_1, v_2\}$ comprise all possible spin and velocity vertices occurring in the HBs in Fig. B.1 and in Eq. (4.3), and $G^{R/A}_{E_F,b}(\mathbf{p})$ is the impurity averaged Green function

$$G^{R/A}(\mathbf{p}, E) = \frac{1}{2} \sum_{s=\pm 1} \frac{1 + s \frac{\mathbf{b}_{\rm eff}(\mathbf{p})}{b_{\rm eff}(\mathbf{p})} \cdot \boldsymbol{\sigma}}{E - E_s(\mathbf{p}) \pm i/2\tau} \tag{B.12}$$

which depends on B-field and SOI by $\mathbf{b}_{\rm eff}(\mathbf{p}) = \alpha \mathbf{p} \times \mathbf{e}_z + \mathbf{b}$ and where $E_\pm(\mathbf{p}) = p^2/2m \pm b_{\rm eff}(\mathbf{p})$. Eventually, by use of the property

$$G^{R/A}_b(p) = \sigma^2 G^{R/A}_{-b}(-p)\sigma^2 \tag{B.13}$$

we find,

$$V^{\mu\rho}_{La}[\sigma^k, \sigma^i] = V[\sigma^k, \sigma^\rho, \sigma^i, \sigma^\mu] \tag{B.14}$$
$$V^{\nu\kappa}_{Ra}[v_j, v_m] = V[\sigma^\kappa, v_m, \sigma^\nu, v_j] \tag{B.15}$$
$$V^{\mu\rho}_{Lb}[\sigma^k, v_j] = k^{\rho l}(dk^t)^{\mu r}(dkk^t)^{kn} V[\sigma^l, v_j, \sigma^r, \sigma^n] \tag{B.16}$$
$$V^{\nu\kappa}_{Rb}[\sigma^i, v_m] = (dk^t)^{\nu l}(\bar{d}kk^t)^{in} k^{\kappa r} V[\sigma^l, \sigma^n, \sigma^r, v_m] \tag{B.17}$$
$$V^{\mu\rho}_{Lc}[\sigma^k, v_m] = V[\sigma^k, v_m, \sigma^\rho, \sigma^\mu] \tag{B.18}$$
$$V^{\nu\kappa}_{Rc}[\sigma^i, v_j] = V[\sigma^i, \sigma^\kappa, \sigma^\nu, v_j] \tag{B.19}$$
$$V^{\mu\rho}_{Ld}[\sigma^k, v_m] = (dk^t)^{\rho l}(dk)^{\mu r} V[\sigma^k, v_m, \sigma^l, \sigma^r] \tag{B.20}$$
$$V^{\nu\kappa}_{Rd}[v_j, \sigma^i] = k^{\kappa l}(k^t)^{\nu r} V[\sigma^l, v_j, \sigma^i, \sigma^r] \tag{B.21}$$

where the matrices k and d are defined by $k^{\mu l} = \mathrm{tr}\{\sigma^2 \sigma^\mu \sigma^l\}/2$ and $d(\bar{d}) = \mathrm{diag}(1, -1, -1, -1, +1(-1), +1(-1))$. Eqs. (B.14-B.21) reduce the task of calculating a large number of similar HBs to the calculation of Eqs. (B.9-B.11). The calculation is performed by expanding Eqs. (B.9-B.11) up to second order in the SOI strength α. Note that HBs containing one momentum vertex p_j with $j = 1, 2$ vanish in zeroth order in α due to the integration over the angle of p_j. Therefore, taking into account both the momentum and the spin-dependent part of the velocity operator $\hat{v}_j = \hat{p}_j/m + \Omega_{kj}\sigma^k$ is required to consistently calculate V. In the dc.-limit, however, the spin-dependent part of $\hat{v}$ is cancelled by the vertex correction (see Sec. 4.1 and Ref. [Chalaev05]).

B.1.2 Calculation of the Cooperon and Diffuson

Next, we evaluate the Diffuson D and Cooperon C in Eq. (4.3) and discuss the appropriate boundary conditions in a mesoscopic sample. In a mesoscopic sample, D and C are given in coordinate representation by integral equations

of the form Eqs. (1.14, 1.15, 1.16). In the regime $x, 1/p_F l \ll 1$ Eq. (C.2) can be approximated by a differential equation $L^{\mu\rho}(\nabla_{\mathbf{x}})D^{\rho\nu}(\mathbf{x},\mathbf{x}') = \delta(\mathbf{x}-\mathbf{x}')\delta^{\mu\nu}$ where L is a second order differential operator (cf. Sec. C). Since L is of block diagonal form, i.e. $L^{0,i} = L^{i,0} = 0$ with $i = 1,2,3$ the charge-charge component D^{00} is decoupled from other components. Therefore, $D^{0,0}$ fulfills the well-known Dirichlet-von-Neumann boundary conditions [Akkermans07] used to describe charge diffusion in a sample with electric contacts at $\mathbf{x} = (0, x_2)$ and $\mathbf{x} = (L, x_2)$ and reflecting boundaries at $\mathbf{x} = (x_1, 0)$ and $\mathbf{x} = (x_1, L)$

$$\begin{aligned} D^{0,0}(\mathbf{x} = (0,x_2),\mathbf{x}') = D^{0,0}(\mathbf{x} = (L,x_2),\mathbf{x}') = 0 \\ \frac{\partial D^{0,0}}{\partial x_2}(\mathbf{x} = (x_1,0),\mathbf{x}') = \frac{\partial D^{0,0}}{\partial x_2}(\mathbf{x} = (x_1,L),\mathbf{x}') = 0. \end{aligned} \tag{B.22}$$

Finding the appropriate boundary conditions for the spin components $D^{i,j}$ $i,j = 1,2,3$ is more intricate and subject to a theoretical debate in the context of the spin-Hall effect [Galitski06, Bleibaum06, Rashba06, Tserkovnyak07]. However, in the regime $l/L \ll x \ll 1$ the main contribution to the fluctuations comes from $D^{0,0}$ such that the result Eq. (4.4) in the main Sec. 4.1 is not sensitive to the specific boundary conditions for the other components.

The finite size of the sample is then accounted for by a discretization of the Diffuson/Cooperon modes $(q_{n_x}, q_{n_y}) = (n_x, n_y)\pi/L$ where $n_y = 0,1,2,\ldots$ and where the zero mode is excluded in $n_x = 1,2,3,\ldots$ due to vanishing boundary conditions at the contacts Eq. (B.22). This way, C and D can be calculated in momentum space [cf. Sec. B.1.4] and, thus, are given by the two relations

$$D_q = \frac{1}{2m\tau}(\mathbb{1} - X_+(q))^{-1} \tag{B.23}$$

$$C_q = \frac{1}{2m\tau}k(\mathbb{1} - X_-(q))^{-1}k \tag{B.24}$$

the latter of which can be obtained by use of Eq. (B.13), where again $k^{\mu l} = \mathrm{tr}\{\sigma^2\sigma^\mu\sigma^l\}/2$. Expanding the matrix kernel

$$X_\pm^{\mu\nu} = \frac{1}{2m\tau}\int\frac{d^2p}{(2\pi)^2}\mathrm{tr}\{\sigma^\mu G^R_{E_F,b}(\mathbf{p})\sigma^\nu G^A_{E_F,\pm b}(\mathbf{p}-\mathbf{q})\} \tag{B.25}$$

in Eqs. (B.23, B.24) in the small quantities $\bar{q} = ql \ll 1$, $\beta = 2b\tau \ll 1$, and x,

we find

$$X_\epsilon = \begin{pmatrix} \frac{1}{\lambda} - \frac{\bar{q}^2}{2} & 0 & 0 & 0 \\ 0 & \frac{1}{\lambda} - \frac{\bar{q}^2}{2} & 0 & \\ 0 & 0 & \frac{1}{\lambda} - \frac{\bar{q}^2}{2} & 0 \\ 0 & 0 & 0 & \frac{1}{\lambda} - \frac{\bar{q}^2}{2} \end{pmatrix} \tag{B.26}$$

$$+ \begin{pmatrix} -\beta^2\delta_{\epsilon,-1} & -i\beta\delta_{\epsilon,-1} & 0 & 0 \\ -i\beta\delta_{\epsilon,-1} & -\frac{x^2}{2} - \beta^2\delta_{\epsilon,-1} & 0 & ix\bar{q}\cos\varphi \\ 0 & 0 & -\frac{x^2}{2} - \beta^2\delta_{\epsilon,+1} & -\beta\delta_{\epsilon,+1} + ix\bar{q}\sin\varphi \\ 0 & -ix\bar{q}\cos\varphi & \beta\delta_{\epsilon,+1} - ix\bar{q}\sin\varphi & -x^2 - \beta^2\delta_{\epsilon,+1} \end{pmatrix},$$

where φ is the polar angle of the momentum $\bar{\mathbf{q}}$, $\lambda = 1 - i\Delta E\tau$, and the magnetic field has been taken along $\mathbf{x}(\varphi_b = 0)$ [1]. The matrix inversion in Eqs. (B.23)-(B.24) of $\mathbb{1} - X_\pm$ yields expressions for the components $D^{\mu\nu}$, $C^{\mu\nu}$. The singlet component $D^{0,0}$ (and $C^{2,2}$ for $\mathbf{b} = 0$) has a particularly simple form given by $D^{0,0} = 1/2m\tau(-i\omega\tau + \bar{q}^2/2)$. In the regime $l/L_\phi, l/L \ll x = 2\alpha p_F\tau \ll 1$ these components $D^{0,0}$ and $C^{2,2}$ (for $b = 0$) yield the dominant contributions to Eq. (4.4) in the main Sec. 4.1.

B.1.3 Vertex correction

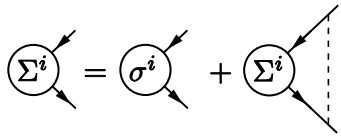

Figure B.2: Diagrammatic equation for the correction of the spin vertex σ^i.

We turn now to the calculation of the spin vertex correction $\Sigma^i \equiv \Sigma^{i\mu}\sigma^\mu$ defined as the solution to the diagrammatic equation in Fig. B.2. Analytically, this can be written as

$$\Sigma^{i\mu} = \delta^{i\mu} + X_+^{i\rho}(q = 0)\Sigma^{\rho\mu}. \tag{B.27}$$

[1] No strong dependence of $\overline{\delta\chi^2}$ on the direction of $\mathbf{b}$ has been found.

yielding the constant solution $\Sigma^{11} = \Sigma^{22} = 2/x^2$ and $\Sigma^{33} = 1/x^2$. This is valid in the regime considered in the paper $l/L \ll x = 2\alpha p_F \tau$, or equivalently $\lambda_{SO} = 1/2m\alpha \ll L$. On the other hand, when $L \approx \lambda_{SO}$ boundary effects start to matter and the matrix elements $\langle x|\Sigma|x'\rangle = \Sigma(x, x')$ are no longer constant. This situation is out of the scope of the paper and we comment on it briefly: For $L \approx \lambda_{SO}$ the diagrammatic equation in Fig. B.2 turns into an integral equation in place of Eq. (B.27), which can be evaluated in the diffusive limit. The boundary effects lead to a cut-off of the $1/x^2$ divergence of Σ for small spin-orbit interaction (small x). Therefore, with Σ remaining finite in the limit $x \to 0$, also the fluctuations (Eqs. (4.5) (4.6) of Sec. 4.1) are convergent and vanish for $x \to 0$.

Eventually, we obtain the main result Eq. (4.4) by inserting the HBs, the Cooperon and the Diffuson, and the renormalized vertex Σ into Eq. (4.3).

B.1.4 Cooperon and Diffuson

In this section we derive equations for the Cooperon and the Diffuson with SOI starting from the initial diagrammatic expressions.

Diffuson

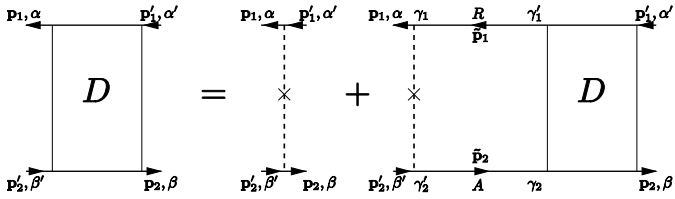

Figure B.3: Diagrammatic equation for the Diffuson.

The Diffuson is given by the diagrammatic equation in Fig. B.1.4. The analytical expression is

$$\begin{aligned} D^{\alpha\alpha'}_{\beta\beta'}(\mathbf{p}_1, \mathbf{p}_1', \mathbf{p}_2, \mathbf{p}_2'|E, \omega) = {} & \frac{1}{m\tau}\delta(\mathbf{p}_1 - \mathbf{p}_1' = -(\mathbf{p}_2 - \mathbf{p}_2'))\delta_{\alpha\alpha'}\delta_{\beta\beta'} \\ & + \frac{1}{m\tau}\int d^2\tilde{p}_1 d^2\tilde{p}_2 \delta(\mathbf{p}_1 - \tilde{\mathbf{p}}_1 = -(\tilde{\mathbf{p}}_2 - \mathbf{p}_2'))\delta_{\alpha\gamma_1}\delta_{\beta'\gamma_2'} \\ & \times G^R_{\gamma_1,\gamma_1'}(\tilde{\mathbf{p}}_1, E + \omega) G^A_{\gamma_2,\gamma_2'}(\tilde{\mathbf{p}}_2, E) D^{\gamma_1'\alpha'}_{\beta,\gamma_2}(\tilde{\mathbf{p}}_1, \mathbf{p}_1', \mathbf{p}_2, \tilde{\mathbf{p}}_2) \end{aligned} \tag{B.28}$$

Since, for a spatially homogeneous system the Green functions $G^{R/A}$ depend only on one momentum argument, we make the ansatz that D depends only on the difference of the left momenta $\mathbf{p}_1 - \mathbf{p}_2'$ in the form

$$D^{\alpha\alpha'}_{\beta\beta'}(\mathbf{p}_1, \mathbf{p}_1', \mathbf{p}_2, \mathbf{p}_2'|E, \omega) = \delta(\mathbf{p}_1 - \mathbf{p}_1' = -(\mathbf{p}_2 - \mathbf{p}_2'))D^{\mu\nu}(\mathbf{p}_1 - \mathbf{p}_2'|E, \omega)\sigma^{\mu}_{\alpha\beta'}\sigma^{\nu}_{\beta\alpha'} \tag{B.29}$$

where $\sigma^{\mu}, \mu = 0, 1, 2, 3$ are the Pauli matrices ($\sigma^0 = \mathbb{1}_2$) and $D^{\mu\nu}(\mathbf{p}_1 - \mathbf{p}_2')$ is a 4×4 matrix. Using the identity $\delta_{\alpha\alpha'}\delta_{\beta\beta'} = 1/2\sum_{\mu=0}^{3}\sigma^{\mu}_{\alpha\beta}\sigma^{\mu}_{\beta'\alpha'}$ Eq. (B.28) factorizes in the momentum and spin arguments and we obtain the equation for the Diffuson

$$D^{\mu\nu}(\mathbf{q}) = \frac{1}{2m\tau}\delta^{\mu\nu} + X_D^{\mu\rho}(\mathbf{q})D^{\rho\nu}(\mathbf{q}) \tag{B.30}$$

where the matrix insertion X_D is given by

$$X_D^{\mu\nu}(\mathbf{q}, \omega) = \frac{1}{2m\tau}\int \frac{d^2p}{(2\pi)^2}\mathrm{tr}\left\{\sigma^{\mu}\, G^R(\mathbf{p}, E_F + \hbar\omega)\, \sigma^{\nu} G^A(\mathbf{p} - \mathbf{q}, E_F)\right\}. \tag{B.31}$$

which is calculated in Chaps. 2, 3 to describe EDSR and in Chap. 4 to describe mesoscopic fluctuations of the spin susceptibility.

Cooperon

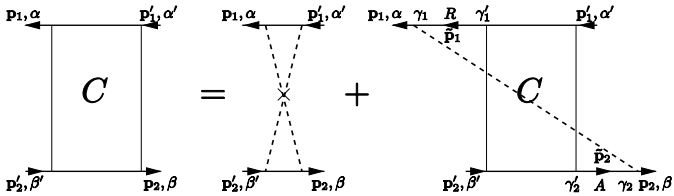

Figure B.4: Diagrammatic equation for the Cooperon.

The Cooperon is given by the diagrammatic equation in Fig. B.1.4. Similar to the previous section we make an ansatz

$$C^{\alpha\alpha'}_{\beta\beta'}(\mathbf{p}_1, \mathbf{p}_1', \mathbf{p}_2, \mathbf{p}_2'|E, \omega) = \delta(\mathbf{p}_1 - \mathbf{p}_1' = -(\mathbf{p}_2 - \mathbf{p}_2'))C^{\mu\nu}(\mathbf{p}_1 + \mathbf{p}_2|E, \omega)\sigma^{\mu}_{\alpha\beta}\sigma^{\nu}_{\beta'\alpha'} \tag{B.32}$$

where C depends only on the sum of the outgoing momenta $\mathbf{p}_1, \mathbf{p}_2$. We obtain for $C^{\mu\nu}$ the equation

$$C^{\mu\nu}(\mathbf{q}) = X_C^{\mu\rho}\left[\frac{1}{2m\tau}\delta^{\rho\nu} + X_C^{\rho\rho'}(\mathbf{q})C^{\rho'\nu}(\mathbf{q})\right] \tag{B.33}$$

where

$$X_C^{\mu\nu}(\mathbf{q},\omega) = \frac{1}{2m\tau}\int\frac{d^2p}{(2\pi)^2}\mathrm{tr}\left\{\sigma^\mu\, G^R(\mathbf{p}, E_F+\hbar\omega)\,\sigma^\nu[G^A(\mathbf{q}-\mathbf{p}, E_F)]^t\right\}. \tag{B.34}$$

Eq. (B.33) is used to calculate the Cooperon contribution to the spin susceptibility fluctuations in Chap. 4.

B.2 List of symbols

$\sigma^i,\ i=1,2,3$	Pauli matrices
σ^0	2×2 identity matrix
p_F	Fermi momentum
$v_F = \frac{p_F}{m}$	Fermi velocity
τ	scattering time
$l = v_F\tau$	mean free path
α	strength of the Rashba spin-orbit interaction
$\lambda_{SO} = \frac{1}{2m\alpha}$	spin-orbit length
$x = 2\alpha p_F\tau$ $= l/\lambda_{SO}$	relative strength of the spin-orbit interaction, spin precession angle between impurity scatterings
$\tau_{\mathrm{DP}}^{-1} = x^2/2\tau$	D'yakonov-Perel spin relaxation rate
τ_ϕ	dephasing rate
$L_\phi = l\sqrt{\tau_\phi/2\tau}$	dephasing length
$\phi = \tau/\tau_\phi$	dephasing rate measured in units of τ
V	Hikami boxes
$V_{(a)}$	empty Hikami box
$V_{(b)}$ $(V_{(c)})$	Hikami box with single impurity line connecting the two advanced(retarded) Green functions
D/C	Diffuson/Cooperon
q	momentum of D/C
ΔE	difference in gate voltages
b	external in-plane magnetic field

$\overline{\chi^{ij}}$	(incoherent) impurity average of the spin-electric susceptibility
$\overline{(\delta\chi^{ij})^2}$	variance of χ^{ij}
L	system size
$\Sigma^i = \Sigma^{i\mu}\sigma^\mu$	vertex correction of the spin vertex σ^i

C

Diffusion equation for the spin polarization

To illustrate the relation of spin diffusion and the ladder-type diagrams shown in Fig. 1.5 we derive a partial differential equation for the spin polarization density $\rho^i(\mathbf{r}) = \sigma^i \delta(\mathbf{r} - \hat{\mathbf{x}})$. We start from the Kubo formula Eq. (1.18) for the spin density $\rho^i(\mathbf{r})$ in linear response to the electric field $\mathbf{E}$. To leading order in $\mathcal{O}(1/p_F l)$ the impurity average of $\rho^i(\mathbf{r})$ is given by the ladder-type diagrams in Eqs. (1.11), (1.14) and, thus, can be written as

$$\rho^i(\mathbf{r}) = \frac{e}{2\pi}(2m\tau) \int d^2x \int d^2y \; d^2y' \; D^{i\nu}(\mathbf{r}, \mathbf{x}) \times \mathrm{tr}\left\{ \sigma^\nu G^R(\mathbf{x}, \mathbf{y}) \langle \mathbf{y}| \hat{v}_j |\mathbf{y}'\rangle G^A(\mathbf{y}, \mathbf{x}) \right\} E_j \tag{C.1}$$

where $\hat{v}_j = \frac{p_j}{m} + \Omega_{kj}\sigma^k$ is the velocity operator and $D^{\mu\nu}(\mathbf{r}, \mathbf{x})$ is the Diffuson defined by the integral equation

$$D^{\mu\nu}(\mathbf{r}, \mathbf{x}) = \frac{\delta^{\mu\nu}\delta(\mathbf{r} - \mathbf{x})}{2m\tau} + \int d^2x' X^{\mu\rho}(\mathbf{r}, \mathbf{x}') D^{\rho\nu}(\mathbf{x}', \mathbf{x}) \tag{C.2}$$

with $X^{\mu\nu}(\mathbf{r}, \mathbf{x}') = \frac{1}{2m\tau}\mathrm{tr}\left\{\sigma^\mu G^R_{E_F+\omega}(\mathbf{r}, \mathbf{x}')\sigma^\nu G^A_{E_F}(\mathbf{x}', \mathbf{r})\right\}$. In the regime $1/p_F l \ll 1$, the impurity-averaged Green functions and, hence, the Kernel $X(\mathbf{r}, \mathbf{x}') \approx e^{-|\mathbf{r}-\mathbf{x}'|/l}$ in Eq. (C.2) are short-ranged on the scale of the mean free path l. The Diffuson on the other hand, which is a concatenation of infinitely many X, is long-ranged and varies slowly on the scale of the mean free path. We therefore expand $D(\mathbf{x}', \mathbf{x}) \approx D(\mathbf{r}, \mathbf{x}) + (x' - r) \cdot \nabla_{\mathbf{r}} D(\mathbf{r}, \mathbf{x}) + \ldots$ around $\mathbf{r}$ to second order. This way, a differential equation

$$L(\boldsymbol{\nabla}_{\mathbf{r}}) D(\mathbf{r}, \mathbf{x}) = \frac{1}{2m\tau}\delta(\mathbf{r} - \mathbf{x}) \mathbb{1}_4 \tag{C.3}$$

$$L(\boldsymbol{\nabla}_{\mathbf{r}}) = \mathbb{1}_4 - X(\mathbf{q}) + i\frac{\partial X(\mathbf{q})}{\partial q_k}\frac{\partial}{\partial r_k} + \frac{\partial^2 X(\mathbf{q})}{\partial q_k \partial q_l}\frac{1}{2}\frac{\partial^2}{\partial r_k \partial r_l}\Big|_{\mathbf{q}=\mathbf{0}}, \tag{C.4}$$

for $D(\mathbf{r}, \mathbf{x})$ is obtained from Eq. (C.2) where $X^{\mu\nu}(\mathbf{q})$ is given in Eq. (B.25) and (B.31), which has been calculated in Eq. (B.26) where the bulk Green functions Eq. (2.3) of an infinite sample were used. Applying now the differential operator L to Eq. (C.1) and by use of Eq. (C.3) we obtain a differential equation for the spin density

$$L(\boldsymbol{\nabla})[\rho(\mathbf{r}) - \mathbf{S}_b] = \left(\frac{1}{\lambda} - 1\right)\mathbf{S}_b \tag{C.5}$$

where $\mathbf{S}_b = -2\nu\boldsymbol{\Omega}(e\mathbf{E}\tau)$ is the bulk, in-plane polarization due to a dc electric field in the magnetoelectric effect [Edelstein90]. To first order in $\omega\tau$, we find

$$[-i\omega + \Gamma - D\nabla^2](\boldsymbol{\rho} - \mathbf{S}_b) + 2[\mathbf{b} + p_F\boldsymbol{\Omega}(l\nabla)] \times (\boldsymbol{\rho} - \mathbf{S}_b) = i\omega\mathbf{S}_b \ , \tag{C.6}$$

where $D = v_F l/2$ is the diffusion constant and $\Gamma^{ij} = [\mathrm{tr}\{(\Omega\Omega^t)\}\delta_{ij} - (\Omega\Omega^t)_{ij}]2p_F^2/\tau$ describes spin relaxation due to the D'yakonov-Perel mechanism [D'yakonov72]. Eq. (C.6) describes the spatially and frequency resolved spin density in a system with SOI.

The individual terms in Eq. (C.6) (from left to right) can be interpreted as spin relaxation towards the equilibrium polarization, diffusion of the spin carrying particles, and precession in the magnetic and spin-orbit induced field. Apart from the latter precession term Eq. (C.6) has the form of a diffusion equation $[-i\omega - D\Delta]\rho = 0$. The precession term describes a coupling of gradients in the spin density to the internal field $\boldsymbol{\Omega}$. Eq. (C.6) can, alternatively, be derived from a quantum kinetic equation [Mishchenko04] [1] and can be applied in a theoretical description of the out-of-plane polarization generated at sample boundaries [Sih05] in the spin-Hall effect.

[1] The approach therein identically yields Eq. (C.6) if generalized to generic SOI, linearized in the electric field, and, as done there, if the charge density is approximated to be independent of spin density.

Bibliography

[Abragam61] A. Abragam. *Principles of Nuclear Magnetism* (Clarendon Press, Oxford, 1961).

[Akkermans07] E. Akkermans and G. Montambaux. *Mesoscopic physics of electrons and photons* (Cambridge University Press, 2007).

[Aleiner01] I. L. Aleiner and V. I. Fal'ko. *Spin-Orbit Coupling Effects on Quantum Transport in Lateral Semiconductor Dots.* Phys. Rev. Lett. **87**, 256801 (2001).

[Altshuler81] B. Altshuler, A. Aronov and D. Khmelnitsky. *Suppression of localization effects by the high frequency field and the Nyquist noise.* Solid State Commun. **39**, 619 (1981).

[Altshuler85] B. L. Altshuler. *Fluctuations in the extrinsic conductivity of disordered conductors.* Sov. JETP Lett. **41**, 648 (1985).

[Altshuler91] B. L. Altshuler, P. A. Lee and R. A. Webb (editors). *Mesoscopic Phenomena in Solids* (Elsevier Science Publishers, 1991).

[Anderson79] P. W. Anderson, E. Abrahams and T. V. Ramakrishnan. *Possible Explanation of Nonlinear Conductivity in Thin-Film Metal Wires.* Phys. Rev. Lett. **43**, 718 (1979).

[Averkiev02] N. S. Averkiev, L. E. Golub and M. Willander. *Spin relaxation anisotropy in two-dimensional semiconductor systems.* J. Phys.: Condens. Matter **14**, R271R283 (2002).

[Awschalom02] D. D. Awschalom, D. Loss and N. Samarth (editors). *Semiconductor Spintronics and Quantum Computation* (Springer, Berlin, 2002).

[Awschalom07] D. D. Awschalom and M. E. Flatté. *Challenges for semiconductor spintronics.* Nature Physics **3**, 153 (2007).

[Baibich88] M. N. Baibich, J. M. Broto, A. Fert, F. N. Van Dau, F. Petroff, P. Eitenne, G. Creuzet, A. Friederich and J. Chazelas. *Giant Magnetoresistance of (001)Fe/(001)Cr Magnetic Superlattices.* Phys. Rev. Lett. **61**, 2472 (1988).

[Bardarson07] J. H. Bardarson, I. Adagideli and P. Jacquod. *Mesoscopic Spin Hall Effect.* Phys. Rev. Lett. **98**, 196601 (2007).

[Baumberg94] J. J. Baumberg, S. A. Crooker, D. D. Awschalom, N. Samarth, H. Luo and J. K. Furdyna. *Ultrafast Faraday spectroscopy in magnetic semiconductor quantum structures.* Phys. Rev. B **50**, 7689 (1994).

[Beenakker91] C. W. J. Beenakker and H. van Houten. *Quantum Transport in Semiconductor Nanostructures.* In H. Ehrenreich and D. Turnbull (editors), *Semiconductor Heterostructures and Nanostructures* (Academic Press, 1991).

[Beenakker97] C. W. J. Beenakker. *Random-matrix theory of quantum transport.* Rev. Mod. Phys. **69**, 731 (1997).

[Bell62] R. L. Bell. *Electric dipole spin transitions in InSb.* Phys. Rev. Lett. **9**, 52 (1962).

[Benoit87] A. Benoit, C. P. Umbach, R. B. Laibowitz and R. A. Webb. *Length-Independent Voltage Fluctuations in Small Devices.* Phys. Rev. Lett. **58**, 2343 (1987).

[Bergmann84] G. Bergmann. *Weak localization in thin films a time-of-flight experiment with conduction electrons.* Phys. Rep. **107**, 1 (1984).

[Binasch89] G. Binasch, P. Grünberg, F. Saurenbach and W. Zinn. *Enhanced magnetoresistance in layered magnetic structures with antiferromagnetic interlayer exchange.* Phys. Rev. B **39**, 4828 (1989).

[Bleibaum06] O. Bleibaum. *Boundary conditions for spin-diffusion equations with Rashba spin-orbit interaction.* Phys. Rev. B **74**, 113309 (2006).

[Bloch57] F. Bloch. *Generalized Theory of Relaxation.* Phys. Rev. **105**, 1206 (1957).

[Bulaev07] D. V. Bulaev and D. Loss. *Electric Dipole Spin Resonance for Heavy Holes in Quantum Dots.* Phys. Rev. Lett. **98**, 097202 (2007).

[Bychkov84] Y. A. Bychkov and E. I. Rashba. *Oscillatory effects and the magnetic susceptibility of carriers in inversion layers.* J. Phys. C **17**, 6039 (1984).

[Chaichian01] M. Chaichian and A. Demichev. *Path integrals in physics* (IOP publishing, 2001).

[Chakravarty86] S. Chakravarty and A. Schmid. *Weak localization: The quasiclassical theory of electrons in a random potential.* Phys. Rep.**140**, 193 (1986).

[Chalaev05] O. Chalaev and D. Loss. *Spin-Hall conductivity due to Rashba spin-orbit interaction in disordered systems.* Phys. Rev. B **71**, 245318 (2005).

[Chandrasekhar90] V. Chandrasekhar, P. Santhanam and D. E. Prober. *Effect of spin-orbit and spin-flip scattering on conductance fluctuations.* Phys. Rev. B **42**, 6823 (1990).

[Cohen-Tannoudji77] C. Cohen-Tannoudji, B. Diu and F. Laloe. *Quantum Mechanics* (Wiley, 1977).

[Coish07] W. A. Coish and D. Loss. *Handbook of Magnetism and Advanced Magnetic Materials*, volume 5, chapter Quantum computing with spins in solids (Wiley, 2007).

[Cremers03] J.-H. Cremers, P. W. Brouwer and V. I. Fal'ko. *Weak localization and conductance fluctuations in a quantum dot with parallel magnetic field and spin-orbit scattering.* Phys. Rev. B **68**, 125329 (2003).

[Datta90] S. Datta and B. Das. *Electronic analog of the electro-optic modulator.* Appl. Phys. Lett. **56**, 665 (1990).

[deAndradaeSilva94] E. A. de Andrada e Silva, G. C. La Rocca and F. Bassani. *Spin-split subbands and magneto-oscillations in III-V asymmetric heterostructures.* Phys. Rev. B **50**, 8523 (1994).

[Dietl02] T. Dietl. *Ferromagnetic semiconductors.* Semiconductor Science and Technology **17**, 377 (2002).

[Dimitrova05] O. V. Dimitrova. *Spin-Hall conductivity in a two-dimensional Rashba electron gas.* Phys. Rev. B **71**, 245327 (2005).

[DiVincenzo00] D. P. DiVincenzo. *The Physical Implementation of Quantum Computation.* Fortschr. Phys. **48**, 771 (2000).

[Dobrowolska84] M. Dobrowolska, A.Witowski, J. K. Furdyna, T. Ichiguchi, H. D. Drew and P. A. Wolff. *Far infrared observation of the electric dipole-spin resonance of donor electrons in* $Cd_1 - xMn_xSe$. Phys. Rev. B **29**, 6652 (1984).

[Dresselhaus55] G. Dresselhaus. *Spin-orbit coupling effects in zinc blende structures.* Phys. Rev. **100**, 580 (1955).

[Drude00] P. Drude. *Zur Elektronentheorie der Metalle.* Annalen der Physik **306**, 566 (1900).

[Duckheim06] M. Duckheim and D. Loss. *Electric-dipole-induced spin resonance in disordered semiconductors.* Nature Physics **2**, 195 (2006).

[Duckheim07] M. Duckheim and D. Loss. *Resonant spin polarization and spin current in a two-dimensional electron gas.* Phys. Rev. B **75**, 201305 (2007).

[Duckheim08] M. Duckheim and D. Loss. *Mesoscopic fluctuations in the spin-electric susceptibility due to Rashba spin-orbit Interaction.* Phys. Rev. Lett. **101**, 226602 (2008).

[D'yakonov71] M. I. D'yakonov and M. I. Perel. *Possibility of orienting electron spins with current.* JETP Lett. **13**, 467 (1971).

[D'yakonov72] M. I. D'yakonov and V. I. Perel. *Spin relaxation of conduction electrons in noncentrosymmetric semiconductors.* Sov. Phys. Solid State **13**, 3023 (1972).

[Dyakonov84] M. I. Dyakonov and V. I. Perel. In F. Meier and B. Zakharchenya (editors), *Optical Orientation* (Elsevier, 1984).

[Edelstein90] V. M. Edelstein. *Spin polarization of conduction electrons induced by electric current in two-dimensional asymmetric electron systems.* Solid State Comm. **73**, 233 (1990).

[Edelstein93] V. M. Edelstein. *Space dispersion feature of the conduction electron spin resonance in two-dimensional electron systems caused by absence of 'up-down' symmetry.* J. Phys C **5**, 2603 (1993).

[Edelstein95] V. M. Edelstein. *Band-spin-orbit-energy effects in conductivity of two-dimensional weakly disordered semiconductor systems.* J. Phys. C **7**, 1 (1995).

[Edwards58] S. F. Edwards. *A new method for the evaluation of electric conductivity in metals.* Philos. Mag. **3**, 1020 (1958).

[Elzerman04] J. M. Elzerman, R. Hanson, L. H. W. van Beveren, B. Witkamp, L. M. K. Vandersypen and L. P. Kouwenhoven. *Single-shot read-out of an individual electron spin in a quantum dot.* Nature **430**, 431 (2004).

[Engel05] H.-A. Engel, B. I. Halperin and E. I. Rashba. *Theory of Spin Hall Conductivity in n-Doped GaAs.* Phys. Rev. Lett. **95**, 166605 (2005).

[Engel06] H.-A. Engel, E. I. Rashba and B. I. Halperin. *Theory of spin Hall effects in semiconductors* (2006). Cond-mat/0603306.

[Engel07] H.-A. Engel, E. I. Rashba and B. I. Halperin. *Out-of-Plane Spin Polarization from In-Plane Electric and Magnetic Fields.* Phys. Rev. Lett. **98**, 036602 (2007).

[Erlingsson05a] S. I. Erlingsson and D. Loss. *Determining the spin Hall conductance via charge transport.* Phys. Rev. B **72**, 121310 (2005).

[Erlingsson05b] S. I. Erlingsson, J. Schliemann and D. Loss. *Spin susceptibilities, spin densities and their connection to spin-currents.* Phys. Rev. B **71**, 035319 (2005).

[Feng89] S. Feng. *Mesoscopic conductance fluctuations in the presence of spin-orbit coupling and Zeeman splitting.* Phys. Rev. B **39**, 8722 (1989).

[Feynman65] R. P. Feynman and A. Hibbs. *Quantum Mechanics and Integrals* (McGraw-Hill, 1965).

[Galitski06] V. M. Galitski, A. A. Burkov and S. D. Sarma. *Boundary conditions for spin diffusion in disordered systems.* Phys. Rev. B **74**, 115331 (2006).

[Ganichev04] S. D. Ganichev, V. V. Bel'kov, L. E. Golub, E. L. Ivchenko, P. Schneider, S. Giglberger, J. Eroms, J. D. Boeck, G. Borghs, W. Wegscheider, D. Weiss and W. Prettl. *Experimental Separation of Rashba and Dresselhaus Spin Splittings in Semiconductor Quantum Wells.* Phys. Rev. Lett. **92**, 256601 (2004).

[Glazov05] M. M. Glazov and E. Y. Sherman. *Nonexponential spin relaxation in magnetic fields in quantum wells with random spin-orbit coupling.* Phys. Rev. B **71**, 241312 (2005).

[Golovach04] V. N. Golovach, A. Khaetskii and D. Loss. *Phonon-Induced Decay of the Electron Spin in Quantum Dots.* Phys. Rev. Lett. **93**, 016601 (2004).

[Golovach06] V. N. Golovach, M. Borhani and D. Loss. *Electric-dipole-induced spin resonance in quantum dots.* Phys. Rev. B **74**, 165319 (2006).

[Gorkov79] L. Gorkov, A. Larkin and D. Khmelnitskii. *Particle conductivity in a two-dimensional random potential.* JETP LETT. **30**, 228 (1979).

[Grünberg86] P. Grünberg, R. Schreiber, Y. Pang, M. B. Brodsky and H. Sowers. *Layered Magnetic Structures: Evidence for Antiferromagnetic Coupling of Fe Layers across Cr Interlayers.* Phys. Rev. Lett. **57**, 2442 (1986).

[Hanson07] R. Hanson, L. P. Kouwenhoven, J. R. Petta, S. Tarucha and L. M. K. Vandersypen. *Spins in few-electron quantum dots.* Rev. Mod. Phys. **79**, 1217 (2007).

[Hikami80] S. Hikami, A. Larkin and Y. Nagoaka. *Spin-orbit interaction and Magnetoresistance in the 2 dimensional random system.* Prog. theoret. phys. **63**, 707 (1980).

[Hikami81] S. Hikami. *Anderson localization in a nonlinear-σ-model representation.* Phys. Rev. B **24**, 2671 (1981).

[Hirsch99] J. E. Hirsch. *Spin Hall Effect.* Phys. Rev. Lett. **83**, 1834 (1999).

[Imry86] Y. Imry. *Active Transmission Channels and Universal Conductance Fluctuations.* Europhys. Lett. **1**, 249 (1986).

[Inoue04] J. Inoue, G. E. W. Bauer and L. W. Molenkamp. *Suppression of the persistent spin Hall current by defect scattering.* Phys. Rev. B **70**, 041303 (2004).

[Jagannathan88] A. Jagannathan, E. Abrahams and M. J. Stephen. *Magnetic exchange in disordered metals.* Phys. Rev. B **37**, 436 (1988).

[Kato04a] Y. K. Kato, R. C. Myers, A. C. Gossard and D. D. Awschalom. *Coherent Spin Manipulation without magnetic fields in strained Semiconductors.* Nature **427**, 50 (2004).

[Kato04b] Y. K. Kato, R. C. Myers, A. C. Gossard and D. D. Awschalom. *Current-Induced Spin Polarization in Strained Semiconductors.* Phys. Rev. Lett. **93**, 176601 (2004).

[Kato04c] Y. K. Kato, R. C. Myers, A. C. Gossard and D. D. Awschalom. *Observation of the Spin Hall Effect in Semiconductors.* Science **306**, 1910 (2004).

[Kato05] Y. K. Kato, R. C. Myers, A. C. Gossard and D. D. Awschalom. *Electrical initialization and manipulation of electron spins in an L-shaped strained n-InGaAs channel.* Appl. Phys. Lett. **87**, 022503 (2005).

[Kikkawa97] J. M. Kikkawa, I. P. Smorchkova, N. Samarth and D. D. Awschalom. *Room-Temperature Spin Memory in Two-Dimensional Electron Gases.* Science **277**, 1284 (1997).

[Kikkawa98] J. M. Kikkawa and D. D. Awschalom. *Resonant Spin Amplification in n-Type GaAs.* Phys. Rev. Lett. **80**, 4313 (1998).

[Koga06] T. Koga, Y. Sekine and J. Nitta. *Experimental realization of a ballistic spin interferometer based on the Rashba effect using a nanolithographically defined square loop array.* Phys. Rev. B **74**, 041302 (2006).

[Krich08] J. J. Krich and B. I. Halperin. *Spin-polarized current generation from quantum dots without magnetic fields.* Phys. Rev. B **78**, 035338 (2008).

[Kroutvar04] M. Kroutvar, Y. Ducommun, D. Heiss, M. Bichler, D. Schuh, G. Abstreiter and J. J. Finley. *Optically programmable electron spin memory using semiconductor quantum dots.* Nature **432**, 81 (2004).

[Larkin86] A. Larkin and D. E. Khmel'nitskii. *Mesoscopic fluctuations of current-voltage characteristics.* Sov. Phys. JETP **64**, 1075 (1986).

[Lee85] P. A. Lee and A. D. Stone. *Universal Conductance Fluctuations in Metals.* Phys. Rev. Lett. **55**, 1622 (1985).

[Lee87] P. A. Lee, A. D. Stone and H. Fukuyama. *Universal conductance fluctuations in metals: Effects of finite temperature, interactions, and magnetic field.* Phys. Rev. B **35**, 1039 (1987).

[Lerner93] I. V. Lerner. *Dependence of the Ruderman-Kittel-Kasuya-Yosida interaction on nonmagnetic disorder.* Phys. Rev. B **48**, 9462 (1993).

[Levitov85] L. S. Levitov, Y. V. Nazarov and G. M. Eliashberg. *Magnetoelectric effects in conductors with mirror isomer symmetry.* Zh. Eksp. Teor. Fiz.(engl. translation: Sov. Phys. JETP 61, 133 (1985)) **88**, 229 (1985).

[Li06] Y. Li and Y.-Q. Li. *Spin relaxation of two-dimensional electrons with a hierarchy of spin-orbit couplings.* J. Phys.: Condens. Matter **19**, 346231 (2006).

[Loss93] D. Loss, H. Schoeller and P. M. Goldbart. *Weak-localization effects and conductance fluctuations: Implications of inhomogeneous magnetic fields.* Phys. Rev. B **48**, 15218 (1993).

[Loss98] D. Loss and D. P. DiVincenzo. *Quantum computation with quantum dots.* Phys. Rev. A **57**, 120 (1998).

[Macedo92] A. M. S. Macedo and J. T. Chalker. *Effects of spin-orbit interactions in disordered conductors: A random-matrix approach.* Phys. Rev. B **46**, 14985 (1992).

[Mal'shukov05] A. G. Mal'shukov, L. Y. Wang, C. S. Chu and K. A. Chao. *Spin Hall Effect on Edge Magnetization and Electric Conductance of a 2D Semiconductor Strip.* Phys. Rev. Lett. **95**, 146601 (2005).

[Maslov93] D. L. Maslov and D. Loss. *Edge-state transport and conductance fluctuations in the metallic phase of the quantum Hall regime.* Phys. Rev. Lett. **71**, 4222 (1993).

[Meier84] F. Meier and B. P. Zakharchenya. *Optical Orientation*, volume 8 of *Modern Problems in Condensed Matter Science series* (North-Holland, Amsterdam, 1984).

[Meier07] L. Meier, G. Salis, I. Shorubalko, E. Gini, S. Schön and K. Ensslin. *Measurement of Rashba and Dresselhaus spinorbit magnetic fields.* Nature Phys. **3**, 650 (2007).

[Melnikov72] V. I. Melnikov and E. I. Rashba. *Influence of impurities on combined resonance in semiconductors.* Sov. Phys. JETP **34**, 1353 (1972).

[Mermin07] N. D. Mermin. *Quantum Computer Science* (Cambridge University Press, 2007).

[Miller03] J. B. Miller, D. M. Zumbühl, C. M. Marcus, Y. B. Lyanda-Geller, D. Goldhaber-Gordon, K. Campman and A. C. Gossard. *Gate-controlled spin-orbit quantum interference effects in lateral transport.* Phys. Rev. Lett. **90**, 076807 (2003).

[Milletarì08] M. Milletarì, R. Raimondi and P. Schwab. *Magneto-spin Hall conductivity of a two-dimensional electron gas.* Europhys. Lett. **82**, 67005 (2008).

[Mishchenko04] E. G. Mishchenko, A. V. Shytov and B. I. Halperin. *Spin Current and Polarization in Impure Two-Dimensional Electron Systems with Spin-Orbit Coupling.* Phys. Rev. Lett. **93**, 226602 (2004).

[Mohanty02] P. Mohanty and R. A. Webb. *Anomalous Conductance Distribution in Quasi-One-Dimensional Gold Wires: Possible Violation of the One-Parameter Scaling Hypothesis.* Phys. Rev. Lett. **88**, 146601 (2002).

[Mott65] N. F. Mott and H. S. W. Massey. *The Theory of Atomic Collisions* (Oxford University Press, New York, 1965).

[Nazarov90] Y. V. Nazarov. *Random spin polarization of carriers in noequilibrium disordered metal.* Pis'ma Zh. Eksp. Teor. Fiz. **51**, 375 (1990).

[Nazarov07] Y. V. Nazarov. *Mesoscopic fluctuations of spin currents.* New J. Phys. **9**, 352 (2007).

[Nielsen00] M. A. Nielsen and I. L. Chuang. *Quantum Computation and Quantum Information* (Cambridge University Press, 2000).

[Nitta97] J. Nitta, T. Akazaki, H. Takayanagi and T. Enoki. *Gate Control of Spin-Orbit Interaction in an Inverted $In_{0.53}Ga_{0.47}As/In_{0.52}Al_{0.48}As$ Heterostructure.* Phys. Rev. Lett. **78**, 1335 (1997).

[Nowack07] K. C. Nowack, F. H. L. Koppens, Y. V. Nazarov and L. M. K. Vandersypen. *Coherent Control of a Single Electron Spin with Electric Fields.* Science **318**, 1430 (2007).

[Oestreich05] M. Oestreich, M. Römer, R. J. Haug and D. Hägele. *Spin Noise Spectroscopy in GaAs.* Phys. Rev. Lett. **95**, 216603 (2005).

[Ohno98] H. Ohno. *Making Nonmagnetic Semiconductors Ferromagnetic.* Science **281**, 951 (1998).

[Papadakis99] S. J. Papadakis, E. P. D. Poortere, H. C. Manoharan, M. Shayegan and R. Winkler. *The Effect of Spin Splitting on the Metallic Behavior of a Two-Dimensional System.* Science **283**, 2056 (1999).

[Pletyukhov07] M. Pletyukhov. *Crossover from diffusive to nondiffusive dynamics in the two-dimensional electron gas with Rashba spin-orbit coupling.* Phys. Rev. B **75**, 155335 (2007).

[Rammer86] J. Rammer and H. Smith. *Quantum field-theoretical methods in transport theory of metals.* Rev. Mod. Phys. **58**, 323 (1986).

[Rammer98] J. Rammer. *Quantum Transport Theory* (Perseus Books, Reading, Massachusetts, 1998).

[Rashba60] E. I. Rashba. *Properties of semiconductors with an extremum loop.* Sov. Phys. Solid State **2**, 1109 (1960).

[Rashba03a] E. I. Rashba. *Spin currents in thermodynamic equilibrium: The challenge of discerning transport currents.* Phys. Rev. B **68**, 241315R (2003).

[Rashba03b] E. I. Rashba and A. L. Efros. *Efficient electron spin manipulation in a quantum well by an in-plane electric field.* App. Phys. Lett. **83**, 5295 (2003).

[Rashba06] E. I. Rashba. *Spinorbit coupling and spin transport.* Physica E **34**, 31 (2006).

[Schäfer96] R. Schäfer, K. Hecker, H. Hegger and W. Langheinrich. *Experimental study of mesoscopic fluctuations in nonlinear conductance and magnetoconductance.* Phys. Rev. B **53**, 15964 (1996).

[Schliemann03] J. Schliemann, J. C. Egues and D. Loss. *Nonballistic Spin-Field-Effect Transistor.* Phys. Rev. Lett. **90**, 146801 (2003).

[Schliemann04] J. Schliemann and D. Loss. *Dissipation effects in spin-Hall transport of electrons and holes.* Phys. Rev. B **69**, 165315 (2004).

[Schliemann05] J. Schliemann, D. Loss and R. M. Westervelt. *Zitterbewegung of Electronic Wave Packets in III-V Zinc-Blende Semiconductor Quantum Wells.* Phys. Rev. Lett. **94**, 206801 (2005).

[Schulte05] M. Schulte, J. G. S. Lok, G. Denninger and W. Dietsche. *Electron spin Resonance on a Two-dimensional Electron Gas in a Single AlAs Quantum Well.* Phys. Rev. Lett. **94**, 137601 (2005).

[Schwabl05] F. Schwabl. *Quantenmechanik für Fortgeschrittene* (Springer, 2005).

[Sih05] V. Sih, R. C. Myers, Y. K. Kato, W. H. Lau, A. C. Gossard and D. D. Awschalom. *Spatial imaging of the spin Hall effect and current-induced polarization in two-dimensional electron gases.* Nature Physics **1**, 31 (2005).

[Sih06] V. Sih, W. H. Lau, R. C. Myers, V. R. Horowitz, A. C. Gossard and D. D. Awschalom. *Generating Spin Currents in Semiconductors with the Spin Hall Effect.* Phys. Rev. Lett. **97**, 096605 (2006).

[Silov04] A. Y. Silov, P. A. Blajnov, J. H. Wolter, R. Hey, K. H. Ploog and N. S. Averkiev. *Current-induced spin polarization at a single heterojunction.* App. Phys. Lett. **85**, 5929 (2004).

[Sinova04] J. Sinova, D. Culcer, Q. Niu, N. A. Sinitsyn, T. Jungwirth and A. H. MacDonald. *Universal intrinsic spin Hall effect.* Phys. Rev. Lett. **92**, 126603 (2004).

[Skocpol86] W. J. Skocpol, P. M. Mankiewich, R. E. Howard, L. D. Jackel, D. M. Tennant and A. D. Stone. *Universal conductance fluctuations in silicon inversion-layer nanostructures.* Phys. Rev. Lett. **56**, 2865 (1986).

[Slichter96] C. Slichter. *Principles of Magnetic Resonance.* Springer Series in Solid-State Sciences (Springer, 1996).

[Stern06] N. P. Stern, S. Ghosh, G. Xiang, M. Zhu, N. Samarth and D. D. Awschalom. *Current-Induced Polarization and the Spin Hall Effect at Room Temperature.* Phys. Rev. Lett. **97**, 126603 (2006).

[Stich07] D. Stich, J. Zhou, T. Korn, R. Schulz, D. Schuh, W. Wegscheider, M. W. Wu and C. Schüller. *Effect of Initial Spin Polarization on Spin Dephasing and the Electron g Factor in a High-Mobility Two-Dimensional Electron System.* Phys. Rev. Lett. **98**, 176401 (2007).

[Tahan05] C. Tahan and R. Joynt. *Rashba spin-orbit coupling and spin relaxation in silicon quantum wells.* Phys. Rev. B **71**, 075315 (2005).

[Trushin07] M. Trushin and J. Schliemann. *Anisotropic current-induced spin accumulation in the two-dimensional electron gas with spin-orbit coupling.* Phys. Rev. B **75**, 155323 (2007).

[Tserkovnyak07] Y. Tserkovnyak, B. I. Halperin, A. A. Kovalev and A. Brataas. *Boundary spin Hall effect in a two-dimensional semiconductor system with Rashba spin-orbit coupling.* Phys. Rev. B **76**, 085319 (2007).

[Tsyplyatyev03] O. Tsyplyatyev, I. L. Aleiner, V. I. Fal'ko and I. V. Lerner. *Applicability of the ergodicity hypothesis to mesoscopic fluctuations.* Phys. Rev. B **68**, 121301 (2003).

[Umbach84] C. P. Umbach, S. Washburn, R. B. Laibowitz and R. A. Webb. *Magnetoresistance of small, quasi-one-dimensional, normal-metal rings and lines.* Phys. Rev. B **30**, 4048 (1984).

[Valenzuela06] S. O. Valenzuela and M. Tinkham. *Direct electronic measurement of the spin Hall effect.* Nature **442**, 176 (2006).

[Walls07] J. Walls and E. Heller. *Spin-Orbit Coupling Induced Interference in Quantum Corrals.* Nano Letters **7**, 3377 (2007).

[Webb88] R. A. Webb, S. Washburn and C. P. Umbach. *Experimental study of nonlinear conductance in small metallic samples.* Phys. Rev. B **37**, 8455 (1988).

[Wilamowski07] Z. Wilamowski, H. Malissa, F. Schäffler and W. Jantsch. *g-Factor Tuning and Manipulation of Spins by an Electric Current.* Phys. Rev. Lett. **98**, 187203 (2007).

[Winkler03] R. Winkler. *Spin-orbit Coupling Effects in Two-Dimensional Electron and Hole Systems* (Springer, 2003).

[Wunderlich05] J. Wunderlich, B. Kaestner, J. Sinova and T. Jungwirth. *Experimental Observation of the Spin-Hall Effect in a Two-Dimensional Spin-Orbit Coupled Semiconductor System.* Phys. Rev. Lett. **94**, 047204 (2005).

[Zumbühl05] D. M. Zumbühl, J. B. Miller, C. M. Marcus, D. Goldhaber-Gordon, J. J. S. Harris, K. Campman and A. C. Gossard. *Conductance fluctuations and partially broken spin symmetries in quantum dots.* Phys. Rev. B **72**, 081305 (2005).

[Zutic04] I. Zutic, J. Fabian and S. D. Sarma. *Spintronics: Fundamentals and applications.* Rev. Mod. Phys. **76**, 323 (2004).

[Zyuzin90] A. Y. Zyuzin. *Spin Polarization Effects in Mesoscopic Conductors.* Europhys. Lett. **12**, 529 (1990).

[Zyuzin92] A. Y. Zyuzin and R. A. Serota. *Mesoscopic fluctuations of electron-spin polarization in disordered conductors.* Phys. Rev. B **45**, 12094 (1992).

[Zyuzin07] V. A. Zyuzin, P. G. Silvestrov and E. G. Mishchenko. *Spin Hall Edge Spin Polarization in a Ballistic 2D Electron System.* Phys. Rev. Lett. **99**, 106601 (2007).

Acknowledgements

I am very appreciative of all the people who have made the time during my PHD research at the university of Basel so enjoyable.

Fist of all, I would like to thank Prof. Daniel Loss for accepting me as a PHD student. The knowledge, views, ideas, and enthusiasm he shared with me in many discussions were always motivating and contributed a lot to the content of this thesis. I moreover benefitted from the excellent research environment in the condensed matter group by being able to participate in conferences and interact with many bright people. I am also grateful to him for being a member of this group.

Also, I want to thank Oleg Chalaev who has introduced me to the subtleties of diagrammatic calculations. Oleg shared his deep knowledge about this subject in conversations on specific questions. He would often start this conversations by stating that he had the answer already written down in his notes which he most often had. I also want to thank my former officemates Joerg Lehmann and Denis Bulaev for the fun we had and for the discussions of physics and matters of life. The same is true for my present officemates K. van Hoogdalem and O. Tsyplyatyev and for the members of whole condensed matter theory group. Specifically, I would like to acknowledge Jan Fischer, Charles Doiron, Mircea Trif, Stefano Chesi, Joël Peguiron, Bill Coish, Beat Roethlisberger, Daniel Saraga, Veronica Cerletti, Daniel Klauser, Massoud Borhani, Vitaly Golovach, Dmitrije Stepanenko, Christoph Bruder, Oded Zilberberg, Dan Bohr, Verena Koerting, John Schliemann, and Sigurdur Erlingsson for scientific and non-scientific discussions and an active social life. I also benefitted from discussions with people (more or less) outside the fourth floor, Carlos Egues, Tobias Kramer, Philippe Jacquod, Oliver Gywat, Hans-Andreas Engel, Jacob Krich, Wolfgang Jantsch, Emmanuel Rashba, Boris Altshuler, Tobias Korn and Dmitrii Maslov. Further, I would like to acknowledge collaboration with Gian Salis and Lorentz Meier at the IBM group in Zuerich who were able to experimentally observe predictions made in this thesis.

I also want to thank Verena and my family for their support.

Last, but not least I would like to thank Prof. Dmitrii Maslov for corefereeing this thesis.

Publications

- Mathias Duckheim and Daniel Loss.
  Mesoscopic fluctuations in the spin-electric susceptibility due to Rashba spin-orbit interaction.
  Phys. Rev. Lett. **101**, 226602 (2008)

- Mathias Duckheim and Daniel Loss.
  Semiconductor spintronics: Snapshots of spins separating.
  Nature Physics **4**, 836 - 837 (2008), News and Views

- Mathias Duckheim and Daniel Loss.
  Resonant spin polarization and spin current in a two-dimensional electron gas.
  Phys. Rev. B **75**, 201305(R) (2007)

- Mathias Duckheim and Daniel Loss.
  Electric-dipole-induced spin resonance in disordered semiconductors.
  Nature Physics **2**, 195-199 (2006)

- Mathias Duckheim and Joachim Ankerhold.
  Influence of low-frequency noise on macroscopic quantum tunneling in superconducting circuits.
  Phys. Rev. B **71**, 134501 (2005)